Experimental and Theoretical Determination of Dissociation Energies of Dispersion-Dominated Aromatic Molecular Complexes

Journal:	*Chemical Reviews*
Manuscript ID	cr-2015-006525.R1
Manuscript Type:	Thematic Review
Date Submitted by the Author:	n/a

Complete List of Authors:	Frey, Jann; Universität Bern, Dept. für Chemie und Biochemie Holzer, Christof; Karlsruhe Institute of Technology, Institute of Physical Chemistry, Theoretical Chemistry Group Klopper, Wim; KIT Karlsruhe, Institut Nanotechnology, Leutwyler, Samuel; Universität Bern, Dept. für Chemie und Biochemie

Experimental and Theoretical Determination of Dissociation Energies of Dispersion-Dominated Aromatic Molecular Complexes

Jann A. Frey,[†] Christof Holzer,[‡] Wim Klopper,[‡] and Samuel Leutwyler[*,†]

Departement für Chemie und Biochemie, Universität Bern, Freiestrasse 3, CH-3012 Bern, Switzerland, and Institute of Physical Chemistry, Karlsruhe Institute of Technology (KIT), Fritz-Haber-Weg 2, D-76131 Karlsruhe, Germany

E-mail: klopper@kit.edu

Abstract

The dissociation energy (D_0) of an isolated and cold molecular complex in the gas-phase is a fundamental measure of the strength of the intermolecular interactions between its constituent moieties. Accurate D_0 values are important for the understanding of intermolecular bonding, for benchmarking high-level theoretical calculations and for the parametrization of force-field models used in fields ranging from crystallography to biochemistry. We review experimental and theoretical methods for determining gas-phase D_0 values of M·S complexes, where M is a (hetero)aromatic molecule and S is a closed-shell "solvent" atom or molecule. The experimental methods discussed involve M-centered ($S_0 \rightarrow S_1$) electronic excitation, which is often followed by ionization to the M^+·S ion. The D_0 is measured by depositing a defined amount of vibrational energy in the neutral ground state, giving $M^{\neq}$·S, the neutral

*To whom correspondence should be addressed

[†]Departement für Chemie und Biochemie, Universität Bern, Freiestrasse 3, CH-3012 Bern, Switzerland

[‡]Institute of Physical Chemistry, Karlsruhe Institute of Technology (KIT), Fritz-Haber-Weg 2, D-76131 Karlsruhe, Germany

S_1 excited state, giving $M^*{\cdot}S$, or the $M^+{\cdot}S$ ion ground state. The experimental methods and their relative advantages and disadvantages are discussed. Based on the electronic structure of M and S, we classify the M·S complexes as type I, II or III, and discuss characteristic properties of their respective potential-energy surfaces that affect or hinder the determination of D_0. Current theoretical approaches are reviewed, which comprise methods based on a Kohn–Sham reference determinant as well as wave function-based methods based on coupled-cluster theory.

Contents

1 Introduction **8**

2 Excitation and Ionization of M·S Complexes: A Classification **11**

2.1 Type I Complexes 12

2.2 Type II Complexes 12

2.3 Type III Complexes 14

3 Experimental Techniques for the Determination of Dissociation Energies of Dispersion-dominated Dimers **15**

3.1 Dispersed Fluorescence Methods (DIS) 15

3.2 Two-color Appearance Energies and Ion Breakdown Measurements 16

3.3 MATI-based Dissociation Energy Measurements of M·S Ions 17

3.4 Velocity Map Imaging (VMI) 18

3.5 Stimulated Emission Pumping/Resonant Two-photon Ionization (SEP-R2PI) 19

4 Quantum Chemical Challenges for Calculating Dispersive Interactions **21**

4.1 Coupled-cluster Theory for Large Systems 22

4.2 Explicitly-correlated Coupled-cluster Theory 24

4.3 Multilevel Schemes 25

4.4 MP2 Complete Basis-set Limit 26

4.5 Spin-component-scaled Methods 28

4.6 Symmetry-adapted Perturbation Theory (SAPT) 29

4.7 Dispersion-corrected Density-functional Theory 30

4.8 Random-phase Approximation (RPA) 30

4.9 Quantum Monte Carlo and Semiempirical Methods 32

4.10 Excited States (S_1) of Weakly Interacting Complexes 32

4.11 Zero-point Vibrational Energy 33

5 Examples of Binding and Dissociation Energies of Dispersively Bound Complexes 34

5.1 Type I Complexes: Two Systems with Localized HOMOs. 34

5.1.1 Ar_2, Kr_2, Xe_2, $(N_2)_2$ and $(CO)_2$ 34

5.1.2 $(H_2O)_2$, $(D_2O)_2$, $H_2O{\cdot}HCl$ and $(NH_3)_2$ 35

5.2 Type II Complexes: A System with Delocalized HOMO and a System with a Localized HOMO 36

5.2.1 Benzene·Argon 36

5.2.2 Complexes with Carbazole 38

5.3 Type III Complexes: Two Systems with Delocalized HOMOs 39

5.3.1 Benzene Dimer 39

5.3.2 Toluene Dimer 42

5.3.3 Indole·Benzene 43

5.3.4 Complexes with Anisole 45

6 Summary and Outlook 46

Biographies

Jann Frey was born in Bern, Switzerland, in 1977. He studied chemistry at the University of Bern where he received his diploma in 2001 and his Ph. D. in 2006. He worked as a postdoctoral researcher in the groups of Prof. John. P. Simons (Univ. of Oxford, 2007) and Prof. Peter Chen (ETH Zürich,2008-2010). He currently teaches chemistry at Gymnasium Liestal and spent a research sabbatical (2014-2015) in the Leutwyler research group. His research interests are in the field of weakly bound complexes.

Christof Holzer was born in Graz, Austria, in 1989. He studied chemistry at the Graz University of Technology (2009-2015). He received his MSc. in 2015 from the Graz University of Technology under the supervision of Nadia Mösch-Zanetti. In 2015 he joined the research group of Wim

Klopper at the Karlsruhe Institute of Technology. His research interests include the development of new (explicitly correlated) methods to improve the description of weakly bonded systems.

Wim Klopper was born in Opperdoes, The Netherlands, in 1961. He studied chemistry at the University of Leiden (1979–1982) and at the Ruhr-Universität Bochum (1982–1985), where he received his Ph.D. in 1989 under the supervision of Werner Kutzelnigg. He was post-doctoral research associate in the groups of Jan Almlöf (University of Minnesota, 1991) and Hans Peter Lüthi (ETH Zurich, 1993–1996) and he spent three years (1996–1999) at the University of Oslo as Førsteamanuensis (Associate Professor) and three years (1999–2002) at the University of Utrecht as Akademie Onderzoeker of the Royal Netherlands Academy of Arts and Sciences (KNAW). In September 2002, he accepted the position of Professor of Theoretical Chemistry at the Universität Karlsruhe (TH) and in 2003 he became Group Leader at the Institute of Nanotechnology at the Forschungszentrum Karlsruhe (since 2009, the Universität Karlsruhe (TH) and the Forschungszentrum Karlsruhe have merged into the Karlsruhe Institute of Technology). Wim Klopper has received the Venia Legendi for Theoretical Chemistry (ETH Zurich, 1998), the Hans G. A. Hellmann Prize of the Arbeitsgemeinschaft Theoretische Chemie (1999), and the Medal of the International Academy of Quantum Molecular Science (1999). He became Member of the International Academy of Quantum Molecular Science in 2011. His research interests include the further development of explicitly correlated electronic structure methods and the accurate computation of molecular energies as well as properties.

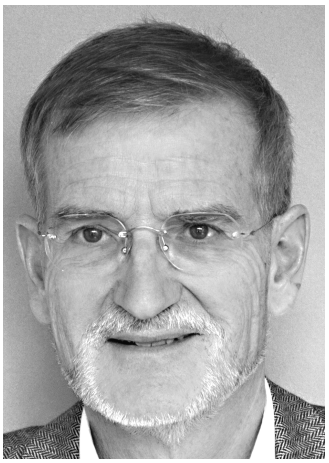

Samuel Leutwyler was born in Switzerland in 1952. He studied chemistry at the University of Bern and received his Ph.D. in 1979 under the supervision of Ernst Schumacher. He was post-doctoral research associate in the research group of Uzi Even and Joshua Jortner (Tel-Aviv University, 1979-1980). He spent four years (1980–1984) at the University of Basel in the groups of J. P. Maier and E. Heilbronner, obtaining a venia legendi (Habilitation) in Physical Chemistry in 1984. He then moved to the University of Bern, where he is Professor of Physical Chemistry since 1990. He was awarded the Nernst-Haber-Bodenstein-Preis of the Deutsche Bunsen-Gesellschaft (1986), the Ruzicka-Preis für Chemie (1989) of the Eidg. Technische Hochschulen (ETH Schulrat) and the Robert-Bunsen Vorlesung of the Deutsche Bunsengesellschaft (2015). His research interests include UV and IR molecular-beam laser spectroscopy of nucleic acid base pair analogues and of van der Waals and H-bonded complexes and clusters, photoinduced proton and hydrogen atom transfer in clusters and high-resolution ultrafast rotational coherence spectroscopy.

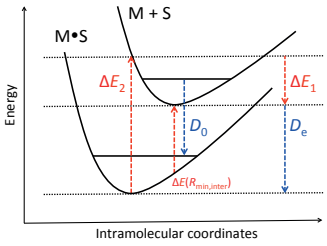

Figure 1: TOC Figure

1 Introduction

Noncovalent interactions between molecules are pivotal for all chemical and biochemical processes, because the mutual approach of two neutral molecules at distances significantly larger than ≈ 4 Å is driven by intermolecular interactions that extend over medium- to long-range intermolecular distances. Noncovalent interactions are at the heart of molecular recognition,[1] and important areas of research like supramolecular chemistry, crystal engineering, biochemical signal transduction or selective catalysis are governed by such processes. A quantitative understanding of intermolecular interactions therefore serves as a basis for the understanding of these complex fields.

The ground state dissociation energy D_0 and well depth D_e are among the most important parameters characterizing intermolecular interactions and the associated intermolecular potential energy surfaces (PESs). However, even today, accurate experimental gas-phase dissociation energies are only known for a very limited number of dispersively bound molecular dimers and hetero-dimers of chemical interest.[2]

Already in 1930, London identified three types of intermolecular interactions:[3] (1) *Electrostatic* interactions between two dipolar (or in general multipolar) molecules. (2) *Inductive* interactions that arise when a dipolar (or quadrupolar) molecule induces a dipole or quadrupole moment in a nearby molecule. Since the induced moments are always oriented in such a way as to give a stabilizing interaction with the inducing molecule, inductive interactions are always binding. (3) The *dispersive* interaction, which – in a semi-classical picture – arises from very rapid *temporal fluctuations* of the electrons in the charge distribution around a closed-shell atom or molecule *A* that induce dipolar (or higher multipolar) charge motions in a neighboring atom or molecule *B*, and vice versa from *B* on *A*.

Non-covalently bonded systems are usually classified according to the dominating attractive interactions in their minimum-energy region into *hydrogen-bonded* (H-bonded) and *dispersion-bonded* (or *van der Waals*) (vdW) complexes. However, not all intermolecular complexes are covered by this classification (such as $NH_3 \cdots Cl_2$), and demarcations between these groups are not always

sharp. H-bonded complexes are dominated by electrostatic interactions between well-defined H-donor and acceptor atoms. The potential minima are well defined with steep walls that are typically separated by high interconversion barriers. In contrast, the potential minima of dispersion-bonded complexes are shallower and less well separated, so experiments often need to consider a number of isomers, and theory needs to characterize not only multiple minima but also the barriers between them, as well as the zero-point vibrational energy (ZPVE) of the intermolecular vibrations. The ZPVE can be larger than the barriers between the minima, leading to large-amplitude zero-point motions. Second, for H-bonded complexes the electrostatic contribution to the interaction energy usually converges with affordable computational efforts (*i.e.*, MP2 at the complete basis set limit), while the dispersion terms require higher order (*e.g.*, CCSD(T)) calculations. Any uncertainties introduced by approximative treatments of the dispersive contribution — be it by corrected density functionals (DFT-D) or by adding Δ(CCSD(T)–MP2) correction values evaluated in small basis sets — only affect a fraction of the total interaction energy of H-bonded systems, but a major part in dispersion-bonded complexes. Third, the dissociation energy of dispersion-bonded complexes is typically smaller than that of hydrogen-bonded dimers.

The research on non-covalently bonded gas-phase complexes has been summarized in several reviews. Most reviews have focused on H-bonded systems.[4–7] Exceptions are the reviews of Topp (1993), who reports on structures and vibrational predissociation dynamics of complexes of small molecules with chromophores such as perylene or 2,5-diphenylfuran determined by fluorescence spectroscopy,[8] and Kendler and Haas (1997),[9] discussing the binding energies of vdW complexes with Ar. In 2015, Hobza and co-workers published a thorough comparison study between theoretical and experimental dissociation energies of 11 hydrogen bonded and 11 dispersive bonded complexes, finding an average agreement of 6%.[10]

Below, we review experimental and theoretical approaches to determining the dissociation energies of dispersion-bonded M·S complexes that consist of an aromatic chromophore, denoted M, and a ”solvent” atom or molecule, denoted S. When comparing calculated and experimental interactions, it is important to note the (subtle) differences between various definitions of the energies. These

definitions are illustrated in Figure 2 and the particular energies are the following:

(1) The intermolecular *interaction* energy $\Delta E(R_{\mathrm{min,inter+intra}})$, which corresponds to the energy difference between the fully optimized complex (or dimer) and the M and S monomers in the structures that they adopt *in the complex*. This energy contribution is also referred to as *two-body energy* ΔE_2. This energy does not include the *deformation energy* ΔE_{def} of the monomers, which comprises the energy differences between the monomers in their isolated, relaxed geometries and their structures in the dimer. The latter contribution is necessarily positive and is also denoted the *one-body energy* ΔE_1. Furthermore, the interaction energy does not take into account the ZPVE of the complex, nor the changes of the monomer ZPVEs upon dimerization. Although the interaction energy is not experimentally accessible, it is valuable, since it is a direct measure of the stabilization arising from the interaction of the M and S wave functions. A further decomposition of the interaction energy into electrostatic, dispersive, inductive and repulsive exchange interactions can be performed by symmetry-adapted perturbation-theory (SAPT). Here the M·S geometry is first fully optimized using a long-range corrected DFT method or correlated quantum-chemical method. The SAPT interaction energy ΔE_{SAPT} and its contributions are calculated at this geometry using a high-quality perturbation-theoretical method. Note that ΔE_{SAPT} needs to be corrected by the monomer deformation energies and the ZPVE of the complex and monomers in order to be comparable with experiment.

(2) The intermolecular electronic *binding* energy $D_e(R_{\mathrm{min,inter+intra}})$, which is evaluated relative to the energies of M and S in their optimized *monomer* structures, $D_e = -\Delta E_1 - \Delta E_2$. Note that $D_e(R_{\mathrm{min,inter+intra}})$ is smaller in magnitude than $\Delta E(R_{\mathrm{min,inter+intra}})$ since it contains the (always positive) deformation energy E_{def}. For weakly bound dimers, the deformation of M and S may be negligible, leading to deformation energies < 0.5 kJ/mol, but E_{def} increases for larger D_e values. For example, E_{def} values of more than 10% of D_e have been reported for H-bonded nucleobase dimers.[11] Because $D_e(R_{\mathrm{min,inter+intra}})$ does not contain any ZPVE contributions, it usually overestimates the intermolecular interaction strength (cf. Figure 2) and is also not directly measurable. However, it corresponds to the minimum of the $3N-6$-dimensional PES of the complex.

(3) The intermolecular *dissociation* energy $D_0(R_{\mathrm{min,inter+intra}})$. Here the vibrational zero-point energies of all the intramolecular and intermolecular vibrations of the complex, $\mathrm{ZPVE_{tot}}(R_{\mathrm{min,inter+intra}})$, as well as the ZPVE of M and S need to be calculated separately at the respective geometries $R_{\mathrm{min,inter+intra}}$, $R_{\mathrm{min,M}}$ and $R_{\mathrm{min,S}}$. The zero-point energy change $\Delta\mathrm{ZPVE} = \mathrm{ZPVE_{tot}} - \mathrm{ZPVE_M} - \mathrm{ZPVE_S}$ is subtracted from D_e to give the dissociation energy D_0 of the complex. In our view, this is the theoretical quantity that should be compared to experimental D_0 values. Note that the ZPVE of M·S contains the intermolecular ZPVE of the six intermolecular vibrational coordinates plus the *change* of the intramolecular $3N_{\mathrm{M}} - 6$ and $3N_{\mathrm{S}} - 6$ ZPVEs of the M and S moieties. The latter are often a large (and unrecognized!) contribution to ΔZPVE, and may outweigh the intermolecular ZPVE contribution. The change of intramolecular ZPVE is especially important in H-bonded complexes, because the ZPVE of the X-H bond is large and in most cases reduced by H-bond formation.

(4) The *fixed-fragments interaction* energy $\Delta E(R_{\mathrm{min,inter}})$ for a complex or dimer that is geometry-optimized with respect to its intermolecular but *not* its intramolecular coordinates. This amounts to the hypothetical interaction energy between two *non-deformed* monomers in their respective monomer geometries. $\Delta E(R_{\mathrm{min,inter}})$ is mostly evaluated for the construction of intermolecular potential energy surfaces. Even for small molecules, the large number of points needed to accurately probe the full six-dimensional intermolecular fixed-fragments interaction-energy surface precludes a geometry relaxation of the complex at every point.

2 Excitation and Ionization of M·S Complexes: A Classification

It is useful to divide M·S complexes into the following three types, which depend on the electronic structure of M and S:

2.1 Type I Complexes

Neither M nor S possesses delocalized π-electrons. While this property excludes aromatic systems – the focus group of this review – we include Type I complexes because the same experimental techniques can be employed for the determination of their dissociation energies as for Type II and III complexes discussed below. Some of the methodological advantages and drawbacks are better documented for Type I complexes than for the other two groups.

Assuming that the adiabatic ionization energy (AIE) of M is lower than that of S, ionization typically occurs by removal of an electron from a non-bonding *n*-orbital (*e.g.*, n_N, n_O, n_S) HOMO of M, leaving a localized "hole" on the heteroatom. This leads to large geometry changes between M·S and M^+·S. In terms of vibronic spectroscopy, the Franck-Condon factors (squares of vibrational overlap integrals) between the neutral and ionic ground states become very small. Experimental schemes for determining D_0 that rely on thermochemical cycles involving ionization and the ion ground state D_0^+, see Figure 3, can therefore be problematic. They are not recommended for type-I and III complexes (see below).

2.2 Type II Complexes

Only M has delocalized π-electrons. The lowest excited singlet state S_1, denoted M^*, is usually a $^1\pi\pi^*$ excitation that lies in the visible or near-UV region. Solvent molecules S whose frontier orbitals are σ- or non-bonding orbitals have high-lying (far-UV) electronic excitations corresponding to $\sigma \rightarrow \sigma^*$, $n \rightarrow \sigma^*$ or Rydberg excitations. For this reason, many common solvents S are transparent down to ≈ 200 nm. In this case, the $S_0 \rightarrow S_1$ excitation of M·S (M^*·S) remains M-centered, and since the π-electron system is delocalized, the electron density change at each atom is quite small. Therefore, the M·S geometry, vibrational frequencies and dissociation energy undergo small changes upon $^1\pi\pi^*$ excitation, as is schematically shown in Figure 4. With regard to ionization, the electron is mainly removed from the π-HOMO of M if the AIE of M is lower than that of S, and analogous considerations apply for the M^+·S ion ground state. In general, the electronic excitation energies change only moderately when an aromatic M is complexed with a non-aromatic closed-

shell S molecule. The small geometry changes ensure good overlaps between the initial and final vibronic wave functions (*i.e.*, large Franck-Condon factors) in excitation. This opens the door to the investigation of the properties of M·S and M^*·S using the toolbox of visible/UV tunable laser experiments that have been developed over the last forty years.

Care must however been taken when investigating the M^+·S state of such complexes when S is not a noble gas atom: upon ionization, the charge on M^+ leads to an additional charge-multipole interaction with S (if S is polar or quadrupolar) and in every case to charge-induced multipole interactions. These may lead to large geometry changes between the neutral and ion ground states. Well known examples are the neutral complexes whose geometries are dominated by X-H$\cdots\pi$ nonclassical hydrogen-bonding interactions, as in the M·HF, M·HCl, M·H_2O and M·methanol complexes. Upon ionization the charge on M^+ renders the X-H$\cdots\pi$ hydrogen bond repulsive, the positive H atom of the H-X bond is repelled and the stable ion ground state minimum has a completely different geometry. This creates several problems for the analysis: (1) The *vertical* ionization (*i.e.*, at the neutral ground-state geometry) is highly efficient, but this can lead to energies close to or above the dissociation energy D_0 of the $M^+ \cdot S$ ion ground state, leading to direct dissociation or vibrational predissociation (VP). (2) Even if vertical ionization leads to an energy below D_0, it may be difficult or impossible to experimentally access the ion ground state minimum (*i.e.*, the adiabatic ionization energy), so that the AIE(M·S) cannot be measured. (3) Due to the larger D_0 in the ion combined with the geometry change, the nascent M^+ and S fragments arising from the M^+·S dissociation may be vibrationally and rotationally hotter than those arising from dissociation on the ground-state surface. It also takes longer for the internal energy in the ion ground state to randomize before VP, giving rise to a wide distribution of time delays ($1 - 10,000$ ns) between the ionization of M·S and the instant of its decay.[12] The dissociation threshold can then only be obtained using unimolecular dissociation models for the kinetic energy release (KER). These involve extensive theoretical modeling and calculations and are subject to uncertainties that are not small and often hard to quantify.[12]

2.3 Type III Complexes

Both M and S have delocalized π-electron systems. This interaction type occurs in many dimers of chemical and biochemical interest (*e.g.*, π-stacked aromatics, DNA bases, charge-transfer complexes, etc.), which are therefore widely studied. Two common geometry types exist, denoted T-shaped and π-stacked (with variations such as slipped-stacked). Since the AIEs of M and S are closer together (or identical for self-dimers M_2) than for type II complexes, the ionization must be viewed as removal of electronic charge from the HOMOs of both M and S. The ion ground state involves stabilizing charge-resonance contributions of the type $M^+ \cdot S \leftrightarrow M \cdot S^+$, which are strongest for symmetric self-dimers $(M{\cdot}M)^+$.[13] Charge-resonance stabilization also remains important in *hetero*dimer ions. The most stable ionic geometry is typically a π-stacked structure which maximizes the charge-resonance interactions. If the neutral structure is T-shaped, the geometry changes completely upon ionization; if the neutral is π-stacked, the M·S interplanar distance contracts strongly upon ionization. In both cases the large differences between the neutral and ionic geometries result in small Franck-Condon factors in ionization. These considerations show that considerable problems arise when trying to determine the experimental dissociation energies of type I and III complexes using ionizative methods.

The review is organized as followed: In Section 3 we review and describe experimental techniques for determining ground state dissociation energies $D_0(S_0)$ of M·S van der Waals complexes. Section 4 summarizes the challenges of a quantum chemical calculation of dissociation energies. In Section 5 we present prominent examples of experimentally and theoretically assessed dissociation energies of vdW complexes.

3 Experimental Techniques for the Determination of Dissociation Energies of Dispersion-dominated Dimers

There has been work on the measurement of M·S dissociation energies, D_0(M·S), since the invention of supersonic-jet spectroscopy. This involves (1) producing the M·S complexes in the supersonic-jet expansion, (2) cooling them to their lowest ($v'' = 0$) vibrational level, and (3) performing different types of vibronic spectroscopic and/or photoionization measurements. One-step photoionization techniques typically involve a vacuum-ultraviolet (VUV) laser, a VUV lamp or a synchrotron light source (the latter two being monochromatized with a VUV monochromator), generating light in the 7 – 12 eV range. The two-step measurements typically involve two tunable UV lasers, where the first laser resonantly excites the M moiety of M·S and the second laser photoionizes the excited M*·S complex. By suitably combining vibronic or vibrational excitation frequencies and photoionization thresholds of M, S and M·S and applying thermochemical cycles, as shown in Figure 5, the dissociation energies D_0(M$^+$·S) and D_0(M·X) can be determined. Alternatively, vibrationally excited M·S complexes, denoted M$^{\neq}$·S, can be populated via infrared (IR) absorption, by stimulated Raman pumping or by vibronic pump-and-dump (stimulated-emission-pumping = SEP) techniques. These methods allow to directly determine D_0(M·X) without passing through the ion ground state.

3.1 Dispersed Fluorescence Methods (DIS)

This method was pioneered by Levy and co-workers in the early 1980s to determine the dissociation energies of I_2·X (X= Ne, Ar, Kr, Xe) vdW complexes.[14] A series of dispersed fluorescence spectra of the I_2·X complex are recorded while exciting the $\tilde{X} \rightarrow \tilde{B}$ electronic origin (0_0^0) band of the I_2 moiety to increasing vibrational quantum number v' of the $\tilde{B}$ excited state. If the energy of the $\tilde{B}; v'$ level exceeds the dissociation energy $D_0'(\tilde{B})$, the I_2^*·X complex undergoes excited state VP, i.e., I_2^*·X $\rightarrow$ I_2^* + X. If the VP rate exceeds the luminescence rate of the $\tilde{B}$ state, the emission from bare I_2^* is observed which can be spectrally discriminated from that of I_2^*·X. The lowest vibronic

level v' of $I_2^*{\cdot}X$ that predissociates to bare I_2^* provides an upper limit of D_0'. A corresponding upper limit to the ground-state dissociation energy D_0'' is obtained from D_0' from the spectral shift $\delta\nu = D_0' - D_0''$ of the 0_0^0 band origins of I_2 and of $I_2{\cdot}X$. A schematic illustration of the method is given in Figure 6.

This method has been extended to M·X complexes such as s-tetrazine·Ar, bracketing D_0 between $3.0 - 4.3$ kJ/mol).[15] An important limit to the DIS method is the existence of excited states above the dissociation limit with lifetimes larger than the experimental time-frame, as it has been observed for example for the benzene·argon complex.[16]

The method requires the emission of $M^*{\cdot}S$ to differ sufficiently from that of M^*, such that the two spectra can be unambiguously separated. Note that emission from the highly excited complex can be shifted to the same region as that of the monomer dissociation product, which can lead to dissociation being incorrectly deduced as having occurred.[17] For larger systems or for complexes with large dissociation energies, the spectra of both M^* and $M^*{\cdot}S$ become more complicated, which often leads to overlapping emission spectra. To overcome this limitation, a two-laser scheme has been introduced by Wittmeyer and Topp[18] in which the first laser vibronically excites the investigated complex. If enough energy for VP in the excited state is deposited into the complex, the formation of vibrationally excited $M^{\neq}$ ground state fragments is expected. These hot fragments are probed by a second laser which is tuned to a hot band and fired ≈ 100 ns after the excitation laser.[18]

3.2 Two-color Appearance Energies and Ion Breakdown Measurements

This technique involves pumping the $S_0 \rightarrow S_1$ 0_0^0 band of M·S, after which the photoionization efficiency (PIE) curve of the excited $M^*{\cdot}S$ state is recorded up to energies that are high enough for VP to occur in the $M^+{\cdot}S$ ion ground state. At the VP threshold the $M^+{\cdot}S$ ion signal disappears and the signal of the daughter M^+ ion appears; both ion signals are simultaneously monitored. A schematic illustration is given in Figure 7. Since ionization produces both $M^+{\cdot}S$ ions and photoelectrons and the energy carried away by the photoelectron is *not* measured in appearance energy measurements,

this unknown partition of energy between M^+, S and the electron leads to a considerable indeterminacy. In practice, the VP thresholds in both the $M^+ \cdot S$ and M^+ ion signals are often unclear, and both are extrapolated to the same VP threshold. Since 2007, Mikami and co-workers have applied this technique to determine the $D_0(M^+ \cdot S)$ of $CH \cdots \pi$ bonded complexes such as benzene·ethene, benzene·acetylene, benzene·CH_2Cl_2 and benzene·$CHCl_3$.[19–23]

To discern between stable and metastable $M^+ \cdot S$ ions, Neusser and co-workers have developed a method to determine the appearance energies of M^+ ions, using a reflectron time-of-flight mass spectrometer (RETOF).[24] The metastable ions that decay in the drift-region of the RETOF have a different kinetic energy than the stable ions. The voltages of the reflector are now adjusted in a way that the flight times of the ions are *not* corrected for the differences in kinetic energy. M^+ daughter ions produced by VP in the drift tube appear between the peaks of the stable ions. The appearance energy is determined from the breakdown of the metastable ion signals upon reducing the ionization energy. Breakdown measurements (BM) have been used to determine the dissociation energy of the benzene dimer[24] as well as the homo- and heterodimers of benzene, toluene and para-difluorobenzenes.[25]

3.3 MATI-based Dissociation Energy Measurements of M·S Ions

The mass-analyzed threshold ionization (MATI) method is a photoionization mass-spectrometric technique that allows to accurately measure the excess vibrational energy E_{exc} that is deposited in the ground state of a molecular ion M^+. This is done by tuning the photoionization light source (laser or VUV photon source) and simultaneously measuring the production of the photoions that are produced simultaneously to threshold (or zero-kinetic energy=ZEKE) photoelectrons. In the MATI technique only the ions are recorded. In a more evolved (but less sensitive) variant, the threshold photoelectrons and photoions are recorded in coincidence (TPEPICO). When measuring ions coincidentally with ZEKE photoelectrons, the vibrational energy E_{exc} of the $M^+ \cdot S$ ion is given by the photon energy minus the adiabatic ionization energy (AIE) of M, AIE(M), see Figure 5.

Neusser and coworkers pioneered an application of MATI for measuring the dissociation energy

$D_0(M^+{\cdot}S)$, by measuring (1) the AIE of M·S and (2) the dissociation threshold of the $M^+{\cdot}S$ ion ground state, $D_0(M^+{\cdot}S)$.[26–29]

The ionization frequency is increased, thereby depositing increasing vibrational energy in the M^+-centered vibrational ladder of the $M^+{\cdot}S$ ion. At (or closely above) the dissociation threshold of $M^+{\cdot}S$, the $M^+{\cdot}S \rightsquigarrow M^+ + S$ process leads to a breakoff of the $M^+{\cdot}S$ ion signal and — correlated with the breakoff — the appearance of the M^+ daughter ion signal; both mother and daughter ions are simultaneously monitored in the mass spectrometer. Since MATI selects for those ions that appear together with ZEKE (near-threshold) photoelectrons, the breakoff energy/appearance energy is much better defined than in the appearance energy measurements (Section 3.2).

Combining $D_0(M^+{\cdot}S)$ with the separately measured adiabatic ionization energies AIE(M^+) and AIE($M^+{\cdot}$ S) yields the dissociation energy D_0(M·S) via the thermochemical cycle shown in Figure 5.[6,26,27,30,31] Alternatively, the neutral D_0(M·S) can be determined by subtracting AIE(M) from AE(M^+), see also Figure 5.[32] Neusser and co-workers have also determined dissociation energies of hydrogen-bonded and π-hydrogen bonded complexes of aromatic molecules with an accuracy of $0.1 - 0.6$ kJ/mol.[6,29,33]

3.4 Velocity Map Imaging (VMI)

Since 2000, the groups of Lawrance[16,17,34,35] and Becucci[36] have applied the velocity map imaging (VMI) technique to determine the D_0 values of aromatic M·S complexes and self-dimers M_2. VMI is an enhanced resolution variant of ion imaging, for a detailed description, see ref. 16. The VMI technique is also discussed in Section 5.1.2 in the context of dissociation energy determination of H-bonded dimers (type I complexes).

The M·S dissociation energy is measured (a) in the S_1 state or (b) in the ion ground state. VMI schemes of both variants (a,b) are shown in Figure 8. In Figure 8(a), the M·S complex is excited into an S_1 state vibronic level that lies slightly above $D_0(S_1)$, leading to S_1 state vibrational predissociation $M^*{\cdot}S \rightarrow M^* + S$. The excited chromophore M^* is then ionized by a second laser. In case (b), the excitation laser pumps M·S into the $v' = 0$ level of S_1. The ionization laser is tuned to an

energy above D_0 of the $M^+ \cdot S$ ion ground state, leading to VP in the ion ground state, $M^+ \cdot S \rightarrow M^+ + S$. In both cases, the translational recoil energy of the M^+ fragment is recorded using VMI. The sharing of the translational recoil energy between the detected M^+ and non-detected S fragments is taken into account. However, the rotational energy deposited in the M and S fragments is not taken into account (for S = X = Ar, Kr there is no rotational energy). The maximum translational energy $E_{\text{trans}}(\text{max})$ measured by VMI is assumed to be the excess energy E_{excess} that is deposited into the complex by the dissociation laser. The dissociation energy of the investigated state corresponds to $D_0 = E_{\text{vib}} - E_{\text{trans}}(\text{max})$.[16] From the spectral shift of the $S_0 \rightarrow S_1$ 0_0^0 band (for a) or the AIE (for b) the ground-state dissociation energy $D_0(S_0)$ is obtained via thermochemical cycles. The Lawrance group has studied para-difluorobenzene (*p*-DFB) with solvents X = Ar, Kr and H_2O.[16,17,34,35] Becucci and co-workers have applied VMI to the anisole dimer.[36] $(\text{Anisole})_2$ is a type-III complex which is expected to undergo large geometry changes after $S_0 \rightarrow S_1$ excitation; indeed the D_0 measured by VMI[36] has recently been questioned and revised, based on calculations.[37] In ref. 37, the possible existence of a low-lying excited state of the dimer ion is discussed, which could act as a sink for the internal energy. The discrepancy between the D_0 values reported in refs. 36 and 37 might be related to the existence of different dissociation channels, where the favored channel does not produce the ion fragment in its ground state. As Tables 1 and 2 show, the VMI method has so far delivered very accurate dissociation energies, with errors in the range of 0.04 – 0.1 kJ/mol.

3.5 Stimulated Emission Pumping/Resonant Two-photon Ionization (SEP-R2PI)

Starting in 1994, the Leutwyler group developed the stimulated-emission pumping/resonant two-photon ionization (SEP-R2PI) method for measuring ground-state D_0 values of type II M·S complexes.[38–41] Similar to the ionization-based appearance potential, ion breakdown, MATI and VMI methods described in Sections 3.2 – 3.4, the method is based on the detection of the $M^+ \cdot S$ ion and is mass- (and isotope-) specific. In contrast to the other ionization-based methods, the SEP-R2PI method involves excitation of S_0 state vibrational levels followed by VP on the *ground-state*

potential-energy surface. This avoids the problems that arise from large geometry changes of M·S between the S_0 and lowest ion states.

The SEP-R2PI method involves vibronic pump and "dump" steps $S_0 \rightarrow S_1 \rightarrow S_0^{\neq}$ akin to stimulated-emission pumping (SEP),[42] which produces vibrationally excited ground-state $M^{\neq}$·S, followed by detection of either vibrationally excited $M^{\neq}$·S or the M fragment, using one-color resonant-two-photon ionization (1C-R2PI). The detection occurs after a time delay Δt that is long enough for $M^{\neq}$·S to undergo intramolecular vibrational redistribution and VP ($\Delta t = 0.1 - 10$ μs).[39–41] The pump, dump and probe steps are induced by three independently tunable UV lasers, as shown in Figure 4. Laser (1) pumps the jet-cooled M·S at the $S_0 \rightarrow S_1$ electronic origin; laser (1) also ionizes a small fraction of the excited molecules, see Figure 3, providing a convenient monitor signal. Laser (2) stimulates "dump" transitions from the $S_1; v' = 0$ state back down to a vibrationally excited $v'' > 0$ level of the S_0 state. Because of the high density of the M-S intermolecular vibrations, rapid coupling among the vibrations ensues, leading to intramolecular vibrational energy redistribution (IVR, wiggly arrows in Figure 4). If laser (2) dumps population into vibrational levels lying above $D_0(S_0)$, see arrow (2') in Figure 4, the metastable $M^{\neq}$·S complex undergoes VP. After a delay of up to 10 μs, which allows VP to go to completion, the presence or absence of vibrationally excited $S_0^{\neq}$ state complexes is probed by laser (3).

In *origin-probed* dump spectroscopy, both the pump laser (1) and probe laser (3') are tuned to the 0_0^0 band of the M·S complex. Scanning the dump frequency (2) yields a signal *decrease* at every resonant dump transition to the S_0 state, irrespective of whether the ground-state vibrational level is above or below $D_0(S_0)$. (*ii*) In *hot-band probed* dump spectroscopy the probe laser (3) is tuned away from the 0_0^0 band to hot-band or sequence-band regions, thereby only probing vibrationally hot levels. A signal *increase* occurs at every resonant dump transition to the S_0 state, until vibrational levels v'' are reached that lie above $D_0(S_0)$; at this energy the M·S complex vibrationally predissociates and no more bands are observed.

$D_0(S_0)$ is thereby bracketed between the highest vibrational level observed in the hot-band-probed dump spectrum (lower limit of D_0) and the lowest-frequency vibration that appears in the origin-

probed but not in the hot-band-probed dump spectrum (upper limit of D_0). When taking into account the frequency shift $\delta\tilde{\nu}$ of the $S_0 \rightarrow S_1$ origin of M·S relative to that of M, the $D_0(S_1)$ is obtained from $D_0(S_1) = D_0(S_0) - \delta\tilde{\nu}$.[38–41,43]

The SEP-R2PI method has been applied to dispersively bound M·S complexes,[39,43] to complexes involving nonclassical OH$\cdots\pi$ hydrogen bonds, to aromatic and aliphatic acceptors,[41,44] and to classically H-bonded complexes.[40,41] The dissociation energies $D_0(S_0)$ of 10 complexes have been determined with a relative accuracy of $\approx 1\%$,[38–41,43,44] and are given in Table 3.

4 Quantum Chemical Challenges for Calculating Dispersive Interactions

In the current issue of this journal on noncovalent interactions, a number of articles provide reviews of quantum chemical methods, computations, and benchmarks. Examples of earlier reviews are found in Refs. 45 and 46. In the present chapter, we will briefly discuss and illustrate some of the methods currently in use, thereby putting emphasis on how these methods could advantageously employ explicitly-correlated wave functions (Slater-type geminals, F12 methods). Such geminal wave functions can not only be employed in coupled-cluster theory but, for example, also within the framework of density-functional theory (DFT) in conjunction with the random-phase approximation, in dispersion-corrected double-hybrid DFT, in spin-component-scaled (SCS) methods, or in symmetry-adapted perturbation theory (SAPT), as we will see below.

We will focus our discussion on noncovalent interactions between molecules in *closed-shell singlet ground states*. Many of the methods discussed in this chapter can be applied to open-shell systems as well, but concerning the corresponding computational challenges, we refer to the recent work by Bozkaya and co-workers[47,48] on orbital-optimized perturbation theory. See also Refs. 49 and 50. Approaches to dimers in excited states (excimers) will be briefly mentioned, but explicitly-correlated wave functions are not yet being widely employed for calculations on excited states (for

example in the framework of explicitly-correlated linear-response coupled-cluster theory).[51–54] We will be very short on semiempirical and quantum Monte Carlo methods, because these methods are being comprehensively reviewed elsewhere in this issue. Finally, we note that it is possible to distinguish between methods that are true first-principles methods — the results of which can be improved in a systematic manner — and between methods that are more empirical in nature, that is, which contain fitted parameters (*e.g.*, in functionals of DFT, in dispersion corrections, or in form of scaling factors). Coupled-cluster methods certainly belong to the first category while for example spin-component-scaled and DFT-based methods belong to the second category. Since the computational demands of the two categories are often very different, it may be advantageous to apply a combination of methods, for example by using a more empirical method for computations of a global PES and high-level coupled-cluster computations at selected points on that surface.

4.1 Coupled-cluster Theory for Large Systems

Today, highly accurate computations of the bond energies of dispersion-dominated systems are possible using approaches based on coupled-cluster theory, for example the coupled-cluster approach with iterative single and double substitutions (CCSD) augmented with noniterative, perturbative triple substitutions, that is CCSD(T),[55–57] or its variant known as quadratic configuration interaction with singles, doubles, and noniterative triples, QCISD(T).[55,57] With respect to computational details of these methods, we refer to the recent short reviews presented in Refs. 58 and 59, respectively. The CCSD(T) method — or alternatively, QCISD(T) — is known as the "gold standard" for work on weakly bound, dispersion-dominated systems such as the benzene dimer and related systems. Such systems are small enough to allow for large basis sets such as the augmented correlation-consistent polarized valence triple-zeta basis (aug-cc-pVTZ)[60,61] or larger.

The CCSD(T) approach can be applied to much larger (than the benzene dimer) hydrogen-bonded and dispersion-dominated vdW complexes by means of composite and fragment-based methods. For a recent review on such methods (of which there are numerous), see Ref. 62. Fragments can be individual molecules (monomers) or parts thereof (*e.g.*, localized orbitals), and computations

are performed on the individual fragments, on pairs of fragments, on triples of fragments, and so forth. Examples are the incremental scheme of Stoll,[63–66] the cluster-in-molecule (CIM) approach of Li,[67–69] the fragment molecular orbital (FMO) method of Kitaura,[70–73] and the divide–expand–consolidate (DEC) coupled-cluster method.[74–76] Furthermore, fragment-based methods can be combined with embedding techniques to yield embedded many-body expansions.[77–79] In 2007, Friedrich, Hanrath, and Dolg reported a fully automated implementation of the incremental scheme,[80] which has since then been developed further to include *explicitly-correlated* coupled-cluster computations.[81–83]

In 1983, the "*localizability of dynamic electron correlation*" was recognized by Pulay and exploited by means of using *localized* occupied Hartree–Fock orbitals in conjunction with a local virtual space that consists of atomic orbitals projected against the occupied space and each other.[84] This has led to the development of *local coupled-cluster* (LCC) methods,[85–89] which can be applied to very large systems such as vdW complexes with large chromophores. LCC methods rely on *pair* and *domain* approximations, and in particular the pair approximation has recently received attention with respect to its application to long-range intermolecular interactions.[90–92] The pair approximation depends on the distance between localized occupied orbitals, and for weak intermolecular interactions, it is crucial to compute the more distant pairs (also) accurately.[90–92] LCC methods have been improved by introducing pair (or pseudo) natural orbitals (PNO) in conjunction with domain approximations.[93–98] Some recent applications to large systems, including the S66 test set,[99,100] can be found in Refs. 101, 102, and 103. Also various explicitly-correlated variants of (PNO-based) local correlation methods have been implemented.[101,104–108] In view of the progress made in recent years, one is tempted to conclude that basically from today on, explicitly-correlated — that is, near complete-basis-set limit — CCSD(T) calculations can be performed with computational effort (computation time and other computer resources) that scales linearly with the size of the molecular system. This would render more approximate and much less accurate approaches redundant, except perhaps for optimizing the required equilibrium structures as long as analytical nuclear gradients have not yet been implemented for the (explicitly-correlated)

PNO-based LCC methods.

4.2 Explicitly-correlated Coupled-cluster Theory

Explicitly-correlated coupled-cluster methods can not only be applied in a standard manner (*i.e*, with canonical Hartree–Fock orbitals) to rather small complexes such as the Li·benzene complex,[109] but also to systems with ca. 20 atoms (with PNO-based local or incremental methods, the systems can of course be much larger). For example, in very recent work focusing on N-H$\cdots\pi$ interactions, CCSD(T)/aug-cc-pVTZ computations were performed for the imidazole·benzene (ImBz) and pyrrole·benzene (PyBz) complexes, see Figure 9.[110]

In this work, the CCSD computations were performed in the large aug-cc-pVQZ basis (augmented correlation-consistent polarized valence quadruple-zeta)[60,61] in conjunction with explicitly-correlated double excitations in the "(F12)" approximation[111] (see Refs. 112, 113 and 114 for recent, comprehensive reviews of explicitly-correlated F12 wave functions with Slater-type geminals). This level of theory is known as the CCSD(F12)/aug-cc-pVQZ approach, and corrections for noniterative, perturbative triple substitions were computed in the aug-cc-pVTZ basis. Following Ref. 115, the latter were corrected for basis-set incompleteness by scaling the triples energy $E_{(\mathrm{T})}$ by the factor $x = E^{\mathrm{corr}}_{\mathrm{MP2\text{-}F12}}/E^{\mathrm{corr}}_{\mathrm{MP2}}$, where $E^{\mathrm{corr}}_{\mathrm{MP2\text{-}F12}}$ is the explicitly-correlated second-order Møller–Plesset correlation energy and $E^{\mathrm{corr}}_{\mathrm{MP2}}$ its conventional counterpart. Hence, the overall level of theory applied in Ref. 110 was

$$E_{\mathrm{CCSD(F12)+(T^*)}} = E_{\mathrm{CCSD(F12)/aug\text{-}cc\text{-}pVQZ}} + E_{\mathrm{(T^*)/aug\text{-}cc\text{-}pVTZ}}, \tag{1}$$

with

$$E_{\mathrm{(T^*)/aug\text{-}cc\text{-}pVTZ}} = x E_{\mathrm{(T)/aug\text{-}cc\text{-}pVTZ}}; \quad x = E^{\mathrm{corr}}_{\mathrm{MP2\text{-}F12/aug\text{-}cc\text{-}pVQZ}}/E^{\mathrm{corr}}_{\mathrm{MP2/aug\text{-}cc\text{-}pVTZ}}\,. \tag{2}$$

At this level of theory, the intermolecular electronic binding energies were determined to be $D_e =$ 22.7 and 20.4 kJ/mol for imidazole·benzene and pyrrole·benzene, respectively, with an estimated

uncertainty of at most a few tenths of a kJ/mol (sometimes denoted as "subchemical accuracy"). Concerning equilibrium structures, the intermolecular distances R of the two complexes were optimized at the level given in Eq. (1). Computations of a scan in terms of one single intermolecular coordinate are possible today without too much computational effort, even including counterpoise corrections,[116,117] but it is less straightforward to compute a counterpoise-corrected intermolecular PES at this high level of theory. Furthermore, large parts of the low-lying PES of a given dimer are required to relate the computed D_e value to the experimentally determined dissociation energy D_0.

4.3 Multilevel Schemes

In attempts to alleviate the restrictions due to the very high computational costs of CCSD(T) computations on large systems, it has become common practice for computational studies of weak intermolecular interactions to approach the *ab initio* limit of a complete basis set (CBS) using a *multilevel scheme*. For example, the CBS limit of the CCSD(T) level may be approached by adding a second-order correction for the basis-set incompleteness error,

$$E_{\mathrm{CCSD(T)/CBS}} \approx E_{\mathrm{CCSD(T)/small\ basis}} + \Delta E_{\mathrm{MP2/CBS}}, \tag{3}$$

$$\Delta E_{\mathrm{MP2/CBS}} = E_{\mathrm{MP2/CBS}} - E_{\mathrm{MP2/small\ basis}}. \tag{4}$$

Note that, fully equivalently, Eq. (3) can also be written as

$$E_{\mathrm{CCSD(T)/CBS}} \approx E_{\mathrm{MP2/CBS}} + \Delta E_{\mathrm{CCSD(T)/small\ basis}}, \tag{5}$$

$$\Delta E_{\mathrm{CCSD(T)/small\ basis}} = E_{\mathrm{CCSD(T)/small\ basis}} - E_{\mathrm{MP2/small\ basis}}. \tag{6}$$

Ref. 118 provides an example of an application of the multilevel scheme, in which the MP2 CBS limit (obtained from explicitly-correlated R12 theory), the CCSD correlation energy, and the (T) triples correction were computed in different basis sets. Recently, Pitoňák and co-workers[119] have proposed a variant of Eqs. (4) and (5), denoted MP2.5, in which third-order Møller–Plesset

perturbation theory is applied in place of CCSD(T) theory, and in which the higher-order ΔE contribution is scaled with a factor 1/2,

$$E_{\text{MP2.5/CBS}} \approx E_{\text{MP2/CBS}} + \tfrac{1}{2}(E_{\text{MP3/small basis}} - E_{\text{MP2/small basis}}). \quad (7)$$

This MP2.5 approach has proven to be quite successful, taking advantage of the error cancelation between the MP2 (overestimation) and MP3 (underestimation) binding energies of dispersion-dominated weakly interacting systems. Alternatively, the overestimation of MP2 theory and thus of the MP2/CBS limit can be corrected by means of an *interference correction*, which consists of applying individual scaling factors $0 \leq c_{ij} \leq 1$ to the pair energies $e^{(ij)}$ of the localized, occupied orbitals i and j,

$$E_{\text{CCSD(T)/CBS}} \approx E_{\text{CCSD(T)/small basis}} + \Delta E_{\text{MP2+INT/CBS}}, \quad (8)$$

$$\Delta E_{\text{MP2+INT/CBS}} = \tfrac{1}{2}\sum_{ij} c_{ij}\left[e^{(ij)}_{\text{MP2-CBS}} - e^{(ij)}_{\text{MP2/small basis}}\right]. \quad (9)$$

Recently,[120] this interference-corrected perturbation theory has been assessed with respect to the S22B database.[121,122] It was also applied recently in Ref. 110 and in computations on noncovalent interactions of carbon dioxide with functional groups of metal-organic frameworks.[123] Promising results were obtained, but a disadvantage of the interference-corrected approach is that it is not invariant with respect to rotations among the occupied orbitals (*i.e.*, localized Hartree–Fock orbitals were used for that reason).

4.4 MP2 Complete Basis-set Limit

Often, the CBS limit at the MP2 level is obtained from MP2 computations in large (augmented) correlation-consistent basis sets followed by extrapolations to the basis set limit. In this respect, the most accurate procedure is to extrapolate individually the Hartree–Fock total energy on the one

hand and the MP2 correlation energy on the other, as recommended in Refs. 124 and 125,

$$E_{\mathrm{HF}/X} \approx E_{\mathrm{HF/CBS}} + A\exp(-aX), \tag{10}$$

$$E^{\mathrm{corr}}_{\mathrm{MP2}/X} \approx E^{\mathrm{corr}}_{\mathrm{MP2/CBS}} + BX^{-3}. \tag{11}$$

Here, X is the cardinal number of the (augmented) correlation-consistent basis set. Alternatively, the MP2/CBS limit may be approached by applying the explicitly-correlated MP2 method in a (large) aug-cc-pVXZ basis,

$$E_{\mathrm{MP2/CBS}} \approx E_{\mathrm{HF}/X} + E^{\mathrm{corr}}_{\mathrm{MP2\text{-}F12}/X} + E_{\mathrm{CABS\ singles}}. \tag{12}$$

Here, $E^{\mathrm{corr}}_{\mathrm{MP2\text{-}F12}/X}$ approximates the CBS limit of the MP2 correlation energy while the term $E_{\mathrm{CABS\ singles}}$ corrects for the basis set incompleteness error in the Hartree–Fock total energy. This correction is computed from single excitations into the complementary auxiliary basis set (CABS) that is used in the explicitly-correlated methods for the resolution-of-the-identity approximation in the evaluation of many-electron integrals. An example of the use of Eq. (12) is provided by the seminal work of Sinnokrot *et al.*[126] on the benzene dimer (in which, however, the energy contribution $E_{\mathrm{CABS\ singles}}$ was not needed and hence not computed, because a very large, optimized basis set of Hartree–Fock-limit quality was used for the MP2-F12 calculations). Furthermore, when using different basis sets for the MP2-F12 calculations, a Schwenke-type extrapolation can be applied to the F12 values obtained in a series of basis sets.[127]

By means of using Eq. (3), large weakly interacting complexes can be treated. In Ref. 128, for example, an octadecane dimer, a stacked guanine trimer, a stacked circumcoronene·adenine dimer, a stacked circumcoronene·GC dimer (GC = hydrogen-bonded guanine·cytosine Watson–Crick pair), a parallel-displaced stacked coronene dimer, two GC pairs arranged as in DNA, and a trimer of phenylalanine were studied at this level.

Besides extensively long computation times and large storage requirements, an additional problem occurs when trying to approach the MP2 CBS limit using aug-cc-pVXZ basis sets: numerical in-

stabilities occur caused by (almost) linear dependent basis functions. In Ref. 128, this problem was avoided by using plain cc-pVXZ basis set for the extrapolation in conjunction with an empirical scaling factor to account for the difference between the aug-cc-pVXZ and cc-pVXZ sets. Also the "seasonal plantings" of diffuse functions as proposed by Papajak and co-workers[129] may help to circumvent the numerical instabilities.

4.5 Spin-component-scaled Methods

Grimme's spin-component-scaled electron-correlation methods,[130] for example SCS-MP2, are widely used in computational studies of dispersion-dominated weakly interacting complexes. These are based on the insight that low-order wave function expansions treat the correlation effects of electron pairs with opposite spin (OS) and same spin (SS) differently. In these methods, the pair energies of orbital pairs with OS and SS are scaled with individual factors c_{OS} and c_{SS}, respectively,

$$E_{\mathrm{SCS}}^{\mathrm{corr}} = c_{\mathrm{OS}} E_{\mathrm{OS}}^{\mathrm{corr}} + c_{\mathrm{SS}} E_{\mathrm{SS}}^{\mathrm{corr}}, \tag{13}$$

$$E_{\mathrm{OS}}^{\mathrm{corr}} = \sum_{i\bar{j}} e^{(i\bar{j})}; \quad E_{\mathrm{SS}}^{\mathrm{corr}} = \tfrac{1}{2}\sum_{ij} e^{(ij)} + \tfrac{1}{2}\sum_{\bar{i}\bar{j}} e^{(\bar{i}\bar{j})}. \tag{14}$$

Here, i refers to an α spin orbital, and $\bar{i}$ to a β spin orbital. Table 1 of Ref. 130 shows a dozen different spin-component-scaled electron-correlation methods, for example the scaled-opposite-spin method (SOS-MP2) and methods optimized for noncovalent interactions (SCS-MI-MP2, SCSN-MP2, SCS-MP2-vdW). It is straightforward to optimize the coefficients c_{OS} and c_{SS} for a particular system under study.

The authors of the present review article have used the spin-component-scaled methods (mostly the original SCS-MP2 method for ground states and the SCS-CC2 method for excited states) extensively in the past, in particular for geometry optimizations.[110,118,131,132] In Ref. 133, the importance of the spin-component-scaled second-order perturbation theory was emphasized for π-stacked aromatic systems while the MP2 method itself was providing excellent results for strong hydrogen bonds. An important advantage of the spin-component-scaled electron-correlation meth-

ods is that these methods can easily and successfully be used for the treatment of low-lying valence excited states of large, weakly interacting chromophores.[134] Examples are methods such as SCS-CC2, SCS-ADC(2), or SCS-CIS(D).[135–138]

4.6 Symmetry-adapted Perturbation Theory (SAPT)

The starting point for SAPT is the (antisymmetrized) product of the wave functions (or Kohn–Sham determinants)[139–141] of the weakly interacting monomers of the complex of interest. Then, the parts of the Hamiltonian that describe the interaction are treated as perturbation. There are various variants of SAPT that provide both the theoretical framework for analyzing intermolecular interactions and a practical tool for calculating these.[142–145] For example, Sherrill has recently shown that the energy-component analysis via SAPT is very useful in understanding noncovalent π-stacking interactions and their substituent and heteroatom effects.[146] Ahnen and co-workers[110] have recently applied the DFT-SAPT[147] approach as implemented by Heßelmann and co-workers,[148,149] using the PBE0 hybrid functional[150] including an asymptotic correction (PBE0AC)[151] to the ImBz and PyBz complexes. See Table 4.

Also SAPT computations suffer from the very slow basis-set convergence that occurs when expanding dynamic-correlation functions in an orbital-product basis. One possible remedy would be to employ explicitly-correlated F12-type functions for the corresponding energy contributions, but in Ref. 110 we have simply scaled the relevant dispersion energies, $E^{(2)}_{\text{disp}}$ and $E^{(2)}_{\text{exch-disp}}$, by the ratio of the corresponding CCSD(F12)+(T*) and CCSD(T) electron-correlation contributions (in the same basis) to the interaction energy. Alternatively, a two-point X^{-3} extrapolation has been applied to the aug-cc-pVDZ and aug-cc-pVTZ energies. For ImBz and PyBz, the scaled PBE0AC-SAPT/aug-cc-pVTZ interaction energies were only $0.2-0.3$ kJ/mol larger in magnitude than the best estimates.

4.7 Dispersion-corrected Density-functional Theory

A recent account of dispersion-corrected density-functional theory [152] for aromatic interactions in complex systems is provided by Ref. 153. The most recent version of Grimme's dispersion correction is denoted "D3", which is used in conjunction with Becke-Johnson damping: D3(BJ). As an example, Table 5 shows results for the ImBz and PyBz complexes, based on GGA, hybrid, and double-hybrid functionals (GGA = generalized gradient approximation). Concerning the latter, Table 5 also shows results obtained by replacing the MP2-type correlation contribution to the double-hybrid functional by the corresponding MP2-F12 one, denoted as B2PLYP-F12, with and without frozen-core (1*s*) orbitals.[110] Using a frozen core is unconventional but yields excellent results and a much reduced basis-set superposition errors (BSSE).

The performance of the DFT-D3(BJ) approach is impressive. The TPSSh-D3(BJ) counterpoise-corrected interaction energies of ImBz and PyBz, for example, agree with the best estimates to within 0.2 kJ/mol.[110] Table 5 also reveals that the BSSE is quite large in the aug-cc-pVTZ basis at the double-hybrid level, due to the MP2-type correlation contribution. This large BSSE is significantly reduced by computing an MP2-F12-type correlation contribution, but overall, the choice of exchange–correlation functional in DFT-D3 appears to be of little relevance for noncovalent interactions when the functional is properly dispersion corrected. Therefore, in view of computational efficiency, it seems most promising to use GGA functionals.

To conclude this subsection, we note that similarly accurate results can be obtained using the density-dependent interatomic vdW potential of Tkatchenko and Scheffler[154,155] or the dispersion correction of Becke and Johnson based on the position-dependent dipole moment of the exchange hole.[156–158]

4.8 Random-phase Approximation (RPA)

This approximation offers a computationally efficient route to the parameter-free computation of dispersion-dominated intermolecular interactions in the framework of DFT. For example, Toulouse and co-workers have developed a range-separated DFT with RPA especially for applications to

noncovalent intermolecular interactions.[159,160] For an excellent recent review on the subject, see Ref. 161. However, as it is the case for DFT-based SAPT (*vide supra*), expanding short-range dynamic-correlation functions in an orbital-product basis leads to slow basis-set convergence.[162] Moreover, methods that go beyond the "direct" random-phase approximation (*i.e.*, methods that go beyond using the Hartree kernel only) exhibit an unphysical short-range behavior of the correlated pair function in large basis sets.[163] Recent developments include a self-consistent treatment of electron correlation in "direct" RPA (dRPA),[164] the analytical calculation of nuclear gradients,[165] the implementation of quasi-relativistic two-component (spin-orbit including) RPA methods,[166,167] and a linear-scaling implementation.[168]

Addressing the basis-set problems, an explicitly-correlated F12-type correction to the dRPA correlation energy has recently been implemented.[169] The corresponding method is denoted dRPA(functional)+F12, where "functional" is the exchange–correlation functional used in the underlying Kohn–Sham calculation. Also a dRPA(functional)(F12) method has been implemented, which is an explicitly-correlated direct ring-coupled-cluster-doubles method, drCCD(F12), with Kohn–Sham orbitals.[170] Table 6 shows corresponding dRPA(PBE)+F12 and -(F12) results for ImBz and PyBz.

We expect that F12 corrections will also dramatically improve the basis-set convergence of the correlation energy in the random-phase approximation when *exchange terms* are taken into account, as for example in calculations with the approximate exchange kernel (AXK)[171] or in the second-order screened exchange (SOSEX) approximation.[172,173]

We conclude this subsection by pointing out that the range-separated RPA method of Toulouse and co-workers[159,160] does *not* suffer from a slow basis set convergence, because in this method only a *long-range* RPA correlation energy is computed.[174]

4.9 Quantum Monte Carlo and Semiempirical Methods

Finally, also semiempirical methods may be applied to dispersion-dominated weakly interacting complexes when empirical corrections for dispersion (and possibly also hydrogen bonding) are added. Examples are the methods PM6, AM1 and OM3[175] as well as the SCC-DFTB-D method.[175–177] These methods were shown to reach the quality of current DFT-D approaches for noncovalent interactions.[175]

Furthermore, it has recently been shown that the fixed-nodes diffusion Monte Carlo (FN-DMC) approach may be seen as an interesting alternative to the "gold standard" CCSD(T)/CBS method.[178–180]

4.10 Excited States (S_1) of Weakly Interacting Complexes

While there are numerous methods available for the computation of the binding energy of a weakly interacting complex in its ground state (S_0), this is no longer true for weakly interacting complexes in their first singlet excited state (S_1). Appropriate methods are the (SCS-)CC2 linear-response coupled-cluster method or multireference approaches such as the CASSCF/CASPT2 approach (complete-active-space self-consistent field plus second-order perturbation theory). Recent examples are found in Refs. 181 and 182 respectively. Also time-dependent density-functional theory (TD-DFT) may be applicable when using appropriate functionals, as shown for example by Huenerbein and Grimme for organic excimers of pyrene and benzene and an exciplex of styrene with trimethylamine.[183]

In our own work, we have used the linear-response SCS-CC2 method as implemented in the program system TURBOMOLE.[184,185] Due to its efficient implementation using the resolution-of-the-identity approximation, it is today possible to compute the harmonic vibrational frequencies of a trimer consisting of imidazole and two benzene molecules at the SCS-CC2/def2-QZVPP[186] level, see Figure 10.

After optimizing the geometry of the (benzene)$_2$·imidazole trimer in its ground state at the SCS-MP2/def2-QZVPP level and its first singlet excited state at the SCS-CC2/def2-QZVPP level, the 0-0 transition is found at 4.72 eV when including the (harmonic) zero-point vibrational energy

(ZPVE). It is assigned to the $1\,^1B_{2u} \leftarrow 1\,^1A_{1g}$ 0-0 transition of benzene.[187] The energy difference at the individual equilibrium structures (T_e value) amounts to 4.91 eV. In the present review article, however, we are *not concerned* with the computations of binding energies of weakly interacting complexes in *excited states*.

4.11 Zero-point Vibrational Energy

Possible methods to compute the anharmonic zero-point vibrational energy (ZPVE) of weakly interacting complexes include quantum diffusion Monte Carlo (as recently applied to the $H_2{\cdot}Li^+{\cdot}$-benzene system)[188] or methods that diagonalize the nuclear Hamiltonian in a discrete-variable-representation (DVR) basis, as pioneered by Bačić and co-workers in the 1990s (using summed empirical atom–atom Lennard-Jones potentials)[189–193] and as for example recently done for PESs of aromatics with rare gases R in ground and excited states.[194–196]

Such methods need a full-dimensional intermolecular PES, which for example can be computed using the modified Shepard interpolation of Bettens and co-workers.[197] Note, however, that these PESs represent the calculated *fixed-fragments* interaction energy $\Delta E(R_{\mathrm{min,inter}})$, which neglects the geometrical relaxation of M and S. Thus the intermolecular electronic binding energy D_e is not the minimum of this PES, but needs to be calculated separately. For type-II and type-III complexes with an aromatic M and a rare gas R, the (reduced) masses are relatively large, and the total ZPVE of the three intermolecular vibrations is in the range of $30-50\ \mathrm{cm}^{-1}$. We estimate the error of the harmonic treatment to be $5-10\ \mathrm{cm}^{-1}$; this is small relative to current error in calculated D_e. Hobza and coworkers have recently shown that ΔZPVE corrections terms for dispersion-bound complexes are small, both harmonic and anharmonic D_0 values being in good agreement with experimental results.[10]

Alternatively, vibrational second-order perturbation theory (VPT2) may be applied, as for example done for the (hydrogen-bonded) formic acid dimer in Ref. 198 using anharmonicity constants computed at the DFT level. Vibrational configuration interaction (VCI) can also be applied to molecular complexes, as demonstrated recently by Panek and Jacob for the intramolecular vibra-

tions of the water tetramer using localized modes.[199] It can of course be used in conjunction with the explicitly-correlated coupled-cluster approach.[200]

5 Examples of Binding and Dissociation Energies of Dispersively Bound Complexes

5.1 Type I Complexes: Two Systems with Localized HOMOs.

5.1.1 Ar_2, Kr_2, Xe_2, $(N_2)_2$ and $(CO)_2$

Due to their simplicity and significance for understanding non-covalent interactions, noble-gas homo- and heterodimers and the related dimers $(N_2)_2$ and $(CO)_2$ are paradigmatic examples of type I complexes. The ionization properties and ion ground-state D_0 values of Ar_2, $(N_2)_2$ and $(CO)_2$ have been reviewed by Weitzel and Mähnert.[201]

The ground-state $^1\Sigma_g^+$ potential curve of Ar_2 has been extracted from the VUV absorption spectrum,[202] yielding D_e = 1.18 kJ/mol, D_0 = 1.03 kJ/mol and a minimum-energy distance $R_e(^1\Sigma_g^+)$= 3.761 Å.[203] Measuring the Ar_2^+ $^2\Sigma_u^+$ ground state and the AIE of Ar_2 has proven challenging: Due to charge-resonance stabilization in the $^2\Sigma_u^+$ state, the equilibrium distance shortens to $R_e(^2\Sigma_u^+)$ = 2.32 Å,[204] and the Franck-Condon overlap between the $^1\Sigma_g^+$ and $^2\Sigma_u^+$ state $v = 0$ wave functions is essentially zero, see Figure 3. Despite this, two research groups have been able to probe Ar_2^+ ground state vibrational levels from $v^+ = 3 - 52$ using pulsed-field ionization zero electronic kinetic energy (PFI-ZEKE) spectroscopy.[204–206] The Franck-Condon factors to vibrations with $v^+ < 25$ are negligible,[204] and the appearance of these bands has been explained by "channel interactions" with high-lying Rydberg series of Ar_2 that converge to electronically excited states of Ar_2^+. Although the detailed mechanism is not clear, the presence of these low-v bands in the PFI-ZEKE spectrum allows to fit the potential energy curve, yielding AIEs of 14.455 eV[205] or 14.457 eV[206] (the differences stem from the different fitting approaches).[206] The resulting dissociation energy of Ar_2^+ is D_0= 127 kJ/mol, which is >100x larger than that of the Ar_2 $^1\Sigma_g^+$ ground

state. As expected from the poor Franck-Condon factors around the spectroscopic origin, ionization energies determined just by the appearance of photoions or photoelectrons tend to overestimate the AIE.

Similar observations have been made for Kr_2 and Xe_2:[207,208] While the ionizative Franck-Condon factors are expected to give spectroscopic access only to vibrational states $v^+ \approx 30-60$, channel interactions with high Rydberg states allowed to identify lower vibrational levels when using the PFI-ZEKE technique. In these cases, even the ion ground state $v^+ = 0$ level was identified, allowing a very accurate description of the cation potential curve. Results of comparable quality have also been obtained for the KrXe and ArXe noble-gas heterodimers.[209,210] This renders PFI-ZEKE a valuable tool for the determination of the AIEs of type I complexes, utilizing thermochemical cycles for the neutral ground state dissociation energies.

5.1.2 $(H_2O)_2$, $(D_2O)_2$, $H_2O{\cdot}HCl$ and $(NH_3)_2$

While the water dimer is H-bonded and is outside the topic of this review, it represents a further type I complex. Furthermore, Reisler and co-workers have recently performed elegant velocity map imaging (VMI) measurements of the dissociation energies of $(H_2O)_2$ and $(D_2O)_2$ that beautifully illustrate the power of the VMI technique.[211,212]

The water dimers are dissociated by pumping the O-H stretch vibration in the ground state using an IR laser pulse, followed by IVR and vibrational predissociation. The two H_2O fragments are then ionized using a 2+1 REMPI scheme (resonance enhanced multiphoton ionization) and their velocity distribution is measured by VMI. Since the rotational levels of H_2O are well-separated, and because the excess energy of the IR photon above D_0 suffices only to populate $v = 1$ of the bending vibration of one of the H_2O fragments, the rotational and vibrational energies of the ionized fragments are determined state-specifically and their respective translational energy distribution yields detailed information on the dissociation process. Apart from D_0, the other unknown parameters are the rotational and vibrational energy of the co-fragments. However, these define the shape of the velocity distributions, and could be established by fitting the velocity distribu-

tion curves obtained by monitoring the velocity distribution of the H_2O fragments in four different rovibrational states.[211] The dissociation energies of $D_0 = 13.2 \pm 0.11$ kJ/mol for $(H_2O)_2$ and $D_0 = 14.9 \pm 0.12$ kJ/mol for $(D_2O)_2$ are in excellent agreement with theory.[213,214] Remarkably, the calculated binding energy D_e amounts to $20.8 - 21.0$ kJ/mol,[215] being ca. 60% larger than D_0! The water dimer is an impressive example of the importance of ZPVE when comparing theory to experiment. Note also that the dissociation energy changes by $\approx 13\%$ upon deuteration.

In contrast to other examples of VMI discussed in Section 3.4, the ground state D_0 is here determined directly from the dissociation kinematics plus detailed spectroscopic knowledge of the monomer and dimer rotational and vibrational energies, without employing thermochemical cycles. The technique has therefore only been applied to small hydride dimers and complexes with well-separated rotational vibrational states. Other complexes studied by VMI so far are H_2O·HCl (D_0 = 15.95±0.12 kJ/mol)[216] and $(NH_3)_2$ (D_0 = 7.89 kJ/mol).[217]

An analogous approach has been applied earlier by the group of Roger Miller, who determined the dissociation energies of a large number of small complexes using photofragment angular distribution (PHOFAD) or position-sensitive translational spectroscopy (POSTS) methods.[218] In this approach, the kinetic energy distribution of the photofragment moieties was probed by recording their deflection angle from the molecular beam axis using a movable liquid He-cooled bolometer. The results of these studies are compiled in Table 1. Due to the quality of the data, it is recommended that this approach should be exploited whenever it is feasible.

5.2 Type II Complexes: A System with Delocalized HOMO and a System with a Localized HOMO

5.2.1 Benzene·Argon

Measurements of the ground-state dissociation energy of benzene·argon (Bz·Ar) have been performed by Neusser and co-workers using ion breakdown measurements ($D_0 = 1.6 \pm 0.5$ kJ/mol)[32] and later by pulsed field mass analyzed threshold ionization (PFI-MATI) spectroscopy ($D_0 < 4.1$

kJ/mol)[27,219]. More recently, Lawrance and co-workers[34] have provided a more accurate $D_0 = 3.77 \pm 0.08$ kJ/mol using velocity map imaging (VMI). While the lower limit of the PFI-MATI measurement agrees with the VMI value, the breakdown measurement[32] yields a much smaller dissociation energy (cf. Table 2).

In the VMI experiment, the dissociation energy has been determined from the cycle D_0(Bz·Ar) = D_0^+(Bz^+·Ar) + AIE(Bz). The AIEs of Bz·Ar and Bz were previously determined using PFI-ZEKE spectroscopy.[220] The cation dissociation energy D_0^+ was determined by ionizing Bz·Ar into a vibrational state above the D_0^+(Bz^+·Ar) dissociation limit. Thereby, the excess energy was chosen as small as possible to prevent the formation of vibrationally excited fragments. As an intermediate state for the two-photon ionization, the 6^1 level of the S_1 state, 521 cm^{-1} above the electronic origin was chosen. VMI was then used to measure the translational energy distribution of the Bz^+ fragments. Subtracting the AIE(Bz·Ar) and the highest observed kinetic energy of the fragment from the excitation energy yielded $D_0^+ = 5.81 \pm 0.05$ kJ/mol. This approach assumes that the Bz^+ is formed in the $N^+ = 0$ rotational level during VP. Thus, the D_0^+ value evaluated by VMI is an upper limit.

The intermolecular potential of Bz·Ar has been constructed based on CCSD(T)/aug-cc-pVDZ calculations, resulting in a fixed-fragments interaction energy $\Delta E(R_{\mathrm{min,inter}}) = -4.66$ kJ/mol.[221] This value agrees with the value of -4.65 kJ/mol reported in Ref. 222, which was obtained by combining the finite-basis MP2 and CCSD(T) values of -5.54 and -3.57 kJ/mol, respectively, with the infinite-basis MP2 limit of -6.62 kJ/mol. Assuming a negligible deformation of benzene by the interaction with the Ar atom, this value may be identified also as the binding energy D_e. Zero-point correction of the D_e using the three intermolecular frequencies calculated from the intermolecular potential of Ref. 221 leads to $D_0 = 3.83$ kJ/mol, which is in excellent agreement with the results of Lawrance and co-workers.[34]

5.2.2 Complexes with Carbazole

Ground-state dissociation energies D_0 of complexes of carbazole with noble gas atoms (Ne, Ar, Kr, Xe) and small molecules (CO, N_2, CH_4) have been measured by the stimulated-emission pumping/resonant two-photon ionization (SEP-R2PI) method.[38,39,43] To illustrate a comparison of experiment with calculation, we have optimized the equilibrium structures of these complexes (and of course also those of the carbazole molecule, CO, N_2, and CH_4) at the SCS-CC2/aug-cc-pVTZ level, see Section 4.5. Figure 11 shows the optimized equilibrium structures of carbazole·CO and carbazole·CH_4.

At these equilibrium structures, we have performed single-point energy calculations at the (SCS-)MP2-F12/cc-pVTZ-F12[223–225] level using the TURBOMOLE program[184,185,226] and at the DFT-SAPT/aug-cc-pVTZ level with the MOLPRO program.[227,228] Concerning DFT-SAPT, we have added a ΔF12 correction that has been obtained by performing an MP2-F12 calculation in which only those second-order pair energies are taken into account where the two occupied orbitals are localized on different fragments (using MOLPRO's Kohn–Sham orbitals and orbital energies). We refer to this level as SAPT-F12(MP2). The PBE0AC functional has been applied using experimental values for the ionization energies.[151] ZPVEs have been computed in the harmonic approximation at the PBE-D3/def2-TZVP level.[229,230] The computed dissociation energies D_0 are summarized in Figure 12. Clearly, dissociation energies are strongly overestimated at the MP2-F12 level while the spin-component-scaled SCS-MP2-F12 energies are much improved for these dispersion-dominated weakly interacting vdW complexes.

Table 7 compares the MP2-F12, SCS-MP2-F12, and SAPT-F12(MP2) results with the experimental D_0 values. The agreement of the SAPT-F12(MP2) results with the experimental values is quite satisfactory, the largest deviation being -1 kJ/mol for carbazole·CO. Note, however, that the experimental uncertainty for this complex is ± 0.38 kJ/mol. The individual contributions to the SAPT-F12(MP2) binding energies are shown in Table 8.

As in Ref. 38, we plot the SAPT-F12(MP2) dispersion energy $E_{\mathrm{disp}}^{(2)}$ and the computed binding energy D_e of the complexes of carbazole with the noble gases X against the static polarizability α_{X}

of these atoms in Figure 13. Clearly these energies depend linearly on the atomic polarizabilities, in accord with London's formula. The polarizabilities α_X were multiplied with the ionization energy factor $I_X I_{Carb}(I_X + I_{Carb})^{-1}$ with I_{Carb} = 7.57 eV and I_X = 21.55, 15.75, 14.00, and 12.13 eV for Ne, Ar, Kr, and Xe, and the polarizabilities were divided by the sixth power of the interfragment distances R = 3.11, 3.32, 3.40, and 3.43 Å that were obtained at the SCS-CC2/aug-cc-pVTZ level. Note that the electronic binding energy D_e is plotted.

Further examples of experimentally determined and computed dissociation energies of type II complexes with small molecules are compiled in Table 9.

5.3 Type III Complexes: Two Systems with Delocalized HOMOs

We denote dispersively bound self-dimers M_2 of aromatic molecules as type III complexes (cf. Table 10). Several problems arise when trying to determine their dissociation energies, which are exemplified using the benzene dimer, Bz_2.

5.3.1 Benzene Dimer

Multiple ground-state structures: Due to the weakness and weak directionality of dispersive intermolecular interactions, the PESs of type III complexes are relatively shallow and exhibit multiple minima, rendering notions such as that of "structure" problematic. For decades Bz_2 was predicted to have a "stacked" or "slipped-stacked" minimum-energy structure with parallel benzene planes. However, already in 1975, molecular-beam electric-deflection measurements showed that isolated and supersonically cooled Bz_2 is polar, and a T-shaped structure was suggested.[231] In 1993, a T-shaped structure with a distance of 5.5 Å between the centers-of-mass of the "T-stem" and "T-cap" Bz moieties was inferred from the microwave rotational spectrum of Bz_2.[232] In 2006, Podeszwa et al.[233] calculated a 6-dimensional intermolecular PES for Bz_2 using DFT-based symmetry-adapted perturbation theory (SAPT) and predicted the tilted T-shaped geometry **M2** shown in Figure 14 as the global minimum. The **M2** minimum (with $D_e = 11.6$ kJ/mol) was calculated to be slightly below the slipped-stacked local minimum denoted **M1** ($D_e = 11.5$ kJ/mol) and much lower than a

previously unknown twisted edge-to-edge local minimum denoted **M3** ($D_e = 7.6$ kJ/mol).

Large-amplitude motions, structural interconversions and internal tunneling processes: The symmetric-top character of the microwave spectrum[232] is surprising because any *rigid* Bz_2 structure is an *asymmetric* top. Indeed, the microwave spectrum exhibits multiple splittings that reflect rapid structural interconversion processes,[234–236] which occur in the vibrational ground state and interchange the Bz monomers between 48 degenerate (but structurally distinct) forms of **M2**.[234] Based on an improved third-order DFT-SAPT PES and supplementary CCSD(T) calculations, van der Avoird and co-workers identified three distinct tunneling paths that interconvert energetically degenerate forms of **M2** (hindered cap C_6 internal rotation, tilt tunneling of the stem Bz, cap turnover).[234,235] Furthermore, The Bz_2 DFT-SAPT PES of Podeszwa et al.[233] revealed four low-lying index-1 saddle points, denoted **S1** to **S4**, that lie merely 0.1–0.5 kJ/mol above the minima, indicating that structural interconversions between **M1** and **M2** are also facile.

Large intermolecular vibrational zero-point energies: Based on the calculation of the vibration-rotation-tunneling levels of Bz_2,[234,235] the vibrational zero-point energy of the six intermolecular vibrations is predicted to be ZPVE = 1.26 kJ/mol. This amounts to nearly 11% of the calculated well depth of the T-shaped **M2** minimum fixed-fragment interaction energy of $\Delta E(R_{\mathrm{min,inter}}) = 11.6$ kJ/mol.[234,235] As shown in Figure 15, the ZPVE places the lowest $v = 0$ intermolecular vibrational level of Bz_2 well above the **S1** to **S4** saddle points of the intermolecular PES.

Large differences between the PESs of the neutral and ion ground states: As shown schematically in Figure 15 for Bz_2, the neutral ground-state PES of M_2 and the ion ground PES of M_2^+ can differ dramatically. The ground-state minimum-energy structure of Bz_2 is T-shaped while the Bz_2^+ minimum-energy structure is slipped-stacked (**M1**).

Experimental dissociation energy of Bz_2: The dissociation energy of Bz_2 has been measured by Hui and co-workers[237] who reported $D_0 = 10.0 \pm 1.7$ kJ/mol and by Neusser and co-workers,[25,238] who reported a distinctly smaller value, $D_0 = 6.75 \pm 1$ kJ/mol. Two different thermochemical

cycles where applied: Hui exploited the relationship given in Eq. (15), cf. Figure 5.

$$D_0 = D_0^+ + \mathrm{AIE}(\mathrm{Bz}_2) - \mathrm{AIE}(\mathrm{Bz}) \tag{15}$$

Using one-photon VUV photoionization, Hui and co-workers measured AIE(Bz_2)$= 8.690 \pm 0.023$ eV.[237] To obtain the dissociation energy of the cation, D_0^+, they extrapolated the value $D_0^+ = 71.1 \pm 6.3$ kJ/mol obtained by Field *et al.*[13] from equilibrium measurements at 300 K down to 0 K using "reasonable estimates for the vibrational modes involved",[237] resulting in $D_0^+ = 69.8 \pm 7.0$ kJ/mol. This uncertainty results in a very broad range for D_0 between 9.3 and 23.3 kJ/mol. Upon including the results of IR spectra of Nishima and Hanazaki[239] who reported an upper limit for $D_0(\mathrm{Bz}_2)$ as 11.87 kcal/mol, Hui and co-workers arrived at a final result of $D_0 = 10.0 \pm 1.7$ kJ/mol. In contrast, Neusser and co-workers based their D_0 determination on the measurement of the appearance energy (AE) of the Bz^+ daughter ion from the ion breakdown of $(Bz_2)^+$, using the thermochemical cycle $D_0 = \mathrm{AE}(\mathrm{Bz}^+) - \mathrm{AIE}(\mathrm{Bz})$ (see also Figure 5). From their measured AE(Bz^+) = 9.31 eV and AIE(Bz)$= 9.24378 \pm 0.00007$ eV as above,[240,241] they obtained a Bz_2 dissociation energy of $D_0 = 6.75 \pm 1$ kJ/mol. When compared to the calculated $D_0 = 10.34$ kJ/mol of Avoird and co-workers,[234,235] this amounts to a difference of about 4 kJ/mol or 50%.

Repeated measurements of VUV one-photon or resonant two-color two-photon ionization (2C-R2PI) photoionization efficiency (PIE) curves of Bz_2 by the groups of Schlag and Baumgärtel resulted in values for AIE(Bz_2) ranging from 8.865 eV[242] to 8.65 eV,[242–244] the latter value being slightly below the Hui and co-workers value of 8.690 eV.[237] However, when inserting the calculated $D_0^+ = 86.6$ kJ/mol of Krylov[245] and the calculated ZPVE-corrected fixed-fragment interaction energy -10.34 kJ/mol of Avoird et al.[234,235] into Eq. (15), one arrives at AIE(Bz_2)$= 8.453$ eV, which is 0.2 eV below the *lowest* experimental value. The reason for this are the large changes between the Bz_2 and $(Bz_2)^+$ minimum geometries, which lead to minute Franck-Condon overlaps in ionization, rendering both one-photon and two-photon ionization measurements of the AIE of Bz_2 nearly impossible. The large errors of the AIE values has a devastating effect on all subsequent

thermochemical cycles.

Therefore, experimental techniques that rely on measurements involving the neutral ground state are recommended. One approach has been presented by Gentry and co-workers who measured the photodissociation dynamics of Bz_2 upon excitation of the ν_{18} level at 1038 cm^{-1} (12.4 kJ/mol), obtaining dissociation times of 2.5 ps.[246] Felker and co-workers used stimulated vibrational Raman scattering (SRS) to populate the ν_1 fundamental of the Bz_2 complex at 992 cm^{-1} (11.87 kJ/mol).[247] The Raman-excited complex was subsequently detected by one-color R2PI. Employing a time delay of $\Delta t \approx 50$ ns between the SRS pulses and the excitation/ionization laser pulse, no decrease of the vibrationally excited population was observed. This led Felker and co-workers to the conclusion that either VP occurs on $\gg 50$ ns time scale or that $D_0 > 11.87$ kJ/mol. This yields limits between $11.87 < D_0 < 12.4$ kJ/mol, which is in acceptable agreement with the calculated ZPVE-corrected fixed-fragment interaction energy of -10.4 kJ/mol.[234,235] This value is based on the calculated $\Delta E(R_{\mathrm{min,inter}})$ of the 6-dimensional rigid-monomer PES and the anharmonic ZPVE of the six intermolecular vibrations, given as 105 cm^{-1} = 1.26 kJ/mol in ref. 234. However, Bz_2 has 66 vibrations, of which the 60 intramolecular vibrations are neglected in the rigid-monomer treatment. The effect of dimer formation on these is not known; it could increase or decrease the ΔZPVE.

5.3.2 Toluene Dimer

Despite their similar chemical structure, the conformational space of $(toluene)_2$ and Bz_2 differ markedly, since T-shaped structures of the toluene dimer are either calculated to be substantially less favorable[248,249] than π-stacked conformers, or could not even be identified as minima.[250] This change of conformational preferences has been ascribed to (1) the compensation of the repulsive quadrupole-quadrupole interactions (which disfavor stacked conformations in Bz_2) by an attractive dipole-dipole interaction in stacked $(toluene)_2$, and (2) the increase in the dispersive interaction due to the additional methyl group.[249] A decomposition of the interaction energy[248] shows that the electrostatic contribution barely changes, while there is an increase of the correlation energy

by $\approx 40\%$ on going from Bz_2 to $(toluene)_2$.

Three different local minima of stacked $(toluene)_2$ have been identified with the CH_3-groups of the toluene moieties either parallel (C_{2h} symmetry), anti-parallel (C_s) or at a $\approx 90^\circ$ angle ("cross-isomer", C_2 symmetric).[248,250] The interaction energies of these three isomers are calculated to be very similar. The most stable isomer is predicted to be either the cross ($\Delta E_2 = -17.1$ kJ/mol, estimated CCSD(T)/CBS)[248] or the anti-parallel isomer with $\Delta E_2 = -14.5$ kJ/mol (CCSD(T)/6-311++G**).[250] We note a considerable difference between the interaction energies evaluated with the two applied protocols.

The 0_0^0 band of the $S_0 \rightarrow S_1$ spectrum of $(toluene)_2$ is only ≈ 100 cm^{-1} wide and consists of sharp transitions and an underlying broad absorption.[251] Hole-burning spectroscopy revealed the presence of at least two different isomers,[252] which were first assigned to a stacked and a T-shaped structure.[251] More recent calculations[248,250] suggest that two (or more) π-stacked isomers coexist in the molecular beam, but their identification is hindered by the absence of distinct spectroscopic features. The dissociation energy has been determined via breakdown measurement (BM) as $D_0 = 14.5 \pm 1$ kJ/mol.[25] It remains unclear which of the isomers was been probed in that investigation. On the other hand, the experimental uncertainty of the D_0 is larger than the calculated energy differences between the various isomers, so even if the method was able to probe the different isomers, it could not resolve the differences of the dissociation energies.

5.3.3 Indole·Benzene

The indole·benzene dimer provides a gas-phase model for the interactions between aromatic amino acids on protein structures, mimicking the tryptophan·phenylalanine interaction. Employing MATI threshold ionization of indole·benzene plus an appearance energy measurement of indole$^+$, Neusser and co-workers determined the dissociation energy of indole·benzene as $D_0 = 21.8 \pm 0.18$ kJ/mol[33] and that of indole·benzene-d_6 as 22.3 ± 0.18 kJ/mol.[29] These are among the most precise D_0s reported to date. As discussed above, the interpretation of this value also requires the identification of the different structural isomers and of the most stable structure. In addition to the π-stacking

and CH$\cdots\pi$ interactions in (benzene)$_2$ and (toluene)$_2$, indole·benzene can also form an nonclassical NH$\cdots\pi$ hydrogen-bond. The 3D PES for parallel $\pi\cdots\pi$ structures has been calculated with the MP2 and SCS-MP2 methods and the aug-cc-pVDZ basis set, yielding two distinctly different minima structures for the two methods. Both structures are found to be weaker than the NH$\cdots\pi$ conformer at the SCS-CCSD(T)/CBS level of theory by more than 4 kJ/mol and therefore are not expected to be observed in the supersonic jet.[253] Due to the large positive electrostatic potential of the NH hydrogen, the interaction energy ΔE_2 of the T-shaped NH$\cdots\pi$ bonded conformer is nearly 5 kJ/mol larger in magnitude than that of the CH$\cdots\pi$ bonded conformers at the SCS-CCSD[T]/CBS level of theory.[253] The calculated interaction energy $\Delta E_2 = -22.9$ kJ/mol of this conformer is slightly larger in magnitude than the measured D_0. However interaction energies are expected to be larger than the dissociation energy D_0, as discussed in Section 1. On the other hand, Braun *et al.* calculated a dissociation energy $D_0 = 22.2$ kJ/mol at the MP2/CBS + ΔCCSD[T]/6-31G**(0.25,0.15) + ΔZPVE(MP2/6-31G*) level of theory for the NH$\cdots\pi$ hydrogen-bonded T-shaped structure.[29]

Based on the excellent agreement between measured and calculated dissociation energies, this structure was assigned to be the observed complex. However, the structure was contested by Biswal and co-workers,[254] who measured the supersonic jet IR spectrum in the NH stretch region of the indole moiety and compared it to the results of dispersion-corrected B97-D/TZVPP calculations. They found an additional T-shaped local minimum, labeled T', with the plane of the indole moiety tilted ≈60° from that of benzene. The dissociation energies of the T- and T'-shaped isomers are very close (20.4 and 20.3 kJ/mol, respectively, including counterpoise corrections), indicating a very flat potential along the coordinate that interconverts the two conformers. Due to the better agreement of the experimental NH stretch frequency (3479 cm^{-1}) with that calculated for the T'-shaped isomer (3487 cm^{-1}) than with the T-shaped structure (3498 cm^{-1}), Biswal *et al.* concluded that the T' structure is observed.[254] Summarizing, one concluded that even relatively strong and strongly directional NH$\cdots\pi$ interactions may lead to two nearly degenerate isomers. In such cases, the comparison of calculated to the experimental dissociation energies must be made with great

care.[254]

5.3.4 Complexes with Anisole

In anisole, both the methoxy group and the π-electrons plane can act as H-bond acceptor sites. In addition to dispersive and OH$\cdots\pi$ interactions that occur in complexes with benzene, OH$\cdots$O hydrogen bonds can now also come into play. The subtle competition between the different possible interactions are the subject of recent spectroscopic studies in supersonic jets.[255–259] For anisole·water[256,257] and anisole·methanol[259] it has been found that complexes with an OH$\cdots$O hydrogen bond are more abundant than structures dominated by purely dispersive or OH$\cdots\pi$ interactions. In contrast to these findings, the experimental rotational constants of anisole·NH_3 measured with high resolution LIF spectroscopy (laser induced fluorescence) fit best for a structure in which ammonia forms an NH$\cdots\pi$ hydrogen bond to the anisole moiety.[258,260] A comparison of the calculated binding energies of the NH$\cdots\pi$ and N-H$\cdots$O complexes yields an unclear picture: depending on the method for the dissociation energy and structure calculation, either the N-H$\cdots\pi$ or the N-H$\cdots$O complex is expected to be more strongly bound.

The D_0 of anisole·benzene has been measured by dispersed fluorescence (see Section 3.1).[255] The D_0 of the S_1 state was bracketed between 20.5 and 22.2 kJ/mol. Subtracting the redshift of $\delta\nu = 354$ cm^{-1} (4.2 kJ/mol) leads to a ground state $D_0 = 16.3 - 18.0$ kJ/mol.

$(\text{Anisole})_2$ is a π-stacked centrosymmetric (C_i) dimer.[261] Due to symmetry restrictions, the $S_1(A_g)$ state cannot be excited by one-photon excitation, the lowest state that can be optically excited is the $S_2(A_u)$ state. An excitonic splitting between the S_1 and S_2 states occurs which has been measured to be 14 cm^{-1}.[262] The dissociation energy has been determined using VMI (velocity mapping ion imaging) in 2013,[36] however, the measured ground-state $D_0(S_0)$ of 47.0 kJ/mol was in stark contrast to the calculated DFT (M05-2X/aug-cc-pVTZ) binding energy of 17.7 kJ/mol.[258] The experimental D_0 has recently been reinvestigated applying a two-color appearance-energy scheme (2C-AE). The revised dissociation energies are 21.5 ± 1.2 in the S_0 state and 48.1 ± 2.4 kJ/mol in the ion ground state. The neutral ground-state D_0 is now in good agreement with the DFT-D3

zero-point-corrected CCSD(T)/CBS dissociation energy $D_0 = 21.1 \pm 0.2$ kJ/mol.[37]

6 Summary and Outlook

Above, we have discussed experimental and theoretical methods for measuring and calculating accurate dissociation energies D_0 of dispersively bound M·S complexes, where M is an aromatic or heteroaromatic molecule and S is a solvent molecule. In Section 2, we propose a classification of dispersively bound M·S complexes according to the frontier orbitals of M and S (with M_2, that is, M = S as a special case): As type-I we denote complexes in which the HOMO and LUMO of M and S are *not* π-electron orbitals, as type-II we classify complexes in which the HOMO and LUMO of M are *both* π-electron orbitals, but those of S are not, and as type-III we classify M·S complexes in which the HOMO and LUMO of *both* M and S are π-electron orbitals.

With regard to type-II complexes, we discussed in Sections 2 and 3 that the dissociation energy can be determined in either the S_0 ground state of M·S, the S_1 excited state M^*·S or the ion ground state M^+·S, giving D_0(M·S), D_0(M^*·S) or D_0(M^+·S), respectively. The S_1 or ion ground state dissociation energies can be converted to D_0(M·S) using a thermochemical cycle and further experimental information, that is, either the $S_0 \rightarrow S_1$ 0_0^0 excitation energy or the adiabatic ionization energy of M.

We point out in Sections 2, 3 and 5 that the electronic structure of type-I and type-III complexes gives rise to severe problems when determining the D_0 values via either the S_1 excited state or the ion ground state. The reason for this is that the change in electronic structure of M·S upon electronic excitation or ionization leads to major changes of the intermolecular potential energy surfaces of M^*·S or M^+·S, relative to the ground state PES. If the minimum-energy geometries of the S_0 and S_1, or S_0 and ion states are sufficiently displaced, it becomes difficult or impossible to measure the $S_0 \rightarrow S_1$ 0_0^0 excitation energy or the adiabatic ionization energy of M·S. Then, the corresponding thermochemical cycle cannot be employed and $D_0(S_0)$ is not accessible. The intrinsic nature of these problems have not always been realized, sometimes leading to experimental pitfalls.

Due to the recent improvements of theoretical methods for calculating intermolecular interactions and potential energy surfaces, the PESs of even large M·S complexes can now be computationally studied and potential problems diagnosed before the experiment.

Details of the experimental methods are discussed in Section 3: Most methods can be classified as *predissociative*, i.e., M·S is first cooled to its lowest S_0 state vibrational level and is then excited to a vibrational level that energetically lies above the dissociation energy D_0, so that vibrational predissociation (VP) can occur. The methods are categorized according to whether the vibrationally "hot" state that undergoes VP is (a) the S_0 state, (b) the S_1 excited state, or (c) the ion ground state M^+·S. Predissociative methods on the *ground* state surface employing infrared excitation or Raman pumping can be employed for type-I and type-III complexes. For type-II complexes, stimulated-emission pumping, S_1-state or ionizative methods can be generally employed. Problems arise when type-II complexes approach type-III, as for example for heterodimers where M and S have similar electronic structure.

For noble-gas dimers (or heterodimers), which are type-I M_2 or M·X complexes, D_0 can be obtained from the time-honored *extrapolative* method. This involves measuring vibronic or ionizative spectroscopic transitions associated with the (single) vibrational coordinate and extrapolating the vibrational energies of the $v', v'+1, ...$ levels to the dissociation limit. If the functional shape of the potential-energy curve is known (often from theory), the parameters of the potential-energy curve can be determined from the frequency *spacings* between a series of vibrational or vibronic bands, if the vibrational quantum numbers v' are correctly established. This directly gives the well depth $D_e(S_0)$; via a calculation of the zero-point vibrational energy, D_0 is also obtained. Unfortunately, it is difficult to extend the spectroscopic-extrapolative method from diatomics to triatomic or larger M·S complexes, since high vibrational levels of multidimensional potential energy surfaces are anharmonically coupled, both between the intramolecular vibrational coordinates and between the intra- and intermolecular vibrational coordinates, and their energy differences do not follow simple extrapolation rules. In many cases, full variational calculations of the high-lying vibrational levels are prohibitively expensive. In such cases, predissociative methods on the *ground* state surface

should be employed.

Today, quantum chemical computations of electronic binding energies D_e can be performed with very high precision, rivalling or even surpassing the accuracy of experimental determinations of dissociation energies of dispersion-dominated aromatic molecular complexes. Computations at high levels of coupled-cluster theory may be performed with unprecedented accuracy for selected points on the relevant potential energy surfaces, using extrapolation techniques or explicitly-correlated two-electron basis functions to approach the limit of a complete one-electron basis set. It may be particularly advantageous to combine various computational methods in a multi-level scheme. Computationally less demanding methods such as spin-component-scaled second-order Møller–Plesset perturbation theory, dispersion-corrected density-functional theory, density-functional-based symmetry-adapted perturbation theory, or methods based on the random-phase approximation offer access to the computation of intermolecular potential energy surfaces and the computation of zero-point vibrational energies, which are required for a direct comparison between experimentally and theoretically determined dissociation energies.

Experimental and computational techniques have both reached a level of accuracy at which they can mutually enrich and reinforce their further methodological development.

Acknowledgments

We thank the Swiss National Science Foundation (SNSF) and the Deutsche Forschungsgemeinschaft (DFG) for financial support through the Priority Programme SPP 1807 "*Control of London dispersion interactions in molecular chemistry*" (grants DFG KL 721/5-1 and SNSF 200021E-160404).

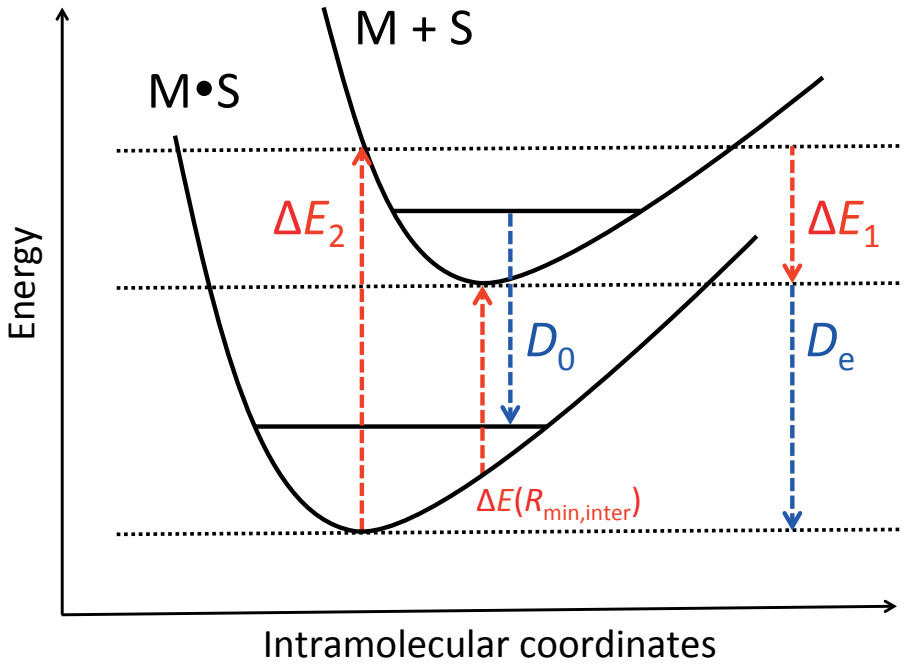

Figure 2: Illustration of the terminology and sign conventions used in the present review. Shown are the interaction energy $\Delta E_2 = \Delta E(R_{\text{min,inter+intra}})$, the electronic binding energy D_e, the dissociation energy D_0 and the fixed-fragments interaction energy $\Delta E(R_{\text{min,inter}})$. Upgoing arrows refer to negative values, downgoing arrows refer to positive values.

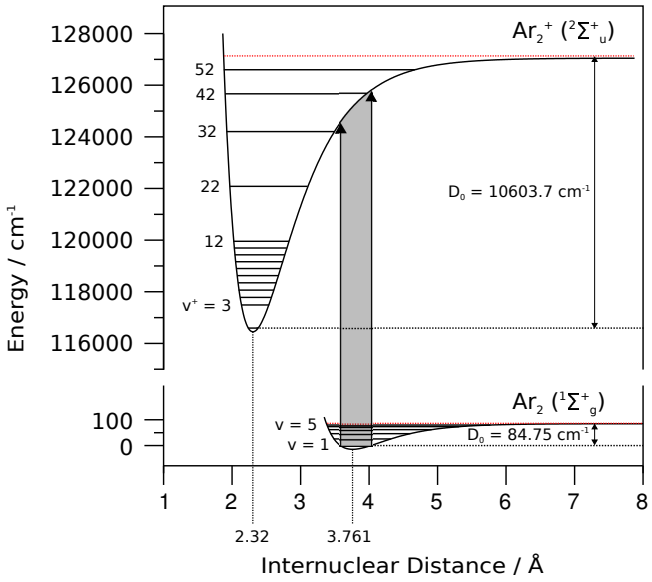

Figure 3: Neutral $^1\Sigma_g^+$ and ion $^2\Sigma_u^+$ ground state potentials of Ar_2. The Franck-Condon window for ionization from the $^1\Sigma_g^+$ $v'' = 0$ vibration is indicated in grey. The energy axis of the ground state is magnified 10x with respect to the ion state.

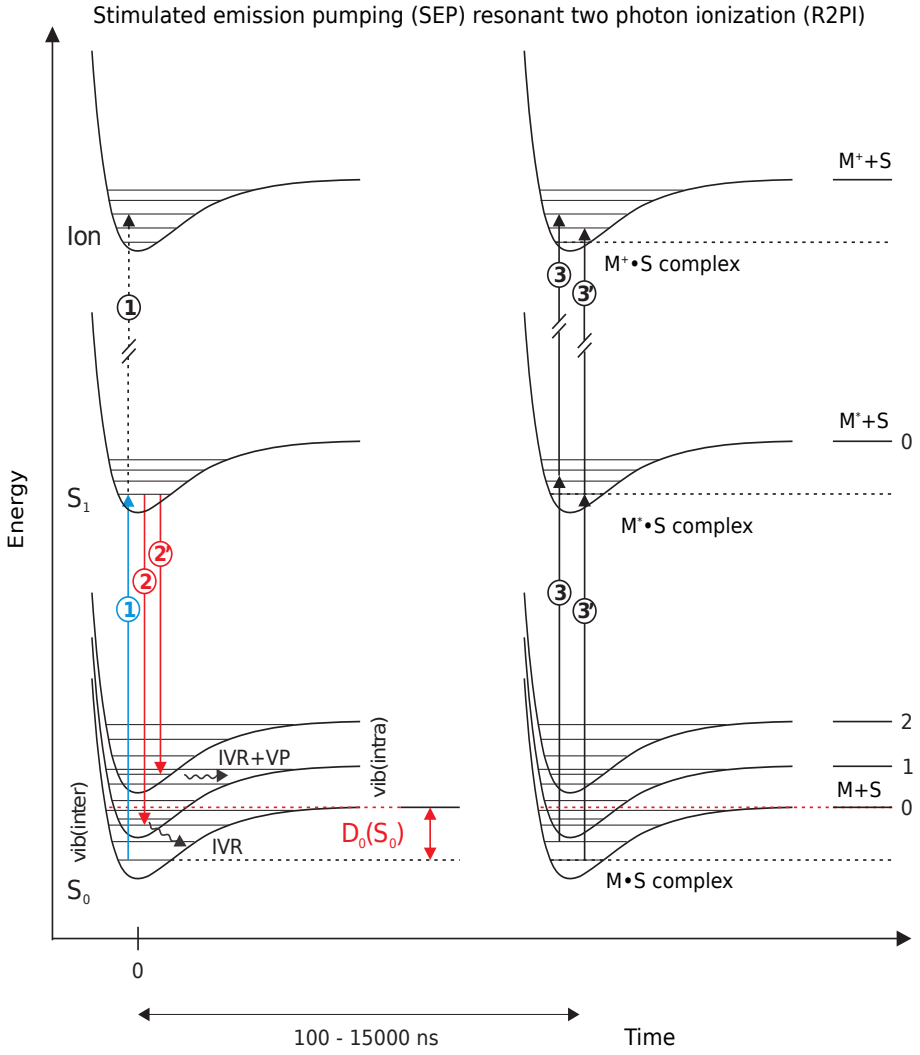

Figure 4: Schematic level diagram of the SEP-R2PI experiment, as applied to a type-II M·S complex. The potential energy curves indicate the S_0 state, S_1 excited-state and ion ground-state potentials plotted against the M···S distance (intermolecular stretching coordinate). The intramolecular vibrational levels of M are indicated as horizontal bars connected to the vertically shifted Morse-type potentials, and are shown for the S_0 state only. The intermolecular stretching vibrational levels are plotted within the Morse potentials. The global horizontal axis indicates the time between the pump/dump steps and the two-photon ionization detection step, which is delayed by 100 ns to 15 μs.

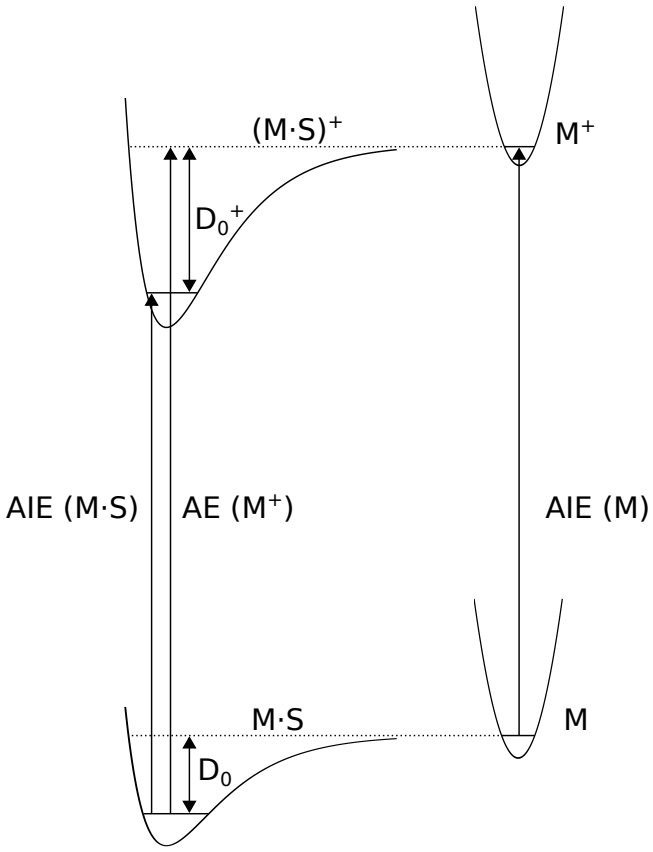

Figure 5: Schematic level diagram of a type II M·S complex in its neutral and cationic ground states. Also indicated are the adiabatic ionization energy (AIE) of M·S and of M, as well as the appearance energy (AE) of the M^+ daughter ion. The scheme illustrates the thermochemical cycles D_0 + AIE(M) = D_0^+ + AIE (M·S), as well as D_0^+= AE(M^+) – AIE (M·S).

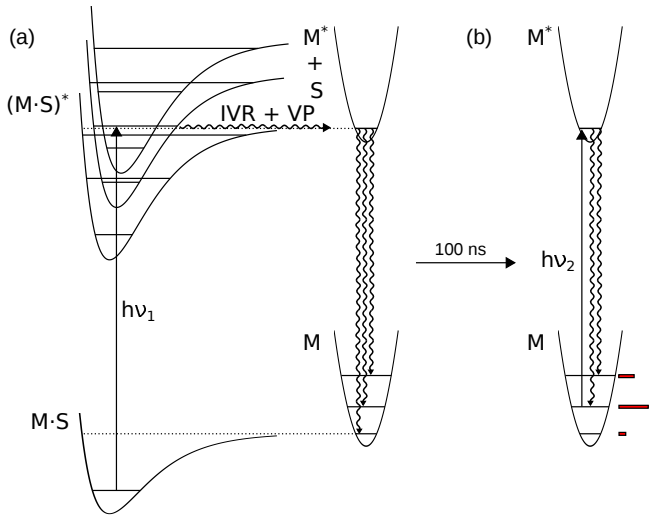

Figure 6: (a) Determination of the excited-state dissociation energy of an M·S complex by dispersed fluorescence. The D_0 of the ground state is then calculated using thermochemical cycles, see Figure 5.(b) A two-laser variant of the method described in ref.[18], detection of the M^* dissociation product is performed on a "hot" level that is not populated in the cold supersonic jet environment.

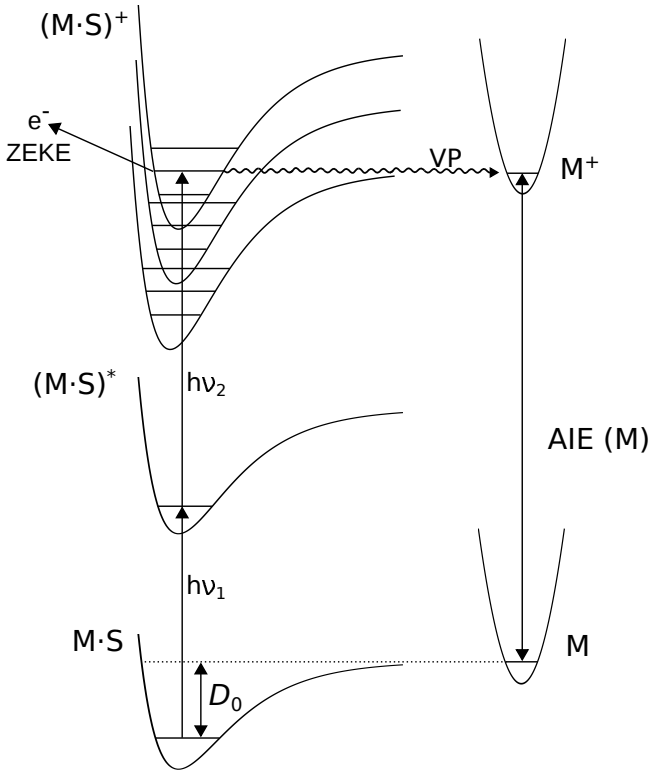

Figure 7: Determination of the ground-state dissociation energy D_0 of an M·S complex by dispersed appearance energy measurements, see section 3.2. Note that the energy of the departing photoelectron (not shown in the Figure9 is not measured but assumed to be zero near the $(M{\cdot}S)^+$ dissociation limit, which introduces considerable ambiguity in the measurement.

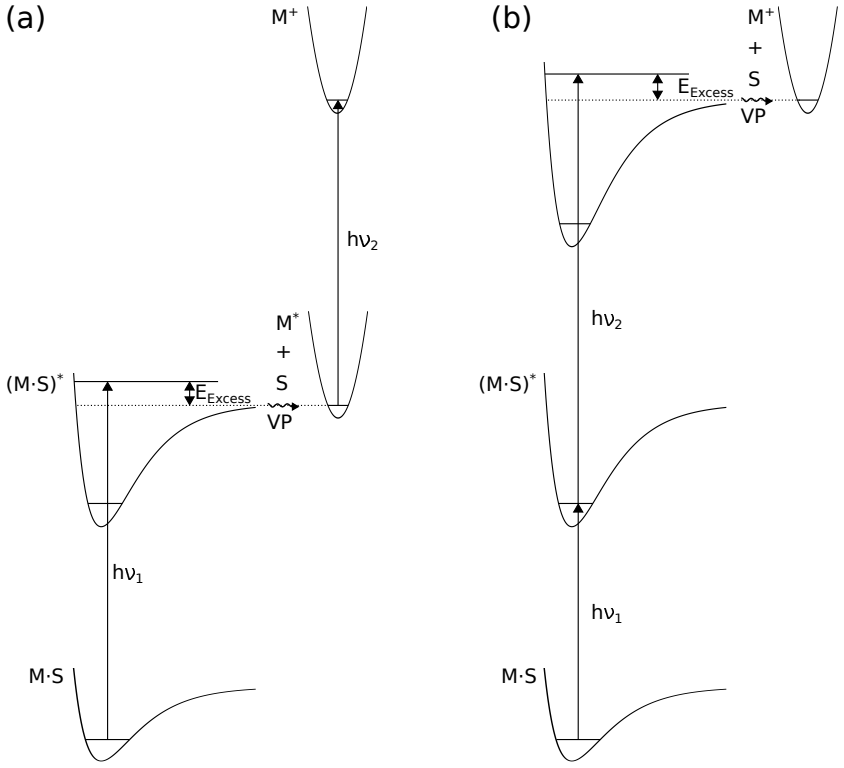

Figure 8: Determination of the dissociation energy in the (a) first excited or (b) ionic ground state using velocity map imaging (VMI). The excess energy E_{excess} is assumed to correspond to the highest measured translational energy E_{trans} of the detected ion fragment M^+. The D_0 of the ground state is then calculated using thermochemical cycles, see Figure 5.

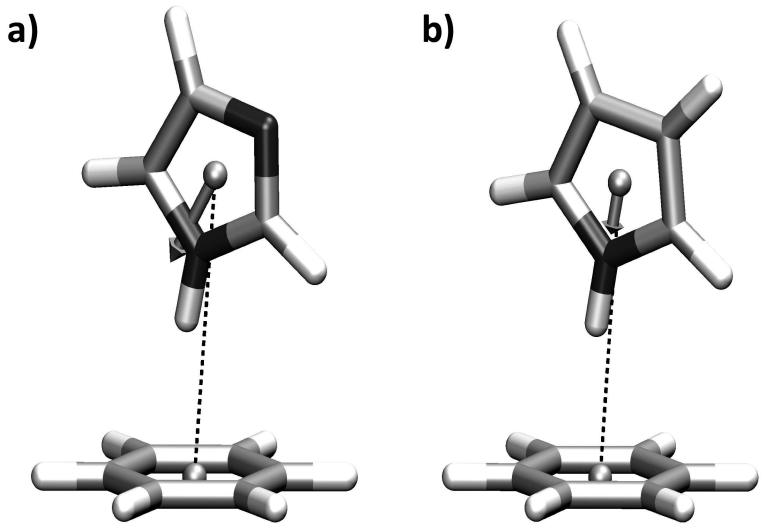

Figure 9: Optimized geometries of the (a) imidazole·benzene and (b) pyrrole·benzene complexes. $R_1 = 8.17\ a_0$ ($R_2 = 8.21\ a_0$) is the distance between the center-of-mass of the imidazole (pyrrole) molecule and the center-of-mass of the benzene molecule. The arrows represent the imidazole and pyrrole monomer dipoles ($2\mu/e$). Reprinted with permission from Ref. 110. Copyright 2014 Elsevier B.V.

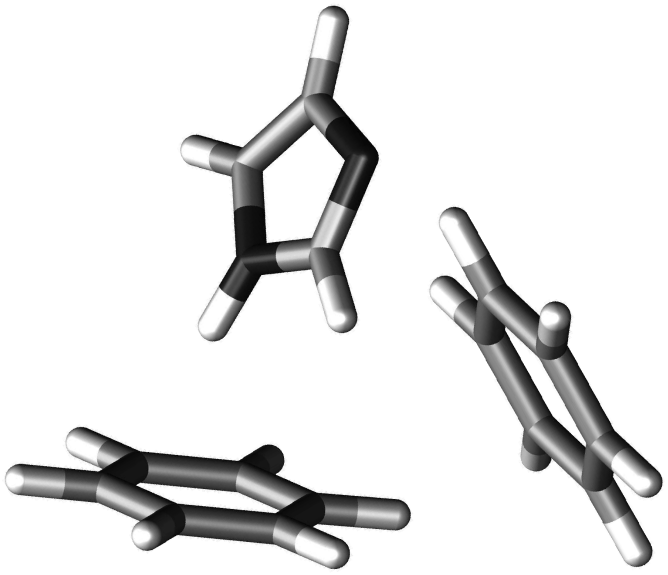

Figure 10: (Benzene)$_2$·imidazole trimer, for which harmonic vibrational frequencies have been computed at the SCS-CC2/def2-QZVPP level in the S_1 state.

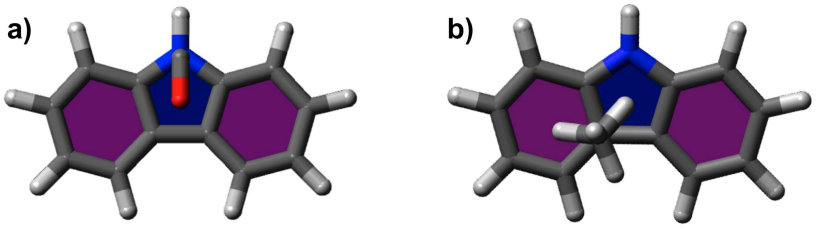

Figure 11: Optimized geometries of the (a) carbazole·CO and (b) carbazole·CH_4 complexes obtained at the SCS-CC2/aug-cc-pVTZ level.

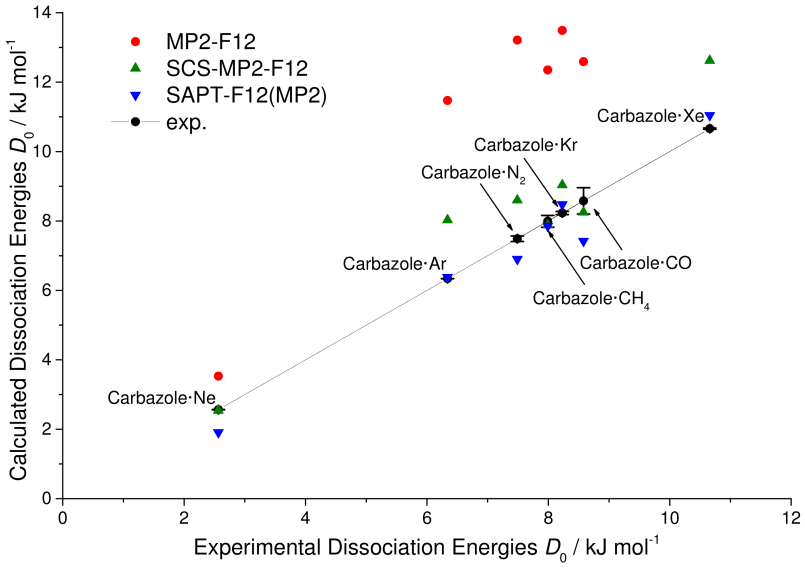

Figure 12: Comparison of experimental and calculated binding energies D_0 of carbazole·X complexes with X = Ne, Ar, Kr, Xe, CO, N_2, and CH_4. The MP2-F12 value for carbazole·Xe is 19.58 kJ/mol and not shown. Harmonic ZPVE from PBE-D3/def2-TZVP computations.

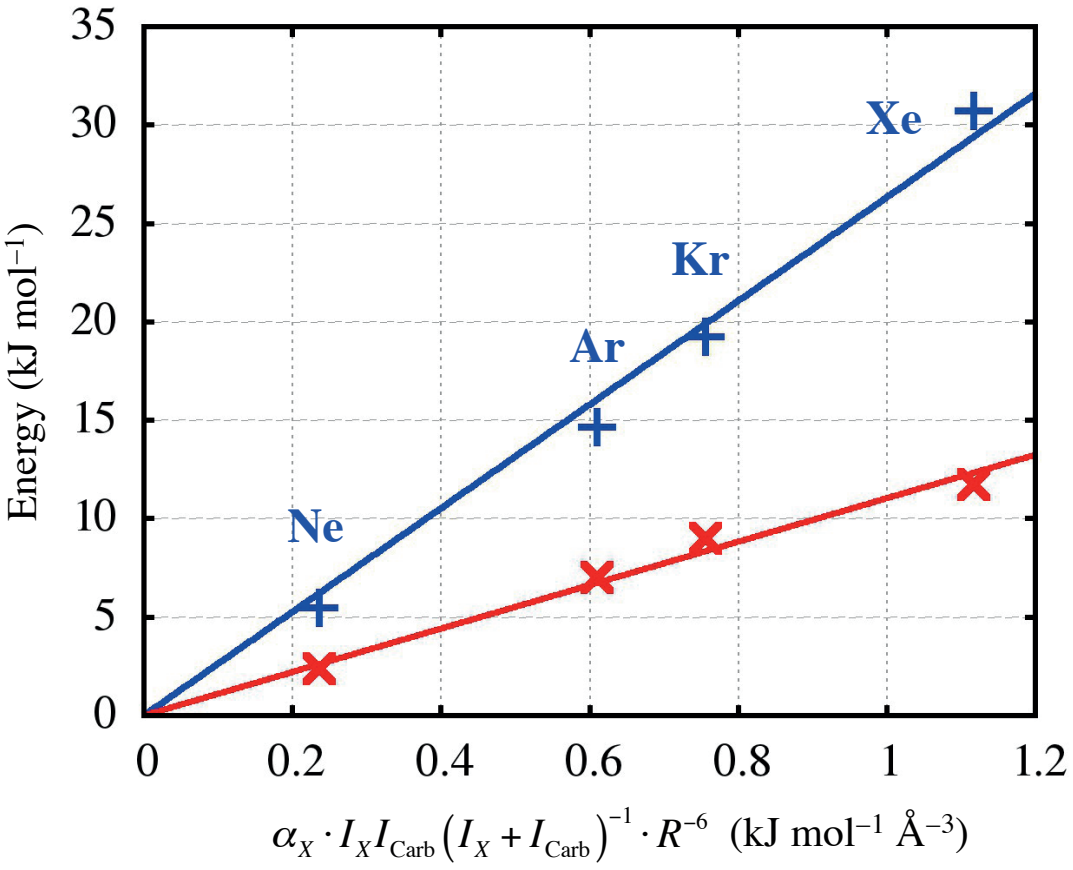

Figure 13: $E_{\mathrm{disp}}^{(2)}$ (blue points and line) and computed binding energy D_e (red points and line) of the carbazole complexes with X = Ne, Ar, Kr, Xe as function of the static polarizability α_{X}.

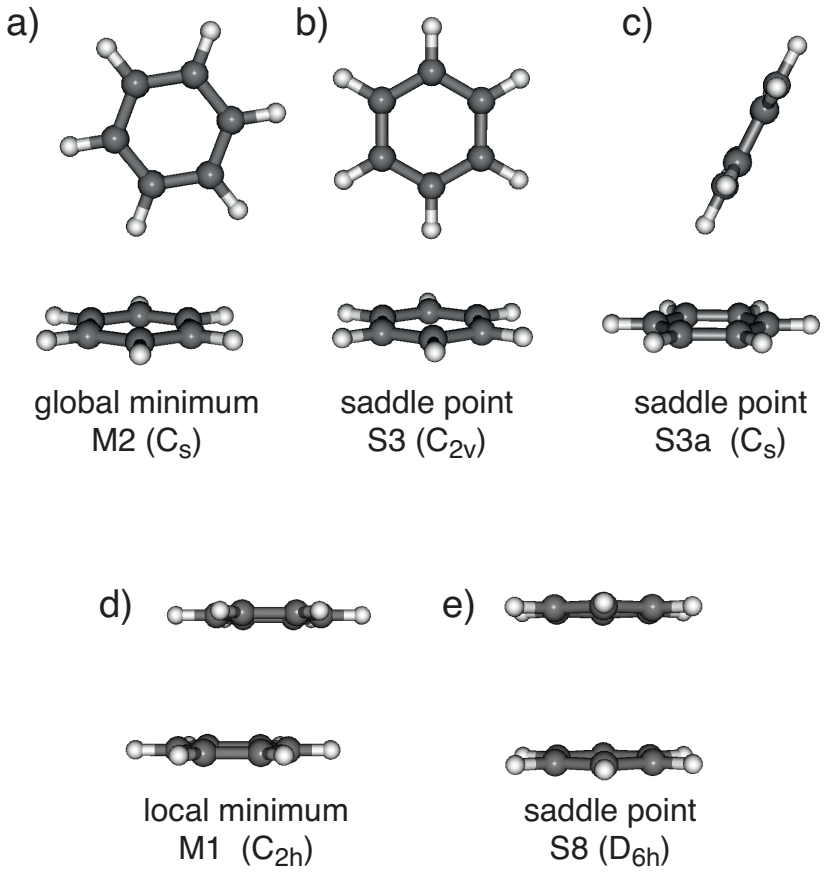

Figure 14: Neutral ground-state stationary points on the $(benzene)_2$ DFT-SAPT intermolecular PES: [233,234] (a) the tipped T-shaped global minimum **M2**, (b) the T-shaped C_{2v} saddle point **S3**, (c) the tilted T-shaped C_s saddle point **S3a**, (d) the parallel-displaced (C_{2h}) local minimum **M1**, (e) the stacked-parallel (D_{6h}) saddle point **S8**. Nomenclature as defined in Refs. 233 and 234.

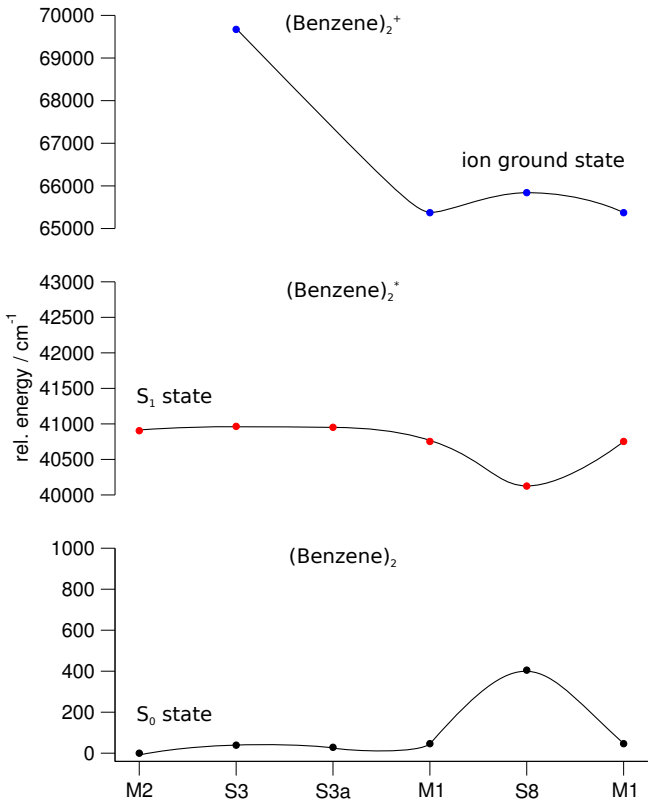

Figure 15: Calculated energies of (benzene)$_2$ in the S_0 state, S_1 state and Bz_2^+ ion ground state energies for the different T-shaped and π-stacked conformers shown in Figure 14. The energies of the different conformers are connected to indicate qualitative features of the S_0 (black), S_1 (red) and ion (blue) potential energy surfaces. The S_0 state energies of the **M2, S3, S3a, M1** and **S8** and $D_e(S_0)$ are from Ref. 234, the vertical SCS-CC2/aug-cc-pVTZ S_1 energies are from Ref. 263, the vertical and adiabatic EOM-CCSD energies are from Ref. 245.

Table 1: Dissociation energies D_0 (in kJ/mol) of neutral type I M·S complexes measured by pulsed-field ionization zero electronic kinetic energy (PFI-ZEKE) spectroscopy, photofragment angular distributions (PHOFAD), position-sensitive translational spectroscopy (POSTS), Doppler spectroscopy and velocity map imaging (VMI).

Complex	Method	Neutral D_0	Calc. D_e	Calc. D_0	Refs.
$(Ar)_2$	PFI-ZEKE	1.03			203
I_2·Ar T-shaped	VMI	2.88 ± 0.04			264
I_2·Ar linear	VMI	2.99 ± 0.03			264
$(H_2O)_2$	VMI	13.2 ± 0.11	20.8	13.2	211,213
$(D_2O)_2$	VMI	14.9 ± 0.12	20.8	14.9 ± 0.06	212,214
H_2O·NH_3	VMI	18.4 ± 0.12	27.0	17.6	265,266
$(NH_3)_2$	VMI	7.90 ± 0.24	13.8	7.91	217,267
$(HCl)_2$	POSTS	5.25 ± 0.01			268
$(HCl)_2$	PHOFAD	5.25 ± 0.1	8.30	5.09	269
H_2O·HCl	VMI	15.96 ± 0.12	23.01	16.12	216,270
$(HF)_2$	PHOFAD	12.70 ± 0.02	19.1	12.7	271,272
HF·DF	PHOFAD	12.94 ± 0.02	19.1	12.9	273,274
DF·HF	PHOFAD	13.84 ± 0.02	19.1	13.8	273,274
C_2H_2·HF	PHOFAD	13.0 ± 0.02			275
C_2H_2·HCl	PHOFAD	9.93 ± 0.07			276
C_2H_2·HCl	VMI	8.37			277
C_2H_2·NH_3	VMI	10.8			278
ortho-D_2·HF	PHOFAD	0.61 ± 0.02			279
para-D_2·HF	PHOFAD	0.81 ± 0.02			279
N_2·HF	PHOFAD	4.76 ± 0.02	9.12	4.98	280,281
CO_2·HF	PHOFAD	8.04 ± 0.5			282
HCN·HF	PHOFAD	23.6 ± 0.12			283
NO·HF	Doppler	5.36			284
$(NO)_2$	Doppler	8.49 ± 0.48			285
NO·CH_4	VMI	1.23 ± 0.02			286

Table 2: Selected ion and neutral dissociation energies D_0 (in kJ/mol) of dispersively bound type-II M·X complexes with X = Ar, Kr, measured by mass-analyzed threshold ionization (MATI), ion breakdown measurements (BM) two-color appearance potential (2C-AP), dispersed fluorescence (DIS) and velocity-map imaging (VMI).

Complex	Method	Ion D_0^+	Neutral D_0	Calc. D_e	Calc. D_0	Refs.
Benzene·Ar	BM	3.7 ± 0.6	1.6 ± 0.5			32
Benzene·Ar	MATI	< 6.1	< 4.1	4.62		26,221,287
Benzene·Ar	VMI	5.82 ± 0.06	3.77 ± 0.08			34
Benzene·Kr	MATI	< 7.6	< 4.8	5.80 -	-	26,287,288
s-Tetrazine·Ar	DIS		$3.0 - 4.3$	$4.9 - 5.0$		15,289
Fluorobenzene·Ar	MATI	6.5	3.84	4.68	4.05	30,290
p-Difluorobenzene·Ar	VMI	6.84 ± 0.07	4.03 ± 0.05	4.77	4.17	16,17,34,195
p-Difluorobenzene·Ar	DIS		$1.91 - 2.54$	4.81	4.20	291,292
p-Difluorobenzene·Kr	VMI	8.61 ± 0.07	4.75 ± 0.08			17
Phenylacetylene·Ar	-			5.01	4.40	194
Styrene·Ar	R2PI		4.7 ± 0.2			293
p-Xylene·Ar	2C-AP		1.4			294
Phenol·Ar	MATI	6.40 ± 0.06	4.35 ± 0.16	5.19	4.65	295
Phenol·Ar				5.02	4.44	296
p-Fluorotoluene·Ar	MATI	6.10 ± 0.24	3.94 ± 0.24			297
Anisole·Ar	MATI	6.95 ± 0.06	4.61 ± 0.06	5.48	4.64	298
Indole·Ar	MATI	6.4 ± 0.1	5.4 ± 0.2			33
Indole·Ar	DIS		< 6.5			299
1-Methylindole·Ar	DIS		$5.4 - 7.8$			300
Dibenzofuran·Ar	MATI	< 7.6	< 6.2			31
Dibenzo-*p*-dioxin·Ar	MATI	8.8 ± 0.1	6.3 ± 0.2			31
Dibenzo-*p*-dioxin·Ar	MATI	8.58	6.04			301
Dibenzo-*p*-dioxin·Kr	MATI	10.98	7.66			301
o-Dichlorobenzene·Ar	MATI	$6.04 - 7.85$	$3.48 - 5.29$			302
m-Dichlorobenzene·Ar	MATI	$4.83 - 7.81$	$2.65 - 5.63$			302
p-Dichlorobenzene·Ar	MATI	$6.90 - 7.85$	$4.90 - 5.85$			302

Table 3: Dissociation energies D_0 of dispersively bound type-II M·X and M·S complexes, measured by the stimulated-emission pumping/resonant two-photon ionization (SEP-R2PI) method, see Figure 4.

Complex	D_0 (kJ/mol)	Refs.
Carbazole·Ne	2.565 ± 0.004	38
Carbazole·Ar	6.339 ± 0.0017	38,43
Carbazole·Kr	8.230 ± 0.046	38
Carbazole·Xe	10.66 ± 0.02	38
Carbazole·N_2	7.49 ± 0.08	39
Carbazole·CO	8.58 ± 0.38	39
Carbazole·CH_4	7.99 ± 0.17	39
1-Naphthol·benzene	21.21 ± 0.25	41
1-Naphthol·benzene-d_6	21.25 ± 0.25	41
1-Naphthol·cyclohexane	28.95 ± 0.13	41

Table 4: PBE0AC-SAPT results (kJ/mol) obtained at the CCSD(F12)+(T*) optimized geometries of the ImBz and PyBz complexes (see Ref. 110 for details). The reference values are $\Delta E_2 = -22.8$ (ImBz) and -20.5 kJ/mol (PyBz). Data taken from Ref. 110.

Contribution[a]	aug-cc-pVDZ		aug-cc-pVTZ		aug-cc-pV(DT)Z[b]	
A=Im, Py	ImBz	PyBz	ImBz	PyBz	ImBz	PyBz
$E^{(1)}_{\text{pol}}$	−17.25	−14.94	−17.34	−15.05		
$E^{(1)}_{\text{exch}}$	23.22	21.69	23.14	21.63		
$E^{(2)}_{\text{ind}}$ (Bz→A)	−2.82	−2.53	−2.99	−2.68		
$E^{(2)}_{\text{ind}}$ (A→Bz)	−7.59	−6.17	−7.71	−6.34		
$E^{(2)}_{\text{exch-ind}}$ (A←Bz)	2.49	2.18	2.66	2.33		
$E^{(2)}_{\text{exch-ind}}$ (Bz←A)	3.74	3.22	3.81	3.33		
$E^{(2)}_{\text{disp}}$	−26.33	−25.53	−24.84	−24.39	−24.32	−24.01
$E^{(2)}_{\text{exch-disp}}$	3.24	3.08	3.13	3.02	3.10	3.00
δ(HF)	−2.89	−2.53	−2.95	−2.61		
Total (ΔE_2)	−24.18	−21.54	−23.08	−20.74		

a) $E^{(2)}_{\text{disp}}$ and $E^{(2)}_{\text{exch-disp}}$ have been scaled by the ratio of the corresponding CCSD(F12)+(T*) and CCSD(T) electron-correlation contributions to the counterpoise-corrected interaction energy ΔE_2^{cp}.

b) Two-point X^{-3} extrapolation from the aug-cc-pVDZ and aug-cc-pVTZ energies.

Table 5: DFT-D3(BJ) results. Interaction energy (ΔE_2 in kJ/mol, with and without counterpoise correction) of the ImBz and PyBz complexes at their CCSD(F12)+(T*) optimized geometries. All results were obtained in the aug-cc-pVTZ basis. The reference values are $\Delta E_2 = -22.8$ (ImBz) and -20.5 kJ/mol (PyBz). Data taken from Ref. 110.

	ImBz		PyBz	
Method	w/o CP	w/CP	w/o CP	w/CP
PBE	−23.08	−22.24	−20.99	−20.16
PBE0	−24.35	−23.51	−21.91	−21.08
TPSS	−22.77	−21.93	−20.67	−19.86
TPSSh	−23.46	−22.59	−21.23	−20.39
B2PLYP	−27.31	−22.25	−25.00	−19.98
B2PLYP-F12	−26.18	−22.52	−23.84	−20.22
Frozen-core-B2PLYP	−24.66	−22.21	−22.40	−19.95
Frozen-core-B2PLYP-F12	−23.53	−22.48	−21.23	−20.19

Table 6: RPA results. Interaction energy (ΔE_2 in kJ/mol, with and without counterpoise correction) of the ImBz and PyBz complexes at their CCSD(F12)+(T*) optimized geometries. All results were obtained in the aug-cc-pVTZ basis. The reference values are $\Delta E_2 = -22.8$ (ImBz) and -20.5 kJ/mol (PyBz). Data taken from Ref. 110.

	ImBz		PyBz	
Method	w/o CP	w/CP	w/o CP	w/CP
dRPA(PBE)	−29.43	−19.34	−27.20	−17.09
dRPA(PBE)+F12	−21.79	−20.78	−19.36	−18.34
dRPA(PBE)(F12)	−22.29	−20.75	−19.87	−18.30

Table 7: MP2-F12, SCS-MP2-F12, and SAPT-F12(MP2) binding energies (D_0 in kJ/mol) obtained at SCS-CC2/aug-cc-pVTZ optimized geometries of the carbazole$\cdots$X complexes (X = Ne, Ar, Kr, Xe, CO, N_2, and CH_4). Harmonic ZPVE from PBE-D3/def2-TZVP computations.

Method	Ne	Ar	Kr	Xe	CO	N_2	CH_4
PBE-D3/def2-TZVP	2.23	5.45	7.19	9.34	9.18	7.79	7.20
SCS-CC2/aug-cc-pVTZ	1.00	5.42	7.39	9.42	7.19	6.78	6.55
MP2-F12	3.53	10.87	13.50	19.58	12.59	13.20	12.36
SCS-MP2-F12	2.54	7.43	9.05	12.62	8.25	8.60	7.88
SAPT-F12(MP2)	1.91	6.38	8.47	11.04	7.42	6.90	7.86
Experiment[38,39,43]	2.57	6.34	8.23	10.66	8.58	7.49	7.99
Exptl. error bar	$\pm$0.004	$\pm$0.002	$\pm$0.05	$\pm$0.02	$\pm$0.38	$\pm$0.08	$\pm$0.17

Table 8: Contributions (kJ/mol) to the PBE0AC-SAPT/aug-cc-pVTZ binding energies obtained at SCS-CC2/aug-cc-pVTZ optimized geometries of the carbazole$\cdots$X complexes (X = Ne, Ar, Kr, Xe, CO, N_2, and CH_4).

Contribution	Ne	Ar	Kr	Xe	CO	N_2	CH_4
$E_{\text{pol}}^{(1)}$	−1.33	−3.88	−5.75	−12.57	−7.12	−6.41	−6.01
$E_{\text{exch}}^{(1)}$	4.32	11.08	15.19	28.70	16.65	16.49	17.58
$E_{\text{ind}}^{(2)}$	−1.63	−5.14	−9.24	−22.39	−6.21	−5.66	−5.29
$E_{\text{exch-ind}}^{(2)}$	1.70	4.95	8.87	19.23	5.68	5.31	4.99
$E_{\text{disp}}^{(2)}$	−5.46	−14.66	−19.25	−30.74	−19.03	−18.84	−21.93
$E_{\text{exch-disp}}^{(2)}$	0.44	1.59	2.39	4.95	2.31	2.21	2.84
δ(HF)	−0.25	−0.63	−0.80	2.31	−1.23	−1.34	−0.99
ΔF12	−0.17	−0.32	−0.43	−1.26	−0.40	−0.38	−0.29
Total (ΔE_2)	−2.39	−7.01	−9.02	−11.76	−9.35	−8.62	−9.10
ΔE_1	0.00	0.03	0.05	0.14	0.16	0.11	0.12
ZPVE/PBE-D3	0.48	0.60	0.49	0.58	1.77	1.61	1.12
D_0 SAPT-F12(MP2)	1.91	6.38	8.47	11.04	7.42	6.90	7.86
D_0 Experiment[38,39,43]	2.57	6.34	8.23	10.66	8.58	7.49	7.99
Exptl. error bar	±0.004	±0.002	±0.05	±0.02	±0.38	±0.08	±0.17

Table 9: Selected ion and neutral dissociation energies D_0 (in kJ/mol) of dispersively bound aromatic M·S type-II complexes, measured by mass-analyzed threshold ionization (MATI), breakdown measurements (BM) two-color appearance potential (2C-AP), dispersed fluorescence (DIS) and velocity-map imaging (VMI).

Complex	Method	Ion D_0^+	Neutral D_0	Calc. D_e	Calc. D_0	Refs.
Benzene-h_6·CH_4	MATI	7.9 ± 0.2	4.5 ± 0.2	5.97	4.73	20
Benzene-d_6·CH_4	MATI	8.7 ± 1.0	5.5 ± 1.0	5.97	4.77	20
Benzene·ethene	2C-AP		5.9 ± 0.8	9.06	7.2	21
Benzene·acetylene	2C-AP		11.3 ± 0.8	11.5	10.0	21
Benzene·CH_2Cl_2	2C-AP	7.6–8.1	15.9 ± 0.8	18.7		22
Benzene·$CHCl_3$	2C-AP	7.6–9.7	21.8 ± 0.8	22.8		22
Benzene·N_2	BM		3.8 ± 0.3			32
Benzene·cyclohexane	BM		7.7 ± 2			32
Benzene·cyclohexane	2C-AP		11.3 ± 1.3			23
p-Difluorobenzene·benzene	BM		7.7 ± 2			25
p-Difluorobenzene·N_2	DIS		< 2.55			303
Anisole·benzene	DIS		$16.3 - 18.0$			255
Perylene·CO_2	DIS		<14.8			18
Perylene·ethylene	DIS		≈ 13.9			18
Indole·CH_4	DIS		< 9.02			299
Indole·benzene	MATI		21.8 ± 0.18		22.2	29,33
Indole·benzene-d_6	MATI		22.3 ± 0.18			29

Table 10: Selected ion and neutral dissociation energies D_0 (in kJ/mol) of dispersively bound M_2 and M·M' (type-III complexes) measured by Raman mass-analyzed threshold ionization (MATI), breakdown measurements (BM) two-color appearance potential (2C-AP), dispersed fluorescence (DIS) and velocity-map imaging (VMI).

Complex	Method	Ion D_0^+	Neutral D_0	Calc. D_e	Calc. D_0	Refs.
$(Benzene)_2$	Raman		$11.87-12.4$	11.7	10.4	234,235,247
	BM	63.7 ± 2	6.75 ± 1			25
	1C-AP	64.03 ± 4	10.0 ± 1.7			237
$(Naphthalene)_2$	BM	65.61	12.1	23.5		304,305
$(Anisole)_2$	VMI	73.5	47.0			36
	2C-AP	48.1 ± 2.4	21.5 ± 1.2	21.1 ± 0.2		37
$(Toluene)_2$	BM		14.5 ± 1	14.52		25,250
Benzene·toluene	BM		12.5 ± 1			25
(p-Difluorobenzene)$_2$	BM		8.7 ± 2			25

References

(1) Meyer, E. A.; Castellano, R. K.; Diederich, F. Interactions with Aromatic Rings in Chemical and Biological Recognition. *Angew. Chem. Int. Ed.* **2003**, *42*, 1210–1250.

(2) Hobza, P.; Müller-Dethlefs, K. *Non-Covalent Interactions: Theory and Experiment*; The Royal Society of Chemistry: Cambridge, 2009.

(3) London, F. Zur Theorie und Systematik der Molekularkräfte. *Z. Phys.* **1930**, *63*, 245–279.

(4) Mons, M.; Dimicoli, I.; Piuzzi, F. Gas Phase Hydrogen-Bonded Complexes of Aromatic Molecules: Photoionization and Energetics. *Int. Rev. Phys. Chem.* **2002**, *21*, 101–135.

(5) Hobza, P.; Havlas, Z. Blue-Shifting Hydrogen Bonds. *Chem. Rev.* **2000**, *100*, 4253–4264.

(6) Braun, J. E.; Mehnert, T.; Neusser, H. J. Binding Energy of van der Waals- and Hydrogen-bonded Clusters by Threshold Ionization Techniques. *Int. J. Mass. Spec.* **2000**, *203*, 1–18.

(7) Wormer, P. E. S.; van der Avoird, A. Intermolecular Potentials, Internal Motions, and Spectra of van der Waals and Hydrogen-Bonded Complexes. *Chem. Rev.* **2000**, *100*, 4109–4144.

(8) Topp, M. R. Dynamics and Structure of Aromatic Molecular van der Waals Complexes. *Int. Rev. Phys. Chem.* **1993**, *12*, 149–204.

(9) Haas, Y.; Kendler, S. Binding Energies of Aromatic 1:1 Hetero-Clusters in a Supersonic Jet. *Isr. J. Chem.* **1997**, *37*, 427–438.

(10) Haldar, S.; Gnanasekaran, R.; Hobza, P. A Comparison of Ab Initio Quantum-mechanical and Experimental D_0 Binding Energies of Eleven H-bonded and Eleven Dispersion-bound Complexes. *Phys. Chem. Chem. Phys.* **2015**, *17*, 26645–26652.

(11) Šponer, J.; Jurečka, P.; Hobza, P. Accurate Interaction Energies of Hydrogen-Bonded Nucleic Acid Base Pairs. *J. Am. Chem. Soc.* **2004**, *126*, 10142–10151.

(12) Baer, T.; Hase, W. L. *Unimolecular Reaction Dynamics*; Oxford University Press (Oxford, New York), 1996.

(13) Meot-Ner, M.; Hamlet, P.; Hunter, E. P.; Field, F. H. Bonding Energies in Association Ions of Aromatic Compounds. Correlations with Ionization Energies. *J. Am. Chem. Soc.* **1978**, *100*, 5466–5471.

(14) Blazy, J. A.; DeKoven, B. M.; Russell, T. D.; Levy, D. H. The Binding Energy of Iodine-Rare Gas van der Waals Molecules. *J. Chem. Phys.* **1980**, *72*, 2439–2444.

(15) Brumbaugh, D. V.; Kenny, J. E.; Levy, D. H. Vibrational Predissociation and Intramolecular Vibrational Relaxation in Electronically Excited s-Tetrazine-Argon van der Waals Complex. *J. Chem. Phys.* **1983**, *78*, 3415–3434.

(16) Bellm, S. M.; Gascooke, J. R.; Lawrance, W. D. The Dissociation Energy of van der Waals Complexes Determined by Velocity Map Imaging: Values for S_0 and S_1 p-Difluorobenzene-Ar and D_0 (p-Difluorobenzene-Ar). *Chem. Phy. Lett.* **2000**, *330*, 103–109.

(17) Bellm, S. M.; Moulds, R. J.; Lawrance, W. D. The Binding Energies of p-Difluorobenzene-Ar, Kr Measured by Velocity Map Imaging: Limitations of Dispersed Fluorescence in Determining Binding Energies. *J. Chem. Phys.* **2001**, *115*, 10709–10717.

(18) Wittmeyer, S. A.; Topp, M. R. Hot-Band Spectroscopy of Ground-State Levels of Perylene Following Predissociation of van der Waals Complexes. *J. Phys. Chem.* **1993**, *97*, 8718–8726.

(19) Tsuzuki, S.; Honda, K.; Uchimaru, T.; Mikami, M.; Fujii, A. Magnitude and Directionality of the Interaction of the Aliphatic CH/pi Interaction: Significant Difference from Hydrogen Bond. *J. Phys. Chem. A* **2006**, *110*, 10163–10168.

(20) Shibasaki, K.; Fujii, A.; Mikami, N.; Tsuzuki, S. Magnitude of the CH/pi Interaction in the

Gas Phase: Experimental and Theoretical Determination of the Accurate Interaction Energy in Benzene-Methane. *J. Phys. Chem. A* **2006**, *110*, 4397–4404.

(21) Shibasaki, K.; Fujii, A.; Mikami, N.; Tsuzuki, S. Magnitude and Nature of Interactions in Benzene-X (X= Ethylene and Acetylene) in the Gas Phase: Significantly Different CH/pi Interaction of Acetylene As Compared with Those of Ethylene and Methane. *J. Phys. Chem. A* **2007**, *111*, 753–758.

(22) Tsuzuki, S.; Fujii, A. Nature and Physical Origins of CH/pi Interaction: Significant Difference from Conventional Hydrogen Bonds. *Phys. Chem. Chem. Phys.* **2008**, *10*, 2584–2594.

(23) Fujii, A.; Hayashi, H.; Park, J. W.; Kazama, T.; Mikami, N.; Tsuzuki, S. Experimental and Theoretical Determination of the Accurate CH/pi Interaction Energies in Benzene-Alkane Clusters: Correlation between Interaction Energy and Polarizability. *Phys. Chem. Chem. Phys.* **2011**, *13*, 14131–14141.

(24) Kiermeier, A.; Ernstberger, B.; Neusser, H. J.; Schlag, E. W. Multiphoton Mass Spectrometry of Clusters: Dissociation Kinetics of the Benzene Cluster Ions. *J. Phys. Chem.* **1988**, *92*, 3785–3789.

(25) Ernstberger, B.; Krause, H.; Kiermeier, A.; Neusser, H. J. Multiphoton Ionization and Dissociation of Mixed van der Waals Clusters in a Linear Reflectron Time-of-flight Mass Spectrometer. *J. Chem. Phys* **1990**, *92*, 5285–5296.

(26) Krause, H.; Neusser, H. J. Dissociation of State-Selected Complex-Ions Studied by Mass-selective Pulsed Field Threshold Ionization Spectroscopy. *J. Chem. Phys.* **1992**, *97*, 5923–5926.

(27) Krause, H.; Neusser, H. J. Dissociation-energy of Neutral and Ionic Benzene-Noble Gas Dimers by Pulsed-Field Threshold Ionization Spectroscopy. *J. Chem. Phys.* **1993**, *99*, 6278–6286.

(28) Neusser, H. J.; Krause, H. Binding Energy and Structure of van der Waals Complexes of Benzene. *Chem. Rev.* **1994**, *94*, 1829–1843.

(29) Braun, J.; Neusser, H. J.; Hobza, P. NH$\cdots\pi$ Interactions in Indole·benzene and Indole·benzene-h_6, d_6 Radical Cation Complexes, Mass Analyzed Threshold Ionization Experiments and Correlated ab Initio Quantum Chemical Calculations. *J. Phys. Chem. A* **2003**, *107*, 3918–3924.

(30) Grebner, T. L.; Neusser, H. J. Vibrational Spectroscopy of Molecular and van der Waals Complex Cations by Mass Analyzed Pulsed Field Threshold Ionization Spectroscopy. *Int. J. Mass Spectrom. Ion Processes* **1996**, *159*, 137–152.

(31) Grebner, T. L.; Stumpf, R.; Neusser, H. J. Mass Analyzed Threshold Ionization of van der Waals Complexes: Binding Energies of Dibenzofuran·Ar and Dibenzo-p-dioxin·Ar. *Int. J. Mass Spectrom. Ion Processes* **1997**, *167/168*, 649–660.

(32) Ernstberger, B.; Krause, H.; Neusser, H. Metastable Decay and Binding Energies of van der Waals Cluster Ions. *Z. Angew. Phys. D* **1991**, *20*, 189–192.

(33) Braun, J. E.; Grebner, T. L.; Neusser, H. J. Van der Waals versus Hydrogen-bonding in Complexes of Indole with Argon, Water, and Benzene by Mass-analyzed Pulsed Field Threshold Ionization. *J. Phys. Chem. A* **1998**, *102*, 3273–3278.

(34) Sampson, R. K.; Lawrance, W. D. The Dissociation Energy of the Benzene-Argon van der Waals Complex Determined by Velocity Map Imaging. *Aust. J. Chem.* **2003**, *56*, 275–277.

(35) Bellm, S. M.; Moulds, R. J.; van Leeuwen, M. P.; Lawrance, W. D. A Velocity Map ion Imaging Study of Difluorobenzene-Water Complexes: Binding Energies and Recoil Distributions. *J. Chem. Phys.* **2008**, *128*, 114314.

(36) Mazzoni, F.; Pasquini, M.; Pietraperzia, G.; Becucci, M. Binding Energy Determination in

a pi-stacked Aromatic Cluster: The Anisole Dimer. *Phys. Chem. Chem. Phys.* **2013**, *15*, 11268–11274.

(37) Řezáč, J.; Nachtigallová, D.; Mazzoni, F.; Pasquini, M.; Pietraperzia, G.; Becucci, M.; Müller-Dethlefs, K.; Hobza, P. Binding Energies of the pi-Stacked Anisole Dimer: New Molecular Beam-Laser Spectroscopy Experiments and CCSD(T) Calculations. *Chem. Eur. J.* **2015**, *21*, 6740–6746.

(38) Droz, T.; Bürgi, T.; Leutwyler, S. Van der Waals Binding Energies and Intermolecular Vibrations of Carbazole-R (R=Ne, Ar, Kr, Xe). *J. Chem. Phys.* **1995**, *103*, 4035–4045.

(39) Bürgi, T.; Droz, T.; Leutwyler, S. Binding Energies of Carbazole-S van der Waals Complexes (S = N_2, CO, and CH_4). *J. Chem. Phys.* **1995**, *103*, 7228–7239.

(40) Bürgi, T.; Droz, T.; Leutwyler, S. Accurate Hydrogen-Bonding Energies Betweeen 1-Naphthol and Water, Methanol and Ammonia. *Chem. Phys. Lett.* **1995**, *246*, 291–299.

(41) Wickleder, C.; Droz, T.; Bürgi, T.; Leutwyler, S. Accurate Intermolecular Binding Energies of 1-Naphthol to Benzene and Cyclohexane. *Chem. Phys. Lett.* **1997**, *264*, 257–264.

(42) Dai, H.-L.; Field, R. W. *Molecular Dynamics and Spectroscopy by Stimulated Emission Pumping*; World Scientific, Singapore, 1995.

(43) Bürgi, T.; Droz, T.; Leutwyler, S. Ground-State Binding Energy and Vibrations of the Carbazole-Ar van der Waals Complex by Pump/Dump-R2PI Measurements. *Chem. Phys. Lett.* **1994**, *225*, 351–358.

(44) Wickleder, C.; Henseler, D.; Leutwyler, S. Accurate Dissociation Energies of O-H$\cdots$O hydrogen-bonded 1-Naphthol Solvent Complexes. *J. Chem. Phys.* **2002**, *116*, 1850–1857.

(45) Riley, K. E.; Pitoňák, M.; Jurečka, P.; Hobza, P. Stabilization and Structure Calculations for Noncovalent Interactions in Extended Molecular Systems Based on Wave Function and Density Functional Theories. *Chem. Rev.* **2010**, *110*, 5023–5063.

(46) Hobza, P. Calculations on Noncovalent Interactions and Databases of Benchmark Interaction Energies. *Acc. Chem. Res.* **2012**, *45*, 663–672.

(47) Soydaş, E.; Bozkaya, U. Accurate Open-Shell Noncovalent Interaction Energies from the Orbital-Optimized Mø ller-Plesset Perturbation Theory: Achieving CCSD Quality at the MP2 Level by Orbital Optimization. *J. Chem. Theory Comput.* **2013**, *9*, 4679–4683.

(48) Bozkaya, U.; Sherrill, C. D. Orbital-optimized MP2.5 and its Analytic Gradients: Approaching CCSD(T) Quality for Noncovalent Interactions. *J. Chem. Phys.* **2014**, *141*, 204105.

(49) Pirani, F.; Maciel, G. S.; Cappelletti, D.; Aquilanti, V. Experimental Benchmarks and Phenomenology of Interatomic Forces: Open-Shell and Electronic Anisotropy Effects. *Int. Rev. Phys. Chem.* **2006**, *25*, 165–199.

(50) Hapka, M.; Żuchowski, P. S.; Szczęśniak, M. M.; Chałasiński, G. Symmetry-adapted Perturbation Theory based on Unrestricted Kohn-Sham Orbitals for High-spin Open-shell van der Waals complexes. *J. Chem. Phys.* **2012**, *137*, 164104.

(51) Neiss, C.; Hättig, C.; Klopper, W. Extensions of R12 Corrections to CC2-R12 for Excited States. *J. Chem. Phys.* **2006**, *125*, 064111.

(52) Neiss, C.; Hättig, C. Frequency-Dependent Nonlinear Optical Properties with Explicitly Correlated Coupled-Cluster Response Theory Using the CCSD(R12) Model. *J. Chem. Phys.* **2007**, *126*, 154101.

(53) Köhn, A. A Modified Ansatz for Explicitly Correlated Coupled-cluster Wave Functions that is Suitable for Response Theory. *J. Chem. Phys.* **2009**, *130*, 104104.

(54) Hanauer, M.; Köhn, A. Response Properties with Explicitly Correlated Coupled-cluster Methods using a Slater-type Correlation Factor and Cusp Conditions. *J. Chem. Phys.* **2009**, *131*, 124118.

(55) Pople, J. A.; Head-Gordon, M.; Raghavachari, K. Quadratic Configuration Interaction. A General Technique for Determining Electron Correlation Energies. *J. Chem. Phys.* **1987**, *87*, 5968–5975.

(56) Raghavachari, K.; Trucks, G. W.; Pople, J. A.; Head-Gordon, M. A Fifth-Order Perturbation Comparison of Electron Correlation Theories. *Chem. Phys. Lett.* **1989**, *157*, 479–483.

(57) Lee, T. J.; Rendell, A. P.; Taylor, P. R. Comparison of the Quadratic Configuration Interaction and Coupled-cluster Approaches to Electron Correlation Including the Effect of Triple Excitations. *J. Phys. Chem.* **1990**, *94*, 5463–5468.

(58) Bartlett, R. J. Coupled-cluster Theory and its Equation-of-motion Extensions. *WIREs Comput. Mol. Sci.* **2012**, *2*, 126–138.

(59) Cremer, D. From Configuration Interaction to Coupled-cluster Theory: The Quadratic Configuration Interaction Approach. *WIREs Comput. Mol. Sci.* **2013**, *3*, 482–503.

(60) Dunning, Jr., T. H. Gaussian Basis Sets for use in Correlated Molecular Calculations. I.The atoms Boron through Neon and Hydrogen. *J. Chem. Phys.* **1989**, *90*, 1007–1023.

(61) Kendall, R. A.; Dunning, Jr., T. H.; Harrison, R. J. Electron Affinities of the First-row Atoms Revisited. Systematic Basis Sets and Wave Functions. *J. Chem. Phys.* **1992**, *96*, 6796–6806.

(62) Raghavachari, K.; Saha, A. Accurate Composite and Fragment-Based Quantum Chemical Models for Large Molecules. *Chem. Rev.* **2015**, *115*, 5643–5677.

(63) Stoll, H. The Correlation Energy of Crystalline Silicon. *Chem. Phys. Lett.* **1992**, *191*, 548–552.

(64) Stoll, H. Correlation Energy of Diamond. *Phys. Rev. B* **1992**, *46*, 6700–6704.

(65) Shukla, A.; Dolg, M.; Fulde, P.; Stoll, H. Wave-Function-Based Correlated *Ab Initio* Calculations on Crystalline Solids. *Phys. Rev. B* **1999**, *60*, 5211–5216.

(66) Stoll, H.; Paulus, B.; Fulde, P. On the Accuracy of Correlation-Energy Expansions in Terms of Local Increments. *J. Chem. Phys.* **2005**, *123*, 144108.

(67) Li, S.; Shen, J.; Li, W.; Jiang, Y. An Efficient Implementation of the ¨Cluster-in-Molecule¨ Approach for Local Electron Correlation Calculations. *J. Chem. Phys.* **2006**, *125*, 074109.

(68) Li, W.; Piecuch, P.; Gour, J. R.; Li, S. Local Correlation Calculations using Standard and Renormalized Coupled-cluster Approaches. *J. Chem. Phys.* **2009**, *131*, 114109.

(69) Li, W.; Chen, C.; Zhao, D.; Li, S. LSQC: Low Scaling Quantum Chemistry Program. *Int. J. Quantum Chem.* **2015**, *115*, 641–646.

(70) Kitaura, K.; Ikeo, E.; Asada, T.; Nakano, T.; Uebayasi, M. Fragment Molecular Orbital Method: An Approximate Computational Method for Large Molecules. *Chem. Phys. Lett.* **1999**, *313*, 701–706.

(71) Fedorov, D. G.; Kitaura, K. Coupled-Cluster Theory based upon the Fragment Molecular-Orbital Method. *J. Chem. Phys.* **2005**, *123*, 134103.

(72) Hirata, S.; Valiev, M.; Dupuis, M.; Xantheas, S. S.; Sugiki, S.; Sekino, H. Fast Electron Correlation Methods for Molecular Clusters in the Ground and Excited States. *Mol. Phys.* **2005**, *103*, 2255–2265.

(73) Nakata, H.; Fedorov, D. G.; Nagata, T.; Kitaura, K.; Nakamura, S. Simulations of Chemical Reactions with the Frozen Domain Formulation of the Fragment Molecular Orbital Method. *J. Chem. Theory Comput.* **2015**, *11*, 3053–3064.

(74) Ziółkowski, M.; Jansík, B.; Kjærgaard, T.; Jørgensen, P. Linear Scaling Coupled Cluster Method with Correlation Energy Based Error Control. *J. Chem. Phys.* **2010**, *133*, 014107.

(75) Kristensen, K.; Ziółkowski, M.; Jansík, B.; Kjærgaard, T.; Jørgensen, P. A Locality Analysis of the Divide-Expand-Consolidate Coupled Cluster Amplitude Equations. *J. Chem. Theory Comput.* **2011**, *7*, 1677–1694.

(76) Høyvik, I.-M.; Kristensen, K.; Jansík, B.; Jørgensen, P. The Divide-Expand-Consolidate Family of Coupled-cluster Methods: Numerical Illustrations using Second order Møller-Plesset Perturbation Theory. *J. Chem. Phys.* **2012**, *136*, 014105.

(77) Dahlke, E. E.; Truhlar, D. G. Electrostatically Embedded Many-Body Correlation Energy, with Applications to the Calculation of Accurate Second-Order Møller-Plesset Perturbation Theory Energies for Large Water Clusters. *J. Chem. Theory Comput.* **2007**, *3*, 1342–1348.

(78) Bygrave, P. J.; Allan, N. L.; Manby, F. R. The Embedded Many-body Expansion for Energetics of Molecular Crystals. *J. Chem. Phys.* **2012**, *137*, 164102.

(79) Friedrich, J.; Yu, H.; Leverentz, H. R.; Bai, P.; Siepmann, J. I.; Truhlar, D. G. Water 26-mers Drawn from Bulk Simulations: Benchmark Binding Energies for Unprecedentedly Large Water Clusters and Assessment of the Electrostatically Embedded Three-Body and Pairwise Additive Approximations. *J. Phys. Chem. Lett.* **2014**, *5*, 666–670.

(80) Friedrich, J.; Hanrath, M.; Dolg, M. Fully Automated Implementation of the Incremental Scheme: Application to CCSD Energies for Hydrocarbons and Transition Metal Compounds. *J. Chem. Phys.* **2007**, *126*, 154110.

(81) Friedrich, J.; Tew, D. P.; Klopper, W.; Dolg, M. Automated Incremental Scheme for Explicitly Correlated Methods. *J. Chem. Phys.* **2010**, *132*, 164114.

(82) Friedrich, J.; Walczak, K. Incremental CCSD(T)(F12)|MP2-F12: A Method to Obtain Highly Accurate CCSD(T) Energies for Large Molecules. *J. Chem. Theory Comput.* **2013**, *9*, 408–417.

(83) Friedrich, J.; Hänchen, J. Incremental CCSD(T)(F12*)|MP2: A Black Box Method To Obtain Highly Accurate Reaction Energies. *J. Chem. Theory Comput.* **2013**, *9*, 5381–5394.

(84) Pulay, P. Localizability of Dynamic Electron Correlation. *Chem. Phys. Lett.* **1983**, *100*, 151–154.

(85) Hampel, C.; Werner, H.-J. Local Treatment of Electron Correlation in Coupled-cluster Theory. *J. Chem. Phys.* **1996**, *104*, 6286–6297.

(86) Schütz, M.; Werner, H.-J. Local Perturbative Triples Correction (T) with Linear Cost Scaling. *Chem. Phys. Lett.* **2000**, *318*, 370–378.

(87) Schütz, M. Low-Order Scaling Local Electron Correlation Methods. III. Linear Scaling Local Perturbative Triples Correction (T). *J. Chem. Phys.* **2000**, *113*, 9986–10001.

(88) Schütz, M.; Werner, H.-J. Low-Order Scaling Local Electron Correlation Methods. IV. Linear Scaling Local Coupled-Cluster (LCCSD). *J. Chem. Phys.* **2001**, *114*, 661–681.

(89) Werner, H.-J.; Schütz, M. An Efficient Local Coupled Cluster Method for Accurate Thermochemistryof Large Systems. *J. Chem. Phys.* **2011**, *135*, 144116.

(90) Masur, O.; Usvyat, D.; Schütz, M. Efficient and Accurate Treatment of Weak Pairs in Local CCSD(T) Calculations. *J. Chem. Phys.* **2013**, *139*, 164116.

(91) Schütz, M.; Masur, O.; Usvyat, D. Efficient and Accurate Treatment of Weak Pairs in Local CCSD(T) Calculations. II. Beyond the Ring Approximation. *J. Chem. Phys.* **2014**, *140*, 244107.

(92) Schwilk, M.; Usvyat, D.; Werner, H.-J. Communication: Improved Pair Approximations in Local Coupled-Cluster Methods. *J. Chem. Phys.* **2015**, *142*, 121102.

(93) Neese, F.; Wennmohs, F.; Hansen, A. Efficient and Accurate Local Approximations to Coupled-Electron Pair Approaches: An Attempt to Revive the Pair Natural Orbital Method. *J. Chem. Phys.* **2009**, *130*, 114108.

(94) Neese, F.; Hansen, A.; Liakos, D. G. Efficient and Accurate Approximations to the Local Coupled Cluster Singles Doubles Method Using a Truncated Pair Natural Orbital Basis. *J. Chem. Phys.* **2009**, *131*, 064103.

(95) Liakos, D. G.; Hansen, A.; Neese, F. Weak Molecular Interactions Studied with Parallel Implementations of the Local Pair Natural Orbital Coupled Pair and Coupled Cluster Methods. *J. Chem. Theory Comput.* **2011**, *7*, 76–87.

(96) Riplinger, C.; Neese, F. An Efficient and Near Linear Scaling Pair Natural Orbital Based Local Coupled Cluster Method. *J. Chem. Phys.* **2013**, *138*, 034106.

(97) Riplinger, C.; Sandhoefer, B.; Hansen, A.; Neese, F. Natural Triple Excitations in Local Coupled Cluster Calculations with Pair Natural Orbitals. *J. Chem. Phys.* **2013**, *139*, 134101.

(98) Rolik, Z.; Szegedy, L.; Ladjánszki, I.; Ladóczki, B.; Kállay, M. An Efficient Linear-Scaling CCSD(T) Method Based on Local Natural Orbitals. *J. Chem. Phys.* **2013**, *139*, 094105.

(99) Řezáč, J.; Riley, K. E.; Hobza, P. S66: A Well-balanced Database of Benchmark Interaction Energies Relevant to Biomolecular Structures. *J. Chem. Theory Comput.* **2011**, *7*, 2427–2438.

(100) Řezáč, J.; Riley, K. E.; Hobza, P. Erratum to ' S66: A Well-balanced Database of Benchmark Interaction Energies Relevant to Biomolecular Structures '. *J. Chem. Theory Comput.* **2014**, *10*, 1359–1360.

(101) Schmitz, G.; Hättig, C.; Tew, D. P. Explicitly Correlated PNO-MP2 and PNO-CCSD and Their Application to the S66 Set and Large Molecular Systems. *Phys. Chem. Chem. Phys.* **2014**, *16*, 22167–22178.

(102) Liakos, D. G.; Sparta, M.; Kesharwani, M. K.; Martin, J. M. L.; Neese, F. Exploring the Accuracy Limits of Local Pair Natural Orbital Coupled-Cluster Theory. *J. Chem. Theory Comput.* **2015**, *11*, 1525–1539.

(103) Liakos, D. G.; Neese, F. Domain Based Pair Natural Orbital Coupled Cluster Studies on Linear and Folded Alkane Chains. *J. Chem. Theory Comput.* **2015**, *11*, 2137–2143.

(104) Adler, T. B.; Werner, H.-J. An Explicitly Correlated Local Coupled Cluster Method for Calculations of Large Molecules Close to the Basis Set Limit. *J. Chem. Phys.* **2011**, *135*, 144117.

(105) Tew, D. P.; Helmich, B.; Hättig, C. Local Explicitly Correlated Second-Order Møller-Plesset Perturbation Theory with Pair Matural Orbitals. *J. Chem. Phys.* **2011**, *135*, 074107.

(106) Hättig, C.; Tew, D. P.; Helmich, B. Local Explicitly Correlated Second- and Third-order Møller-Plesset Perturbation Theory with Pair Natural Orbitals. *J. Chem. Phys.* **2012**, *136*, 204105.

(107) Krause, C.; Werner, H.-J. Comparison of Explicitly Correlated Local Coupled-cluster Methods with various Choices of Virtual Orbitals. *Phys. Chem. Chem. Phys.* **2012**, *14*, 7591–7604.

(108) Pavošević, F.; Neese, F.; Valeev, E. F. Geminal-Spanning Orbitals make Explicitly Correlated Reduced-Scaling Coupled-Cluster Methods Robust, Yet Simple. *J. Chem. Phys.* **2014**, *141*, 054106.

(109) Harding, M. E.; Klopper, W. Benchmarking the Lithium-Thiophene Complex. *ChemPhysChem* **2013**, *14*, 708–715.

(110) Ahnen, S.; Hehn, A.-S.; Vogiatzis, K. D.; Trachsel, M. A.; Leutwyler, S.; Klopper, W. Accurate Computations of the Structures and Binding Energies of the Imidazolebenzene and Pyrrolebenzene Complexes. *Chem. Phys.* **2014**, *441*, 17–22.

(111) Fliegl, H.; Klopper, W.; Hättig, C. Coupled-cluster Theory with Simplified Linear-R12 Corrections: The CCSD(R12) Model. *J. Chem. Phys.* **2005**, *122*, 084107.

(112) Ten-no, S.; Noga, J. Explicitly Correlated Electronic Structure Theory from R12/F12 Ansätze. *WIREs Comput. Mol. Sci.* **2012**, *2*, 114–125.

(113) Kong, L.; Bischoff, F. A.; Valeev, E. F. Explicitly Correlated R12/F12 Methods for Electronic Structure. *Chem. Rev.* **2012**, *112*, 75–107.

(114) Hättig, C.; Klopper, W.; Köhn, A.; Tew, D. P. Explicitly Correlated Electrons in Molecules. *Chem. Rev.* **2012**, *112*, 4–74.

(115) Knizia, G.; Adler, T. B.; Werner, H.-J. Simplified CCSD(T)-F12 Methods: Theory and Benchmarks. *J. Chem. Phys.* **2009**, *130*, 054104.

(116) van Duijneveldt, F. B.; van Duijneveldt-van de Rijdt, J. G. C. M.; van Lenthe, J. H. State of the Art in Counterpoise Theory. *Chem. Rev.* **1994**, *94*, 1873–1885.

(117) Burns, L. A.; Marshall, M. S.; Sherrill, C. D. Comparing Counterpoise-Corrected, Uncorrected, and Averaged Binding Energies for Benchmarking Noncovalent Interactions. *J. Chem. Theory Comput.* **2014**, *10*, 49–57.

(118) Leist, R.; Frey, J.; Ottiger, P.; Frey, H.-M.; Leutwyler, S.; Bachorz, R.; Klopper, W. Nucleobase-Fluorobenzene Interactions: Hydrogen Bonding Wins over π Stacking. *Angew. Chem. Int. Ed.* **2007**, *46*, 7449–7452.

(119) Pitoňák, M.; Neogrády, P.; Černý, J.; Grimme, S.; Hobza, P. Scaled MP3 Non-Covalent Interaction Energies Agree Closely with Accurate CCSD(T) Benchmark Data. *ChemPhysChem* **2009**, *10*, 282–289.

(120) Vogiatzis, K. D.; Klopper, W. Accurate Non-Covalent Interactions with Basis-Set Corrections from Interference-Corrected Perturbation Theory: Comparison with the S22B Database. *Mol. Phys.* **2013**, *111*, 2299–2305.

(121) Jurečka, P.; Šponer, J.; Černý, J.; Hobza, P. Benchmark Database of Accurate (MP2 and CCSD(T) Complete Basis Set Limit) Interaction Energies of Small Model Complexes, DNA Base Pairs, and Amino Acid Pairs. *Phys. Chem. Chem. Phys.* **2006**, *8*, 1985–1993.

(122) Marshall, M. S.; Burns, L. A.; Sherrill, C. D. Basis Set Convergence of the Coupled-cluster Correction, MP2CCSD(T): Best Practices for Benchmarking Non-covalent Interactions and the Attendant Revision of the S22, NBC10, HBC6, and HSG Databases. *J. Chem. Phys.* **2011**, *135*, 194102.

(123) Vogiatzis, K. D.; Klopper, W.; Friedrich, J. Non-Covalent Interactions of CO_2 with Functional Groups of Metal-Organic Frameworks from a CCSD(T) Scheme Applicable to Large Systems. *J. Chem. Theory Comput.* **2015**, *11*, 1574–1584.

(124) Halkier, A.; Helgaker, T.; Jørgensen, P.; Klopper, W.; Koch, H.; Olsen, J.; Wilson, A. K. Basis-set Convergence in Correlated Calculations on Ne, N_2, and H_2O. *Chem. Phys. Lett.* **1998**, *286*, 243–252.

(125) Halkier, A.; Helgaker, T.; Jørgensen, P.; Klopper, W.; Olsen, J. *Chem. Phys. Lett.* **1999**, *302*, 437–446.

(126) Sinnokrot, M. O.; Valeev, E. F.; Sherrill, C. D. Estimates of the Ab Initio Limit for π-π Interactions: The Benzene Dimer. *J. Am. Chem. Soc.* **2002**, *124*, 10887–10893.

(127) Schwenke, D. W. The Extrapolation of One-Electron Basis Sets in Electronic Structure Calculations: How it Should Work and How it Can Be Made to Work. *J. Chem. Phys.* **2005**, *122*, 014107.

(128) Sedlak, R.; Janowski, T.; Pitoňák, M.; Řezáč, J.; Pulay, P.; Hobza, P. Accuracy of Quantum Chemical Methods for Large Noncovalent Complexes. *J. Chem. Theory Comput.* **2013**, *9*, 3364–3374.

(129) Papajak, E.; Zheng, J.; Xu, X.; Leverentz, H. R.; Truhlar, D. G. Perspectives on Basis Sets Beautiful: Seasonal Plantings of Diffuse Basis Functions. *J. Chem. Theory Comput.* **2011**, *7*, 3027–3034.

(130) Grimme, S.; Goerigk, L.; Fink, R. F. Spin-component-scaled Electron Correlation Methods. *WIREs Comput. Mol. Sci.* **2012**, *2*, 886–906.

(131) Pfaffen, C.; Frey, H.-M.; Ottiger, P.; Leutwyler, S.; Bachorz, R. A.; Klopper, W. Large-Amplitude Vibrations of an NH-π Hydrogen Bonded cis-Amide-Benzene Complex. *Phys. Chem. Chem. Phys.* **2010**, *12*, 8208–8218.

(132) Ottiger, P.; Pfaffen, C.; Leist, R.; Leutwyler, S.; Bachorz, R. A.; Klopper, W. Strong NH$\cdots\pi$ Hydrogen Bonding in Amide-Benzene Interactions. *J. Phys. Chem. B* **2009**, *113*, 2937–2943.

(133) Bachorz, R. A.; Bischoff, F. A.; Hofener, S.; Klopper, W.; Ottiger, P.; Leist, R.; Frey, J. A.; Leutwyler, S. Scope and Limitations of the SCS-MP2 Method for Stacking and Hydrogen Bonding Interactions. *Phys. Chem. Chem. Phys.* **2008**, *10*, 2758–2766.

(134) Goerigk, L.; Grimme, S. Assessment of TD-DFT Methods and of Various Spin-scaled CIS(D) and CC2 Versions for the Treatment of Low-lying Valence Excitations of Large Organic Dyes. *J. Chem. Phys.* **2010**, *132*, 184103.

(135) Grimme, S.; Izgorodina, E. I. Calculation of 0âĂŞ0 Excitation Energies of Organic Molecules by CIS(D) Quantum Chemical Methods. *Chem. Phys.* **2004**, *305*, 223–230.

(136) Hättig, C. In *Response Theory and Molecular Properties (A Tribute to Jan Linderberg and Poul Jørgensen)*; Jensen, H. J. A., Ed.; Adv. Quantum Chem.; Academic Press, 2005; Vol. 50; pp 37–60.

(137) Rhee, Y. M.; Head-Gordon, M. Scaled Second-Order Perturbation Corrections to Configuration Interaction Singles: Efficient and Reliable Excitation Energy Methods. *J. Phys. Chem. A* **2007**, *111*, 5314–5326.

(138) Hellweg, A.; Grün, S. A.; Hättig, C. Benchmarking the Performance of Spin-component-

scaled CC2 in Ground and Electronically Excited States. *Phys. Chem. Chem. Phys.* **2008**, *10*, 4119–4127.

(139) Misquitta, A. J.; Szalewicz, K. Intermolecular Forces from Asymptotically Corrected Density Functional description of Monomers. *Chem. Phys. Lett.* **2002**, *357*, 301–306.

(140) Misquitta, A. J.; Jeziorski, B.; Szalewicz, K. Dispersion Energy from Density-Functional Theory Description of Monomers. *Phys. Rev. Lett.* **2003**, *91*, 033201.

(141) Misquitta, A. J.; Szalewicz, K. Symmetry-Adapted Perturbation-Theory Calculations of Intermolecular Forces employing Density-Functional Description of Monomers. *J. Chem. Phys.* **2005**, *122*, 214109.

(142) Jeziorski, B.; Moszynski, R.; Szalewicz, K. Perturbation Theory Approach to Intermolecular Potential Energy Surfaces of van der Waals Complexes. *Chem. Rev.* **1994**, *94*, 1887–1930.

(143) Szalewicz, K. Symmetry-Adapted Perturbation Theory of Intermolecular Forces. *WIREs Comput. Mol. Sci.* **2012**, *2*, 254–272.

(144) Jansen, G. Symmetry-adapted Perturbation Theory based on Density Functional Theory for Noncovalent Interactions. *WIREs Comput. Mol. Sci.* **2014**, *4*, 127–144.

(145) Lao, K. U.; Herbert, J. M. Accurate and Efficient Quantum Chemistry Calculations for Noncovalent Interactions in Many-Body Systems: The XSAPT Family of Methods. *J. Phys. Chem. A* **2015**, *119*, 235–252.

(146) Sherrill, C. D. Energy Component Analysis of π Interactions. *Acc. Chem. Res.* **2013**, *46*, 1020–1028.

(147) Misquitta, A. J.; Podeszwa, R.; Jeziorski, B.; Szalewicz, K. Intermolecular Potentials based on Symmetry-adapted Perturbation Theory with Dispersion Energies from Time-dependent Density-functional calculations. *J. Chem. Phys.* **2005**, *123*, 214103.

(148) Heßelmann, A.; Janssen, G. *Chem. Phys. Lett.* **2002**, *362*, 319–325.

(149) Heßelmann, A.; Janssen, G.; Schütz, M. Density-functional Theory-symmetry-adapted Intermolecular Perturbation Theory with Density Fitting: A new Efficient Method to Study Intermolecular Interaction Energies. *J. Chem. Phys.* **2005**, *122*, 014103.

(150) Perdew, J. P.; Ernzerhof, M.; Burke, K. Rationale for Mixing Exact Exchange with Density Functional Approximations. *J. Chem. Phys.* **1996**, *105*, 9982–9985.

(151) Grüning, M.; Gritsenko, O. V.; van Gisbergen, S. J. A.; Baerends, E. J. Shape Corrections to Exchange-correlation Potentials by Gradient-regulated Seamless Connection of Model Potentials for Inner and Outer Region. *J. Chem. Phys.* **2001**, *114*, 652–660.

(152) Grimme, S. Density Functional Theory with London Dispersion Corrections. *WIREs Comput. Mol. Sci.* **2011**, *1*, 211–228.

(153) Ehrlich, S.; Moellmann, J.; Grimme, S. Dispersion-Corrected Density Functional Theory for Aromatic Interactions in Complex Systems. *Acc. Chem. Res.* **2013**, *46*, 916–926.

(154) Tkatchenko, A.; Scheffler, M. Accurate Molecular van der Waals Interactions from Ground-State Electron Density and Free-Atom Reference Data. *Phys. Rev. Lett.* **2009**, *102*, 073005.

(155) Ferri, N.; DiStasio, Jr., R. A.; Ambrosetti, A.; Car, R.; Tkatchenko, A. Electronic Properties of Molecules and Surfaces with a Self-Consistent Interatomic van der Waals Density Functional. *Phys. Rev. Lett.* **2015**, *114*, 176802.

(156) Becke, A. D.; Johnson, E. R. Exchange-hole Dipole Moment and the Dispersion Interaction. *J. Chem. Phys.* **2005**, *122*, 154104.

(157) Becke, A. D.; Johnson, E. R. A Density-functional Model of the Dispersion Interaction. *J. Chem. Phys.* **2005**, *123*, 154101.

(158) Becke, A. D.; Johnson, E. R. Exchange-hole Dipole Moment and the Dispersion Interaction Revisited. *J. Chem. Phys.* **2007**, *127*, 154108.

(159) Toulouse, J.; Zhu, W.; Ángyán, J. G.; Savin, A. Range-Separated Density-Functional Theory with the Random-Phase Approximation: Detailed Formalism and Illustrative Applications. *Phys. Rev. A* **2010**, *82*, 032502.

(160) Zhu, W.; Toulouse, J.; Savin, A.; Ángyán, J. G. Range-Separated Density-Functional Theory with Random Phase Approximation Applied to Noncovalent Intermolecular Interactions. *J. Chem. Phys.* **2010**, *132*, 244108.

(161) Eshuis, H.; Bates, J. E.; Furche, F. Electron Correlation Methods based on the Random-phase Approximation. *Theor. Chem. Acc.* **2012**, *131*, 1084.

(162) Eshuis, H.; Furche, F. Basis Set Convergence of Molecular Correlation Energy Differences within the Random-phase Approximation. *J. Chem. Phys.* **2012**, *136*, 084105.

(163) Heßelmann, A.; Görling, A. On the Short-Range Behavior of Correlated Pair Functions from the Adiabatic-Connection Fluctuation-Dissipation Theorem of Density-Functional Theory. *J. Chem. Theory Comput.* **2013**, *9*, 4382–4395.

(164) Bleiziffer, P.; Heßelmann, A.; Görling, A. Efficient Self-consistent Treatment of Electron Correlation within the Random Phase Approximation. *J. Chem. Phys.* **2013**, *139*, 084113.

(165) Burow, A. M.; Bates, J. E.; Furche, F.; Eshuis, H. Analytical First-Order Molecular Properties and Forces within the Adiabatic Connection Random Phase Approximation. *J. Chem. Theory Comput.* **2014**, *10*, 180–194.

(166) Krause, K.; Klopper, W. Communication: Two-component Ring-coupled-cluster Computation of the Correlation Energy in the Random-phase Approximation. *J. Chem. Phys.* **2013**, *139*, 191102.

(167) Kühn, M. Correlation Energies from the Two-Component Random Phase Approximation. *J. Chem. Theory Comput.* **2014**, *10*, 623–633.

(168) Kállay, M. Linear-scaling Implementation of the Direct Random-phase Approximation. *J. Chem. Phys.* **2015**, *142*, 204105.

(169) Hehn, A.-S.; Klopper, W. Communication: Explicitly-correlated Second-order Correction to the Correlation Energy in the Random-phase Approximation. *J. Chem. Phys.* **2013**, *138*, 181104.

(170) Hehn, A.-S.; Tew, D. P.; Klopper, W. Explicitly Correlated Ring-coupled-cluster-doubles Theory. *J. Chem. Phys.* **2015**, *142*, 194106.

(171) Bates, J. E.; Furche, F. Communication: Random Phase Approximation Renormalized Many-body Perturbation Theory. *J. Chem. Phys.* **2013**, *139*, 171103.

(172) Grüneis, A.; Marsman, M.; Harl, J.; Schimka, L.; Kresse, G. Making the Random-phase Approximation to Electronic Correlation Accurate. *J. Chem. Phys.* **2009**, *131*, 154115.

(173) Ren, X.; Rinke, P.; Scuseria, G. E.; Scheffler, M. Renormalized Second-Order Perturbation Theory for the Electron Correlation energy: Concept, Implementation, and Benchmarks. *Phys. Rev. B* **2013**, *88*, 035120.

(174) Franck, O.; Mussard, B.; Luppi, E.; Toulouse, J. Basis Convergence of Range-separated Density-functional Theory. *J. Chem. Phys.* **2015**, *142*, 074107.

(175) Korth, M.; Pitoňák, M.; Řezáč, J.; Hobza, P. A Transferable H-Bonding Correction for Semiempirical Quantum-Chemical Methods. *J. Chem. Theory Comput.* **2010**, *6*, 344–352.

(176) Elstner, M.; Hobza, P.; Frauenheim, T.; Suhai, S.; Kaxiras, E. Hydrogen Bonding and Stacking Interactions of Nucleic Acid Base Pairs: A Density-functional Theory based Treatment. *J. Chem. Phys.* **2001**, *114*, 5149–5155.

(177) Brandenburg, J. G.; Grimme, S. Accurate Modeling of Organic Molecular Crystals by Dispersion-Corrected Density Functional Tight Binding (DFTB). *J. Phys. Chem. Lett.* **2014**, *5*, 1785–1789.

(178) Dubecký, M.; Jurečka, P.; Derian, R.; Hobza, P.; Otyepka, M.; Mitas, L. Quantum Monte Carlo Methods Describe Noncovalent Interactions with Subchemical Accuracy. *J. Chem. Theory Comput.* **2013**, *9*, 4287–4292.

(179) Dubecký, M.; Derian, R.; Jurečka, P.; Mitas, L.; Hobza, P.; Otyepka, M. Quantum Monte Carlo for Noncovalent Interactions: An Efficient Protocol Attaining Benchmark Accuracy. *Phys. Chem. Chem. Phys.* **2014**, *16*, 20915–20923.

(180) Řezáč, J.; Dubecký, M.; Jurečka, P.; Hobza, P. Extensions and Applications of the A24 Data Set of Accurate Interaction Energies. *Phys. Chem. Chem. Phys.* **2015**, *17*, 19268–19277.

(181) Gosling, M. P.; Cockett, M. C. R. Hydrogen-bonding in the Pyrimidine-NH_3 van der Waals Complex: Experiment and Theory. *Phys. Chem. Chem. Phys.* **2014**, *16*, 14195–14205.

(182) Cui, G.; Guan, P.-J.; Fang, W.-H. Photoinduced Proton Transfer and Isomerization in a Hydrogen-Bonded Aromatic Azo Compound: A CASPT2//CASSCF Study. *J. Phys. Chem. A* **2014**, *118*, 4732–4739.

(183) Huenerbein, R.; Grimme, S. Time-dependent Density Functional Study of Excimers and Exciplexes of Organic Molecules. *Chem. Phys.* **2008**, *343*, 362–371.

(184) Furche, F.; Ahlrichs, R.; Hättig, C.; Klopper, W.; Sierka, M.; Weigend, F. Turbomole. *WIREs Comput. Mol. Sci.* **2014**, *4*, 91–100.

(185) TURBOMOLE, Version 7.0, a Development of Universität Karlsruhe (TH) and Forschungszentrum Karlsruhe GmbH, 1989-2007, TURBOMOLE GmbH, since 2007. Available from `http://www.turbomole.com`.

(186) Weigend, F.; Furche, F.; Ahlrichs, R. Gaussian Basis Sets of Quadruple Zeta Valence Quality for Atoms H-Kr. *J. Chem. Phys.* **2003**, *119*, 12753–12762.

(187) Christiansen, O.; Stanton, J. F.; Gauss, J. A Coupled-cluster Study of the $^1A_{1g}$ and $^1B_{2u}$ States of Benzene. *J. Chem. Phys.* **1998**, *108*, 3987–4001.

(188) Kolmann, S. J.; D'Arcy, J. H.; Jordan, M. J. T. Quantum Effects and Anharmonicity in the H2-Li+-Benzene Complex: A Model for Hydrogen Storage Materials. *J. Chem. Phys.* **2013**, *139*, 234305.

(189) Mandziuk, M.; Bačić, Z. Van der Waals Vibrational States of Atom-Large Molecule Complexes by a 3D Discrete Variable Representation Method: Naphthalene-Ar. *J. Chem. Phys.* **1993**, *98*, 7165–7178.

(190) Mandziuk, M.; Bačić, Z.; Droz, T.; Leutwyler, S. Intermolecular Vibrations of the 2,3-Dimethylnaphthalene-Ar van der Waals complex: Experiment and Quantum Three-dimensional Calculations. *J. Chem. Phys.* **1994**, *100*, 52–62.

(191) Droz, T.; Leutwyler, S.; Mandziuk, M.; Bačić, Z. Intermolecular Vibrations of o-Xylene-Ar in the S_0 and S_1 States: Experiment and Quantum Three Dimensional Calculations. *J. Chem. Phys.* **1994**, *101*, 6412–6423.

(192) Droz, T.; Leutwyler, S.; Mandziuk, M.; Bačić, Z. Van der Waals Vibrations and Isomers of 2,3-Dimethylnaphthalene-Ne: Experiment and Quantum Three-Dimensional Calculations. *J. Chem. Phys.* **1995**, *103*, 4855–4868.

(193) Bach, A.; Leutwyler, S.; Sabo, D.; Bačić, Z. Very Large Amplitude Intermolecular Vibrations and Wave Function Delocalization in 2,3-Dimethylnaphthalene-He van der Waals Complex. *J. Chem. Phys.* **1997**, *107*, 8781–8793.

(194) Cybulski, H.; Fernández, B.; Henriksen, C.; Felker, P. M. Ab Initio Ground State Phenylacetylene–Argon Intermolecular Potential Energy Surface and Rovibrational Spectrum. *J. Chem. Phys.* **2012**, *137*, 074305.

(195) Cagide Fajín, J. L.; Fernández, B.; Felker, P. M. p-Difluorobenzene-Argon Ground State Intermolecular Potential Energy Surface. *J. Phys. Chem. A* **2005**, *109*, 11602–11608.

(196) Cagide Fajín, J. L.; Fernández, B.; Felker, P. M. The p-Difluorobenzene-Argon S_1 Excited State Intermolecular Potential Energy Surface. *J. Phys. Chem. A* **2006**, *110*, 13259–13263.

(197) Bettens, R. P. A.; Collins, M. A. Learning to Interpolate Molecular Potential Energy Surfaces with Confidence: A Bayesian Approach. *J. Chem. Phys.* **1999**, *111*, 816–826.

(198) Kalescky, R.; Kraka, E.; Cremer, D. Accurate Determination of the Binding Energy of the Formic Acid Dimer: The Importance of Geometry Relaxation. *J. Chem. Phys.* **2014**, *140*, 084315.

(199) Panek, P. T.; Jacob, C. R. Efficient Calculation of Anharmonic Vibrational Spectra of Large Molecules with Localized Modes. *ChemPhysChem* **2014**, *15*, 3365–3377.

(200) Pfeiffer, F.; Rauhut, G.; Feller, D.; Peterson, K. A. Anharmonic Zero Point Vibrational Energies: Tipping the Scales in Accurate Thermochemistry Calculations? *J. Chem. Phys.* **2013**, *138*, 044311.

(201) Weitzel, K.-M.; Mähnert, J. The Binding Energies of Small Ar_n, $(CO)_n$ and $(N_2)_n$ Cluster Ions. *Int. J. Mass Spectrom.* **2002**, *214*, 175–212.

(202) Colbourn, E. A.; Douglas, A. E. The Spectrum and Ground State Potential Curve of Ar_2. *J. Chem. Phys.* **1976**, *65*, 1741–1745.

(203) Herman, P. R.; LaRocque, P. E.; Stoicheff, B. P. Vacuum Ultraviolet Laser Spectroscopy. V. Rovibronic Spectra of Ar_2 and Constants of the Ground and Excited States. *J. Chem. Phys.* **1988**, *89*, 4535–4549.

(204) Signorell, R.; Merkt, F. The First Electronic States of Ar_2^+ Studied by High Resolution Photoelectron Spectroscopy. *J. Chem. Phys.* **1998**, *109*, 9762–9771.

(205) Signorell, R.; Wüst, A.; Merkt, F. The First Adiabatic Ionization Potential of Ar_2. *J. Chem. Phys.* **1997**, *107*, 10819–10822.

(206) Onuma, T.; Yoshii, H.; Ishijima, H.; Itou, Y.; Hayaishi, T.; Morioka, Y. Pulsed-Field Ionization Zero-Kinetic-Energy Photoelectron Spectra of Ar_2. *J. Mol. Spectrosc.* **1999**, *198*, 209–217.

(207) Signorell, R.; Hollenstein, U.; Merkt, F. High-Resolution Photoelectron Spectroscopic Study of the First Electronic States of Kr_2^+. *J. Chem. Phys.* **2001**, *114*, 9840–9851.

(208) Rupper, P.; Zehnder, O.; Merkt, F. Potential Energy Curves of Diatomic Molecular Ions from High-Resolution Photoelectron Spectra. II. The First Six Electronic States of Xe_2^+. *J. Chem. Phys.* **2004**, *121*, 8279–8290.

(209) Zehnder, O.; Merkt, F. The Low-Lying Electronic States of $KrXe^+$ and their Potential Energy Functions. *Mol. Phys.* **2008**, *106*, 1215–1226.

(210) Zehnder, O.; Merkt, F. The Low-Lying Electronic States of $ArXe^+$ and their Potential Energy Functions. *J. Chem. Phys.* **2008**, *128*, 014306.

(211) Rocher-Casterline, B. E.; Ch´ ng, L. C.; Mollner, A. K.; Reisler, H. Communication: Determination of the Bond Dissociation Energy (D_0) of the Water Dimer, $(H_2O)_2$, by Velocity Map Imaging. *J. Chem. Phys* **2011**, *134*, 211101.

(212) Ch´ng, L. C.; Samanta, A. K.; Czakó, G.; Bowman, J. M.; Reisler, H. Experimental and Theoretical Investigations of Energy Transfer and Hydrogen-Bond Breaking in the Water Dimer. *J. Am. Chem. Soc.* **2012**, *134*, 15430–15435.

(213) Shank, A.; Wang, Y.; Kaledin, A.; Braams, B. J.; Bowman, J. M. Accurate *ab initio* and "Hybrid" Potential Energy Surfaces, Intramolecular Vibrational Energies, and Classical IR Spectrum of the Water Dimer. *J. Chem. Phys.* **2009**, *130*, 144314.

(214) Czakó, G.; Wang, Y.; Bowman, J. M. Communication: Quasiclassical Trajectory Calculations of Correlated Product-state Distributions for the Dissociation of $(H_2O)_2$ and $(D_2O)_2$. *J. Chem. Phys* **2011**, *135*, 151102.

(215) Klopper, W.; van Duijneveldt-van de Rijdt, J. G. C. M.; van Duijneveldt, F. B. Computational Determination of Equilibrium Geometry and Dissociation Energy of the Water Dimer. *Phys. Chem. Chem. Phys.* **2000**, *2*, 2227–2234.

(216) Samanta, A. K.; Czakó, G.; Wang, Y.; Mancini, J. S.; Bowman, J. M.; Reisler, H. Experimental and Theoretical Investigations of Energy Transfer and Hydrogen-Bond Breaking in Small Water and HCl Clusters. *Acc. Chem. Res.* **2014**, *47*, 2700–2709.

(217) Case, A. S.; Heid, C. G.; Kable, S. H.; Crim, F. F. Dissociation Energy and Vibrational Predissociation Dynamics of the Ammonia Dimer. *J. Chem. Phys.* **2011**, *135*, 084312.

(218) Oudejans, L.; Miller, R. E. Photofragment Translational Spectroscopy of Weakly Bound Complexes: Probing the Interfragment Correlated Final State Distributions. *Annu. Rev. Phys. Chem.* **2001**, *52*, 607–637.

(219) Neusser, H. J.; Sussmann, R.; Smith, A. M.; Riedle, E.; Weber, T. High-Resolution UV Spectroscopy of Molecular Complexes. *Ber. Bunsenges. Phys. Chem.* **1992**, *96*, 1252–1259.

(220) Chewter, L. A.; Müller-Dethlefs, K.; Schlag, E. W. Determination of the Ionization Energy of the Benzene-Argon Complex by Zero Kinetic Energy Photoelectron Spectroscopy. *Chem. Phys. Lett.* **1987**, *135*, 219–222.

(221) Koch, H.; Fernández, B.; Makarewicz, J. Ground State Benzene-Argon Intermolecular Potential Energy Surface. *J. Chem. Phys.* **1999**, *111*, 198–204.

(222) Klopper, W.; Lüthi, H. P.; Brupbacher, T.; Bauder, A. Ab initio Computations close to the One-particle Basis Set Limit on the weakly bound van der Waals Complexes Benzene-Neon and Benzene-Argon. *J. Chem. Phys.* **1994**, *101*, 9747–9754.

(223) Peterson, K. A.; Adler, T. B.; Werner, H.-J. Systematically Convergent Basis Sets for Explicitly Correlated Wavefunctions: The atoms H, He, B-Ne, and Al-Ar. *J. Chem. Phys.* **2008**, *128*, 084102.

(224) Yousaf, K. E.; Peterson, K. A. Optimized Auxiliary Basis Sets for Explicitly Correlated Methods. *J. Chem. Phys.* **2008**, *129*, 184108.

(225) Hill, J. G.; Peterson, K. A. Correlation Consistent Basis Sets for Explicitly Correlated Wavefunctions: Pseudopotential-based Basis Sets for the post-d Main Group Elements Ga - Rn. *J. Chem. Phys.* **2014**, *141*, 094106.

(226) Bachorz, R. A.; Bischoff, F. A.; Glöß, A.; Hättig, C.; Höfener, S.; Klopper, W.; Tew, D. P. The MP2-F12 Method in the TURBOMOLE Program Package. *J. Comput. Chem.* **2011**, *32*, 2492–2513.

(227) MOLPRO, version 2012.1, a Package of Ab Initio Programs, H.-J. Werner, P. J. Knowles, G. Knizia, F. R. Manby, M. Schütz, P. Celani, T. Korona, R. Lindh, A. Mitrushenkov, G. Rauhut, K. R. Shamasundar, T. B. Adler, R. D. Amos, A. Bernhardsson, A. Berning, D. L. Cooper, M. J. O. Deegan, A. J. Dobbyn, F. Eckert, E. Goll, C. Hampel, A. Hesselmann, G. Hetzer, T. Hrenar, G. Jansen, C. Köppl, Y. Liu, A. W. Lloyd, R. A. Mata, A. J. May, S. J. McNicholas, W. Meyer, M. E. Mura, A. Nicklass, D. P. O'Neill, P. Palmieri, D. Peng, K. Pflüger, R. Pitzer, M. Reiher, T. Shiozaki, H. Stoll, A. J. Stone, R. Tarroni, T. Thorsteinsson, and M. Wang, see `http://www.molpro.net`.

(228) Werner, H.-J.; Knowles, P. J.; Knizia, G.; Manby, F. R.; Schütz, M. Molpro: a General-Purpose Quantum Chemistry Program Package. *WIREs: Comput. Mol. Sci.* **2012**, *2*, 242–253.

(229) Perdew, J. P.; Burke, K.; Ernzerhof, M. Generalized Gradient Approximation Made Simple. *Phys. Rev. Lett.* **1996**, *77*, 3865–3868.

(230) Weigend, F.; Ahlrichs, R. Balanced Basis Sets of Split Valence, Triple Zeta Valence and Quadruple Zeta Valence Quality for H to Rn: Design and Assessment of Accuracy. *Phys. Chem. Chem. Phys.* **2005**, *7*, 3297–3305.

(231) Steed, J. M.; Dixon, T. A.; Klemperer, W. Molecular-Beam Studies of Benzene Dimer, Hexafluorobenzene Dimer and Benzene-Hexafluorobenzene. *J. Chem. Phys.* **1979**, *70*, 4940–4946.

(232) Arunan, E.; Gutowsky, H. S. The Rotational Spectrum, Structure and Dynamics of a Benzene Dimer. *J. Chem. Phys.* **1993**, *98*, 4294–4296.

(233) Podeszwa, R.; Bukowski, R.; Szalewicz, K. Potential Energy Surface for the Benzene Dimer and Perturbational Analysis of pi-pi Interactions. *J. Phys. Chem. A* **2006**, *110*, 10345–10354.

(234) van der Avoird, A.; Podeszwa, R.; Szalewicz, K.; Leforestier, C.; van Harrevelt, R.; Bunker, P. R.; Schnell, M.; von Helden, G.; Meijer, G. Vibration-Rotation-Tunneling States of the Benzene Dimer: An Ab Initio Study. *Phys. Chem. Chem. Phys.* **2010**, *12*, 8219–8240.

(235) Schnell, M.; Erlekam, U.; Bunker, P. R.; von Helden, G.; Grabow, J.-U.; Meijer, G.; van der Avoird, A. Structure of the Benzene Dimer - Governed by Dynamics. *Angew. Chem. Int. Ed.* **2013**, *52*, 5180–5183.

(236) Schnell, M.; Erlekam, U.; Bunker, P. R.; von Helden, G.; Grabow, J.-U.; Meijer, G.; van der Avoird, A. Unraveling the Internal Dynamics of the Benzene Dimer: A Combined Theoretical and Microwave Spectroscopy Study. *Phys. Chem. Chem. Phys.* **2013**, *15*, 10207–10223.

(237) Grover, J. R.; Walters, E. A.; Hui, E. T. Dissociation Energies of the Benzene Dimer and Dimer Cation. *J. Phys. Chem.* **1987**, *91*, 3233–3237.

(238) Krause, H.; Ernstberger, B.; Neusser, H. Binding Energies of small Benzene Clusters. *Chem. Phys. Lett.* **1991**, *184*, 411–417.

(239) Nishiyama, I.; Hanazaki, I. Infrared Photodissociation of the Benzene Dimer. Translational Energy Distribution of Dissociation Fragments. *Chem. Phys. Lett.* **1985**, *117*, 99–102.

(240) Chewter, L. A.; Sander, M.; Müller-Dethlefs, K.; Schlag, E. W. High Resolution Zero Kinetic Energy Photoelectron Spectroscopy of Benzene and Determination of the Ionization Potential. *J. Chem. Phys.* **1987**, *86*, 4737–4744.

(241) Nemeth, G. I.; Selzle, H. L.; Schlag, E. W. Magnetic {ZEKE} Experiments with Mass Analysis. *Chem. Phys. Lett.* **1993**, *215*, 151–155.

(242) Boernsen, K. O.; Selzle, H. L.; Schlag, E. W. Photoionization of Benzene Complexes. *J. Phys. Chem.* **1988**, *92*, 5482–5485.

(243) Grover, J. R.; Walters, E. A.; Baumgaertel, H. Comparison of One-photon with Two-photon Photoionization of Benzene Dimer near Threshold: Comment. *J. Phys. Chem.* **1989**, *93*, 7534–7535.

(244) Selzle, H. L.; Neusser, H. J.; Ernstberger, B.; Krause, H.; Schlag, E. W. Ionization Potential of the Benzene Dimer: Reply to Comment. *J. Phys. Chem.* **1989**, *93*, 7535–7536.

(245) Pieniazek, P. A.; Krylov, A. I.; Bradforth, S. E. Electronic Structure of the Benzene Dimer Cation. *J. Chem. Phys.* **2007**, *127*, 044317.

(246) Johnson, R. D.; Burdenski, S.; Hoffbauer, M. A.; Giese, C. F.; Gentry, W. R. Infrared Photodissociation of Benzene Dimers in the 1000 cm^{-1} Frequency Region. *J. Chem. Phys.* **1986**, *84*, 2624–2629.

(247) Henson, B. F.; Hartland, G. V.; Venturo, V. A.; Felker, P. M. Time-resolved Raman spectroscopy of Benzene Dimer: Nanosecond-plus Lifetime at 992 cm^{-1} Vibrational Energy. *J. Chem. Phys.* **1989**, *91*, 2751–2753.

(248) Tsuzuki, S.; Honda, K.; Uchimaru, T.; Mikami, M. Ab Initio Calculations of Structures and Interaction Eenergies of Toluene Dimers Including CCSD(T) Level Electron Correlation correction. *J. Chem. Phys.* **2005**, *122*, 144323.

(249) Chipot, C.; Jaffe, R.; Maigret, B.; Pearlman, D. A.; Kollman, P. A. Benzene Dimer:âĂĽ A Good Model for pi-pi Interactions in Proteins? A Comparison between the Benzene and the Toluene Dimers in the Gas Phase and in an Aqueous Solution. *J. Am. Chem. Soc.* **1996**, *118*, 11217–11224.

(250) Rogers, D. M.; Hirst, J. D.; Lee, E. P.; Wright, T. G. Ab Initio Study of the Toluene Dimer. *Chem. Phys. Lett.* **2006**, *427*, 410–413.

(251) Law, K.; Schauer, M.; Bernstein, E. R. Dimers of Aromatic Molecules: $(Benzene)_2$, $(Toluene)_2$, and Benzene-Toluene. *J. Chem. Phys.* **1984**, *81*, 4871–4882.

(252) Ishikawa, S.; Ebata, T.; Ishikawa, H.; Inoue, T.; Mikami, N. Hole-Burning and Stimulated RamanâĹŠUV Double Resonance Spectroscopies of Jet-Cooled Toluene Dimer. *J. Phys. Chem.* **1996**, *100*, 10531–10535.

(253) Geng, Y.; Takatani, T.; Hohenstein, E. G.; Sherrill, C. D. Accurately Characterizing the pi-pi Interaction Energies of Indole-Benzene Complexes. *J. Phys. Chem. A* **2010**, *114*, 3576–3582.

(254) Biswal, H. S.; Gloaguen, E.; Mons, M.; Bhattacharyya, S.; Shirhatti, P. R.; Wategaonkar, S. Structure of the Indole-Benzene Dimer Revisited. *J. Phys. Chem. A* **2011**, *115*, 9485–9492.

(255) Lahmani, F.; Lardeux-Dedonder, C.; Solgadi, D.; Zehnacker, A. Spectroscopic Study of the Anisole-Benzene Complex Formed in a Supersonic Free Jet. *J. Phys. Chem.* **1989**, *93*, 3984–3989.

(256) Reimann, B.; Buchhold, K.; Barth, H.-D.; Brutschy, B.; Tarakeshwar, P.; Kim, K. S. Anisole-$(H_2O)_n$ (n=1-3) Complexes: An Experimental and Theoretical Investigation of the Modulation of Optimal Structures, Binding Energies, and Vibrational Spectra in Both the Ground and First Excited States. *J. Chem. Phys.* **2002**, *117*, 8805–8822.

(257) Ribblett, J. W.; Sinclair, W. E.; Borst, D. R.; Yi, J. T.; Pratt, D. W. High Resolution Electronic Spectra of Anisole and Anisole-Water in the Gas Phase: Hydrogen Bond Switching in the S_1 State. *J. Phys. Chem. A* **2006**, *110*, 1478–1483.

(258) Biczysko, M.; Piani, G.; Pasquini, M.; Schiccheri, N.; Pietraperzia, G.; Becucci, M.; Pavone, M.; Barone, V. On the Properties of Microsolvated Molecules in the Ground (S0) and Excited (S1) States: The Anisole-Ammonia 1:1 Complex. *J. Chem. Phys.* **2007**, *127*, 144303.

(259) Heger, M.; Altnoder, J.; Poblotzki, A.; Suhm, M. A. To pi or Not to pi - How does Methanol Dock onto Anisole? *Phys. Chem. Chem. Phys.* **2015**, *17*, 13045–13052.

(260) Giuliano, B. M.; Maris, A.; Melandri, S.; Caminati, W. Pure Rotational Spectrum and Model Calculations of Anisole-Ammonia. *J. Phys. Chem. A* **2009**, *113*, 14277–14280.

(261) Pietraperzia, G.; Pasquini, M.; Schiccheri, N.; Piani, G.; Becucci, M.; Castellucci, E.; Biczysko, M.; Bloino, J.; Barone, V. The Gas Phase Anisole Dimer: A Combined High-Resolution Spectroscopy and Computational Study of a Stacked Molecular System. *J. Phys. Chem. A* **2009**, *113*, 14343–14351.

(262) Pasquini, M.; G.Pietraperzia,; Piani, G.; Becucci, M. Excitonic Coupling in van der Waals Complexes: The Anisole Dimers. *J. Mol. Struct.* **2011**, *993*, 491–494.

(263) Balmer, F. A.; Trachsel, M. A.; van der Avoird, A.; Leutwyler, S. The Elusive S_2 State, the S_1/S_2 Splitting, and the Excimer States of the Benzene Dimer. *J. Chem. Phys.* **2015**, *142*, 234306.

(264) Wei, J.; Makarem, C.; Reinitz, A. L.; Darr, J. P.; Loomis, R. A. Accurate Measurement of the T-Shaped and Linear Binding Energies Using Vibronic-Specific I_2(B, v) Fragment Velocity-Map Imaging. *Chem. Phys.* **2012**, *399*, 172–179.

(265) Mollner, A. K.; Casterline, B. E.; Ch´ ng, L. C.; Reisler, H. Imaging the State-Specific Vibrational Predissociation of the Ammonia – Water Hydrogen-Bonded Dimer. *J. Phys. Chem. A* **2009**, *113*, 10174–10183.

(266) Lane, J. R.; Vaida, V.; Kjaergaard, H. G. Calculated Electronic Transitions of the Water Ammonia Complex. *J. Chem. Phys.* **2008**, *128*, 034302.

(267) Slipchenko, M. N.; Sartakov, B. G.; Vilesov, A. F.; Xantheas, S. S. Study of NH Stretching Vibrations in Small Ammonia Clusters by Infrared Spectroscopy in He Droplets and ab Initio Calculations. *J. Phys. Chem. A* **2007**, *111*, 7460–7471.

(268) Ni, H.; Serafin, J. M.; Valentini, J. J. Dynamics of the Vibrational Predissociation of HCl Dimer. *J. Chem. Phys.* **2000**, *113*, 3055–3066.

(269) Vissers, G. W. M.; Oudejans, L.; Miller, R. E.; Groenenboom, G. C.; van der Avoird, A. Vibrational Predissociation in the HCl Dimer. *J. Chem. Phys.* **2004**, *120*, 9487–9498.

(270) Mancini, J. S.; Bowman, J. M. A New Many-Body Potential Energy Surface for HCl Clusters and Its Application to Anharmonic Spectroscopy and Vibration-Vibration Energy Transfer in the HCl Trimer. *J. Phys. Chem. A* **2014**, *118*, 7367–7374.

(271) Bohac, E. J.; Marshall, M. D.; Miller, R. E. Initial State Effects in the Vibrational Predissociation of Hydrogenfluoride Dimer. *J. Chem. Phys.* **1992**, *96*, 6681–6695.

(272) Klopper, W.; Quack, M.; Suhm, M. A. HF Dimer: Empirically Refined Analytical Potential Energy and Dipole Hypersurfaces from Ab Initio Calculations. *J. Chem. Phys.* **1998**, *108*, 10096–10115.

(273) Oudejans, L.; Miller, R. E. Dissociation Dynamics of Oriented DF-HF and HF-DF Complexes: Evidence for Direct and Indirect Dissociation. *J. Phys. Chem. A* **1997**, *101*, 7582–7592.

(274) Klopper, W.; Quack, M.; Suhm, M. A. A New Ab Initio Based Six-dimensional Semi-empirical Pair Interaction Potential for HF. *Chem. Phys. Lett.* **1996**, *261*, 35–44.

(275) Oudejans, L.; Moore, D. T.; Miller, R. E. State-to-State Vibrational Predissociation Dynamics of the Acetylene-HF complex. *J. Chem. Phys.* **1999**, *110*, 209–219.

(276) Oudejans, L.; Miller, R. E. State-to-State Vibrational Predissociation Dynamics of the Acetylene-HCl Complex. *J. Phys. Chem. A* **1999**, *103*, 4791–4797.

(277) Li, G.; Parr, J.; Fedorov, I.; Reisler, H. Imaging Study of Vibrational Predissociation of the HCl-Acetylene Dimer: Pair-correlated Distributions. *Phys. Chem. Chem. Phys.* **2006**, *8*, 2915–2924.

(278) Parr, J. A.; Li, G.; Fedorov, I.; McCaffery, A. J.; Reisler, H. Imaging the State-Specific Vibrational Predissociation of the C_2H_2-NH_3 Hydrogen-Bonded Dimer. *J. Phys. Chem. A* **2007**, *111*, 7589–7598.

(279) Bohac, E. J.; Miller, R. E. State-to-state Vibrational Predissociation of H_2-HF and D_2-HF. Direct Comparisons between Theory and Experiment. *J. Chem. Phys.* **1993**, *98*, 2604–2613.

(280) Bemish, R. J.; Bohac, E. J.; Wu, M.; Miller, R. E. Photofragment Vibrational, Rotational, and Translational Distributions for N_2-HF (v=1). *J. Chem. Phys.* **1994**, *101*, 9457–9468.

(281) Jankowski, P.; Tsang, S. N.; Klemperer, W.; Szalewicz, K. Spectra of N_2-HF from Symmetry-adapted Perturbation Theory Potential. *J. Chem. Phys.* **2001**, *114*, 8948–8963.

(282) Oudejans, L.; Miller, R. E. Intermolecular V-V Energy Transfer in the Photodissociation of CO_2-HF(v=1). *J. Chem. Phys.* **1998**, *109*, 3474–3484.

(283) Oudejans, L.; Miller, R. Mode Dependence of the State-to-State Vibrational Dynamics of HCN-HF. *Chem. Phys.* **1998**, *239*, 345 – 356.

(284) Shorter, J. H.; Casassa, M. P.; King, D. S. Fragment State Correlations in the Dissociation of NO-HF(v=1). *J. Chem. Phys.* **1992**, *97*, 1824–1831.

(285) Hetzler, J. R.; Casassa, M. P.; King, D. S. Product Energy Correlations in the Dissociation of Overtone Excited Nitric Oxide Dimer. *J. Phys. Chem.* **1991**, *95*, 8086–8095.

(286) Wright, D. S.; Holmes-Ross, H. L.; Lawrance, W. D. Dissociation of the NO-CH_4 van der Waals Complex: Binding Energy and Correlated Motion of the Molecular Fragments. *Chem. Phys. Lett.* **2007**, *435*, 19–23.

(287) Krause, H.; Neusser, H. J. The van der Waals modes of the (Benzene-Ar)$^+$ Complex Studied by Mass-selective Pulsed-field Threshold Ionization. *Chem. Phys. Lett.* **1993**, *213*, 603–609.

(288) Hobza, P.; Bludsky, O.; Selzle, H. L.; Schlag, E. W. Ab-Initio Second- and Fourth-order Moller-Plesset Study on Structure, Stabilization Energy, and Stretching Vibration of Benzene-X (X=He, Ne, Ar, Kr, Xe) van der Waals molecules. *J. Chem. Phys.* **1992**, *97*, 335–340.

(289) Makarewicz, J. Fully Dimensional Ab Initio Description of the Structure and Energetics of Azabenzene-Argon Complexes. *J. Chem. Phys.* **2005**, *123*, 154302.

(290) Cagide Fajín, J. L.; López Cacheiro, J.; Fernández, B.; Makarewicz, J. Fluorobenzene·Argon Ground-state Intermolecular Potential Energy Surface. *J. Chem. Phys.* **2004**, *120*, 8582–8586.

(291) Su, M.-C.; O, H.-K.; Parmenter, C. S. A Fluorescence Characterization of the p-Difluorobenzene-Argon van der Waals Complex. Energy Levels, Geometries and Dissociation Energies. *Chem. Phys.* **1991**, *156*, 261–280.

(292) Makarewicz, J. Potential-energy Surface, Dynamics of van der Waals Motions, and Vibronic Transitions in p-Difluorobenzene-Argon Complex. *J. Chem. Phys.* **2005**, *122*, 114312.

(293) Dimopoulou-Rademann, O.; Even, U.; Amirav, A.; Jortner, J. Binding energy of the Styrene-Argon van der Waals Molecule. *J. Phys. Chem.* **1988**, *92*, 5371–5373.

(294) Dao, P.; Morgan, S.; Jr., A. C. Two-color Resonance Enhanced Multiphoton Ionization of van der Waals Molecules: Studies of Spectroscopy Shifts and Ionization Thresholds of p-Xylene Clustered with Argon. *Chem. Phys. Lett.* **1985**, *113*, 219–224.

(295) Černý, J.; Tong, X.; Hobza, P.; Müller-Dethlefs, K. State of the Art Theoretical Study and Comparison to Experiment for the Phenol···Argon Complex. *J. Chem. Phys.* **2008**, *128*, 114319.

(296) Makarewicz, J. Potential Energy Surface, van der Waals Motions, and Vibronic Transitions in Phenol-Argon Complex. *J. Chem. Phys.* **2006**, *124*, 084310.

(297) Georgiev, S.; Chakraborty, T.; Neusser, H. J. Binding Energy and Intermolecular Vibrations of Neutral and Ionized p-Fluorotoluene-Ar Cluster by Mass Analyzed Threshold Ionization. *J. Phys. Chem. A* **2004**, *108*, 3304–3307.

(298) Mazzoni, F.; Becucci, M.; Rezac, J.; Nachtigallová, D.; Michels, F.; Hobza, P.; Müller-Dethlefs, K. Structure and Energetics of the Anisole-Ar_n (n = 1, 2, 3) Complexes: High-resolution Resonant Two-photon and Threshold Ionization Experiments, and Quantum Chemical Calculations. *Phys. Chem. Chem. Phys.* **2015**, 12530–12537.

(299) Outhouse, E. A.; Bickel, G. A.; Demmer, D. R.; Wallace, S. C. Vibrational Predissociation in S_1 Indole van der Waals Clusters. *J. Chem. Phys.* **1991**, *95*, 6261–6270.

(300) Outhouse, E. A.; Demmer, D. R.; Leach, G. W.; Wallace, S. C. Vibrational Predissociation in S_1 1-Methylindole van der Waals Clusters. *J. Chem. Phys.* **1993**, *99*, 80–90.

(301) Grebner, T. L.; Neusser, H. J. Pulsed Field Threshold Ionization of van der Waals Complexes. The Dissociation Energy of Ionic and Neutral Dibenzo-p-dioxin·Ar and -84Kr. *Chem. Phys. Lett.* **1995**, *245*, 578–584.

(302) Gaber, A.; Riese, M.; Witte, F.; Grotemeyer, J. Determination of the Binding Energies in Aromatic Clusters: Resonance-enhanced Multi-photon Ionization and Mass Analyzed

Threshold Ionization Investigation of the Dichlorobenzene-Argon Complexes. *Eur. J. Mass Spectrom.* **2009**, *15*, 349–359.

(303) Gilbert, B. D.; Parmenter, C. S.; Oh, H.-K. Vibrational Predissociation Dynamics of p-Difluorobenzene-N_2 Complexes. Comparison with p-Difluorobenzene-Ar. *J. Phys. Chem.* **1995**, *99*, 2444–2458.

(304) Fujiwara, T.; Lim, E. C. Binding Energies of the Neutral and Ionic Clusters of Naphthalene in Their Ground Electronic States. *J. Phys. Chem. A* **2003**, *107*, 4381–4386.

(305) Podeszwa, R.; Szalewicz, K. Physical Origins of Interactions in Dimers of Polycyclic Aromatic Hydrocarbons. *Phys. Chem. Chem. Phys.* **2008**, *10*, 2735–2746.